AN ABSTRACT OF THE THESIS OF

Donald Joseph Gordon for the Doctor of Philosophy in

Physical Chemistry presented on March 10, 1971 .

Title: Infrared Spectrum of Isotopic Cyanate Ion in

Potassium Chloride and Potassium Bromide.

Abstract approved: _____

Dr. John Courtney Decius

Cyanate ion enriched in ^{15}N, ^{13}C, or ^{18}O has been prepared by direct oxidation reactions and introduced into pressed disks and single crystals of potassium chloride and potassium bromide grown from the melt. The infrared absorption spectra of $^{14}N^{12}C^{16}O^-$, $^{15}N^{12}C^{16}O^-$, $^{14}N^{13}C^{16}O^-$, $^{14}N^{12}C^{18}O^-$, $^{14}N^{13}C^{18}O^-$, $^{15}N^{12}C^{18}O^-$, $^{15}N^{13}C^{16}O^-$, and $^{15}N^{13}C^{18}O^-$ have together exhibited over 250 bands. The infrared spectra of such matrix isolated molecular ions have been observed between 550 cm^{-1} and 5000 cm^{-1} from 320°K to liquid-N_2 temperatures. More than 70 new spectral features of the cyanate ion's spectra including $2\nu_3$ have been discovered. On the basis of isotopic frequency shifts and changes in the relative intensities, an earlier assignment of ν_1 and $2\nu_2$ is reversed. Noether's rule has been found applicable to di-substituted cyanates. Calculations based upon cyanate spectra have lead to a complete determination of the general internal coordinate potential function through quartic terms for cyanate ion in KCl, KBr, and KI. Normal coordinate potential constants for each isotopic species have been determined in all three lattices. Anharmonicity constants, and the cubic and quartic internal coordinate potential constants are independent of the matrix.

Infrared Spectrum of Isotopic Cyanate Ion in Potassium Chloride and Potassium Bromide

by

Donald Joseph Gordon

A THESIS

submitted to

Oregon State University

in partial fulfillment of
the requirements for the
degree of

Doctor of Philosophy

June 1971

APPROVED:

Redacted for Privacy

Professor of Chemistry

Redacted for Privacy

Chairman of the Chemistry Department

Redacted for Privacy

Dean of the Graduate School

Date thesis presented: March 10, 1971

Typed by Judith Lee Gordon for:

Donald Joseph Gordon

Preface

This paper presents a thorough study of the cyanate ion's vibrational spectra in potassium chloride and potassium bromide crystals. Initially this problem was undertaken to provide a more thorough study of this ion in potassium chloride and to prepare and study isotopic cyanates. Under the direction of Dr. John C. Decius, Art Maki had done the initial studies on cyanate in crystals but had only been able to study the normally abundant isotopic species in KBr and KI. Maki completed his work in 1959. The problem was presented to me January 1964, and from that time until August 1967 a great deal of additional data was discovered. In August 1967, we published a paper (18) indicating our reinvestigation of cyanate ion and its isotopes. Concurrently, I went on active duty in the Army.

At the time of my departure from Oregon State University, the only part of this thesis which was written was most of Chapter Five and most of the tables and charts in Chapter Six. Owing to my extensive duties in the Army which included a year in Viet Nam, I was unable to complete this thesis. During that span, Schettino and Hisatsune, at Pennsylvania State University, independently completed their reinvestigation of cyanate ion. They published their data, which includes much of the new data that my work would have presented though not all of it, in January 1970 (84).

In July 1970, the Army allowed me to go on excess leave to complete my doctorial dissertation. Since Dr. Decius was to be at the University of Minnesota for the 1970 fall term, that was where I went. This was indeed fortuitous for it not only gave me the opportunity of becoming acquainted with the fine spectroscopy laboratory there, but also made it possible for my data to be used to obtain a potential function (including cubic and quartic terms) for cyanate. This does indeed represent a unique contribution.

Also, using their modified spectrometer, we were able to find many weak features in the cyanate spectra above 4000 cm^{-1} including an overtone of the C-N stretch which has never been seen before and is a very necessary bit of information in any force constant or anharmonic determination.

This work, which spans better than six years, not only represents an original and worthwhile scientific contribution but also has served as a very complete learning vehicle. Through my studies, I have aquired a great deal of knowledge of molecular vibration, especially with respect to linear triatomic molecules. And yet, there is still plenty of room for further research in this area.

Many people made this thesis possible. Thanks are due to: Dr. Bert Christensen who arranged my matriculation at Oregon State University and obtained a NASA fellowship for my studies; to Drs. Allen B. Scott and Bob Sievers for the use of their crystal growing apparatus; to Dr. Robert Hexter who graciously provided me a place to work at the University of Minnesota; to Dr. John Overend and D. Foss Smith, Jr. whose aid and interest in the potential energy calculations and in further vibrational research was invaluable; to Maj. Leonard of the Office of Personnel Operations, United States Army, who obtained excess leave which permitted me time to write this paper; and to Drs. Ken Hedberg, Tom Norris, and Olaf Boedtker, members of my graduate committee for their incisive and helpful criticisms in the reading of this work. More words of thanks can't express the depth of my graditude for the contributions made by Dr. John Decius to this dissertation and for the guidance he provided during all of my graduate studies. It has been a rare priviledge for me to have been able to have worked under his supervision.

Behind every endeaver there is a woman. My wife's constant interest and prodding truly provided that extra bit of motivation I needed to complete this work. Her love, understanding, and

dedication to the completion of this work was indespensible. She even typed this thesis.

Donald J. Gordon

TABLE OF CONTENTS

INFRARED SPECTRUM OF ISOTOPIC CYANATE ION IN POTASSIUM CHLORIDE AND POTASSIUM BROMIDE

CHAPTER 1

INTRODUCTION

The subject of the research reported upon in this thesis is the study of the chemical and vibrational behavior of the cyanate ion in potassium chloride and potassium bromide host lattices.

BACKGROUND

The cyanate ion is composed of three atoms, nitrogen, carbon and oxygen. In this thesis, they will always be referred to in that order; and, "normal" cyanate will refer to the 14 12 16 isotopic species.

Previous studies have satisfactorily demonstrated that cyanate ion is a linear triatomic structure having carbon-oxygen and carbon-nitrogen bonds (32). Valence theory and Pauling's Charge Rule (74,p.200) gives the following resonant structures as the most important contributions:

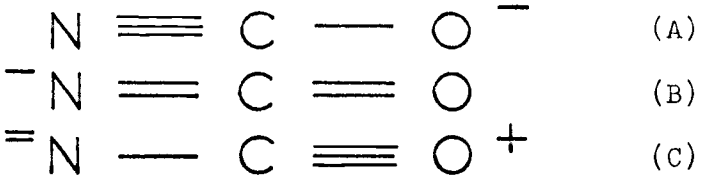

(A)
(B)
(C)

Studies performed by L. H. Jones (39,40) on thiocyanate ion (NCS^-) for structures analogous to (A), (B), and (C) accounted for 71%, 12% and 17%, respectively, of the bonding character within that ion. Maki (54,p.139) has calculated the contributions to the bond character of cyanate ion for resonant structures to be 76% (A), 6% (B) and 18% (C); the increased contribution of (A) being expected as the oxygen is more electro-negative than sulfur.

The only reliable x-ray diffraction studies of cyanate were early works by Hendricks and Pauling (32,p.2912-2916). These indicated that r_{NC} and r_{CO} equilibrium bond lengths were approximately the same and equal to ca. 1.16 Å. This is a doubtful result in view of the bond order calculations of Maki (54,p.139) but this value at least gives us a feel for the (perhaps) average value of the bond lengths. Throughout this paper (and for that matter, for all cyanate studies to date), an accurate value for the respective r_i^e is not experimentally known, and reasonable values are assumed. Table 1-1 illustrates various calculated equilibrium bond lengths.

TABLE 1-1. VARIOUS CYANATE EQUILIBRIUM BOND LENGTHS, (Å).

Item	Structure	r_{NC}	r_{CO}	Reference
1.	$N \equiv C - O^-$ (A)	1.15	1.43	74,p.169
2.	$^-N = C = O$ (B)	1.265	1.215	74,p.169
3.	$^=N - C \equiv O^+$ (C)	1.47	1.10	74,p.169
4.	NCO^-	1.14	1.27	this work
5.	NCO^-	1.17	1.23	55,p.780
6.	NCO^-		1.22	46, this work

The bond lengths shown in the first three rows correspond to the bond orders depicted for the respective bond in the resonant structures. Row four shows bond lengths calculated from Maki's resonant structure contribution percentages, and Pauling's Covalent bond lengths, scaled to the cyanate total (r_{NO}) bond length given by Dixon (23,p.165). The fifth row shows cyanate bond lengths calculated from Badger's Rule (4,p.713). These distances will be the ones used througout this work. The sixth

row shows a CO length calculated from the empirical equation $f_{CO} = 35.5\ r_{CO}^{-5.79}$ which Ladd, et al. (46) have found to be representative of most carbon-oxygen bonds. The f_{CO}'s used in this latter calculation came from the results in Chapter Seven of this paper. All of the above bond lengths demonstrate the predominance of resonant structure (A). This is in accord with cyanate's general chemical behavior toward hydrogen. However, the abundance of isocyanates in many covalent compounds argue for (B) and (C) contributions. The lack of recent bond length data does strongly recommend this area for further study.

Early vibrational studies on cyanate ion were performed in aqueous media using Raman spectroscopic techniques (10,29,68). Early infrared studies were undertaken by Williams (94) in 1940. These works were complicated by the profusion of water bands and the hydrolysis that cyanate undergoes in water. The latter may be presented as:

$$NCO^- + 3H_2O \rightleftharpoons HCO_3^- + NH_4^+ + OH^-$$
$$2NCO^- + 4H_2O \rightleftharpoons 2CO_3^= + 2NH_4^+ \qquad (1\text{-}1)$$

These ions formed by hydrolysis as well as their hydrolytic products caused many impurity bands which further confused their spectra. In addition, the polarizing effect of water upon cyanate changes the cyanate spectrum. Miller and Wilkins (60) obtained infrared spectra of KNCO in Nujol emulsions but their results were confused by carbonate and bicarbonate ion contamination.

More recently Maki and Decius have uncovered a wealth of vibrational detail by isolating cyanate ion in alkali halide matrices of potassium iodide (55), potassium bromide and to a more limited extent in potassium chloride and sodium chloride (56). Table 1-2 outlines early cyanate findings.

TABLE 1-2. EARLY CYANATE RESULTS.

Researcher (technique)	ν_1 (cm-1)	ν_2 (cm-1)	ν_3 (cm-1)	Reference
1. Cleveland (Raman)			2171	10
2. Pal and Sen Gupta (Raman)	{1229 1314}	838	2183	68
3. Goubeau (Raman)	857	970($2\nu_2$)	2192	29
4. Williams (IR)	870		2180	94
5. Maki (IR) in KBr Crystal	{1205.5 1292.6}	629.4	2169.6	56

The 820-880 cm^{-1} bands have been shown (56,p.773) to be due to carbonate ion. The earlier investigations disregarded the doublet between 1200 and 1300 cm^{-1} as due to impurity ions, whereas Maki ascertained that Fermi resonance (see Chapter Three) occurs between ν_1 and $2\nu_2$ in that region. Williams' work was hampered by resolution problems and water solvent opacity to infrared radiation. As a result of this current study some of Maki's data are refined and a comparison of significant changes are presented in this thesis, as the subjects arise.

Decius, et al. continued to study the ion's vibrational spectrum with emphasis upon external modes and the presentation of further vibrational detail (19). Decius and Gordon, as an early result of this work, presented refinements of earlier cyanate assignments and indicated that cyanate isotope spectra were being studied (18). Subsequently, Schettino and Hisatsune (84) described a large number of cyanate ion frequencies in KCl, KBr and KI. Guided by the reassignment of ν_1 and $2\nu_2$ established by Decius and Gordon (18) on the basis of isotopic dependence of the relative intensities of the Fermi diad (see Chapter Four),

Schettino and Hisatsune redetermined the cyanate ion spectroscopic constants (ω_i and X_{ij}). Chapter Eight presents a comparison of Schettino and Hisatsune's work to ours.

One deficiency in all previous work has been the lack of observation of the overtone of ν_3. This piece of data is essential to the evaluation of ω_{33}, X_{33}, f_{NC}, and the potential energy constants. This work remedies this situation. Let us now turn to a discussion of the cyanate ion's symmetry.

CYANATE AND THE $C_{\infty v}$ SYMMETRY GROUP

By virtue of the fact that cyanate ion is a linear, XYZ molecule, it falls into the $C_{\infty v}$ point group. In this group, there can be no symmetry types antisymmetric with respect to the molecular axis. Thus only certain combinations of symmetry properties of vibrational eigenfunctions are possible. For this reason, there are two non-degenerate symmetry types, conventionally designated Σ^+ and Σ^-. The linear XYZ has $3(3)-5=4$ internal degrees of freedom and so two will be non-degenerate normal modes of vibration, and one degenerate, or three observable fundamentals.

Since there are an infinite number of perpendicular planes containing the molecular axis, there are an infinite number of degenerate symmetry types which can be generated. These symmetry species and characters are shown in Appendix Three, Table One. The linear XYZ fundamentals belong to Σ^+ and Π species but eigenfunctions of the higher vibrational levels of the degenerate species may have Σ, Δ , Φ, etc. symmetry. This also is true for combinations. Table Two and Three in Appendix Three shows how these states are generated and the species to be expected.

A splitting of overtones of the degenerate Π mode is predicted from angular momentum considerations but the magnitude of the splitting is determined by the anharmonic potential function. A Π

vibration may be considered as having an angular momentum of one unit (ℓ =1) about the internuclear axis. If the Π vibration is excited to v_n=2, a triply degenerate state is predicted, which splits into one non-degenerate Σ^+ and one doubly degenerate Δ. Based on the Π mode, Figure 1-1 illustrates the excitation of its degeneracies.

The symmetry considerations introduced here will assist in the elucidation of the cyanate spectra. It will be noted that the 000 to 02 ^{2}0 transition has not been observed directly but transitions from this level have been seen. An immediate conclusion from this is that the $\Delta\ell$= $\pm$1, 0 selection rule apparently holds and also that cyanate is very much like CO_2 in that respect.

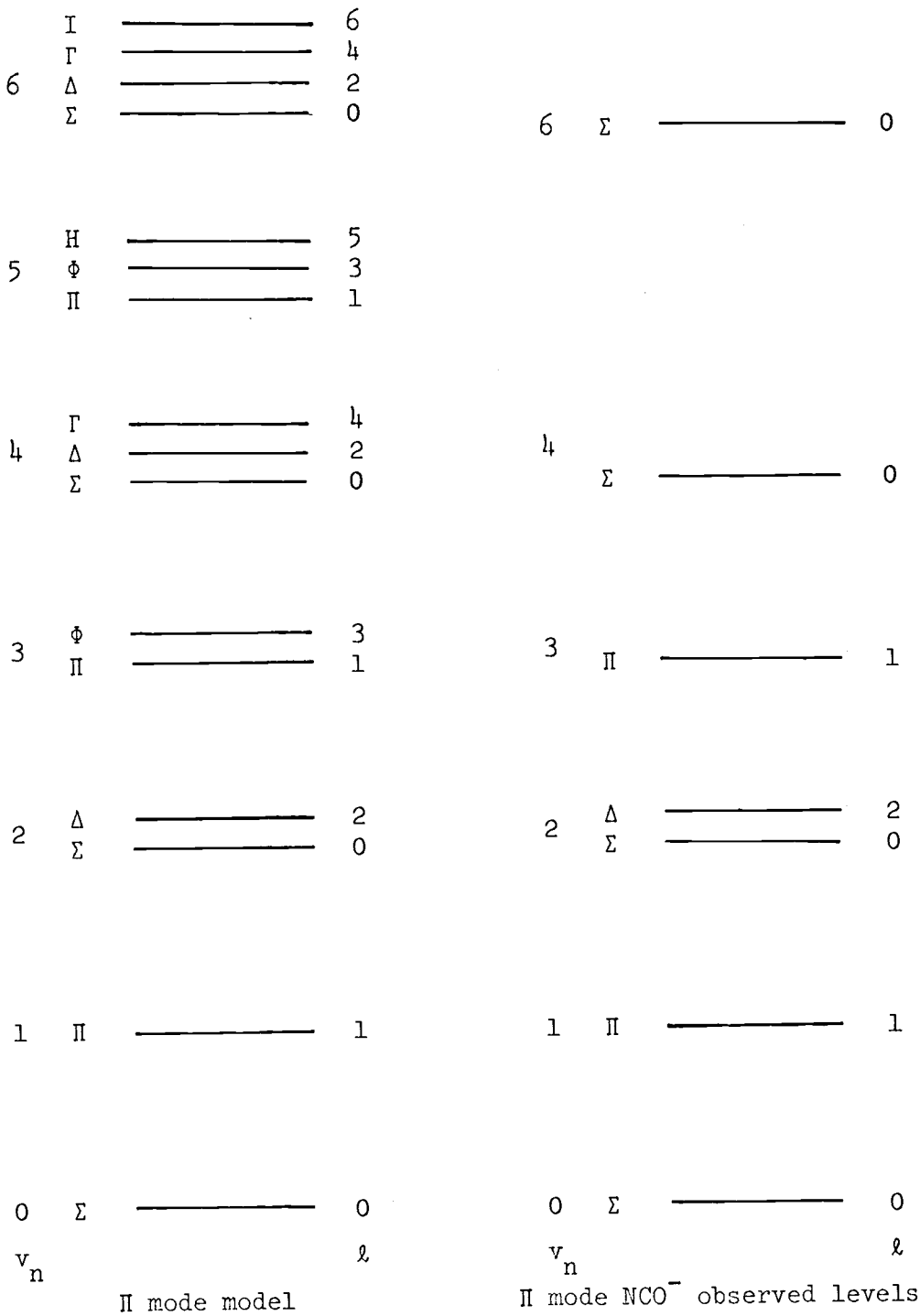

Figure 1-1. Excitation of Π mode degeneracies showing: (a) those levels theoretically possible; and (b) those levels observed in the cyanate ion vibrational spectrum.

CHAPTER 2

A MOLECULAR VIBRATION MODEL FOR THE CYANATE ION

In this section, a brief survey of the high points of vibrational theory will be presented. The discussion will be restricted for the most part to the linear XYZ polyatomic molecule in order to develop a theoretical model of the vibrating cyanate ion in an alkali halide environment. This presentation will proceed in three phases. The classical harmonic treatment of an isolated three partical linear ion will be followed by a quantum mechanical model including anharmonicity. The concluding portion will qualitatively discuss the effects of the alkali halide lattices on the impurity ion.

The rotational effects of the cyanate ion will not formally be considered. Assuming that the z-axis in Figure 2-1 is the body diagonal of the alkali halide cell, true rotation about the x or y axis is assumed unlikely. However, librational motions (coupled with restricted translation-like motions) which occur as the cyanate "bounces" around inside the matrix cell deserves brief comment. For the cyanate ion in the alkali halide "cage", we may write the total energy as:

$$E_{total}=E_{electronic}+E_{translational}+E_{librational}+E_{vibrational}$$

Two plausible assumptions allow us to treat cyanate vibrations separate of the other energy contributions. The Born-Oppenheimer approximation (95,p.273) separates out the E (electronic) and since we will be dealing with only the ground state, we set E (electronic) equal to zero. The translational and rotational (librational) are considered to be low frequency (external) modes (95,p.183) which are negligible with respect to the high frequency internal modes, and will not be analyzed in this thesis.

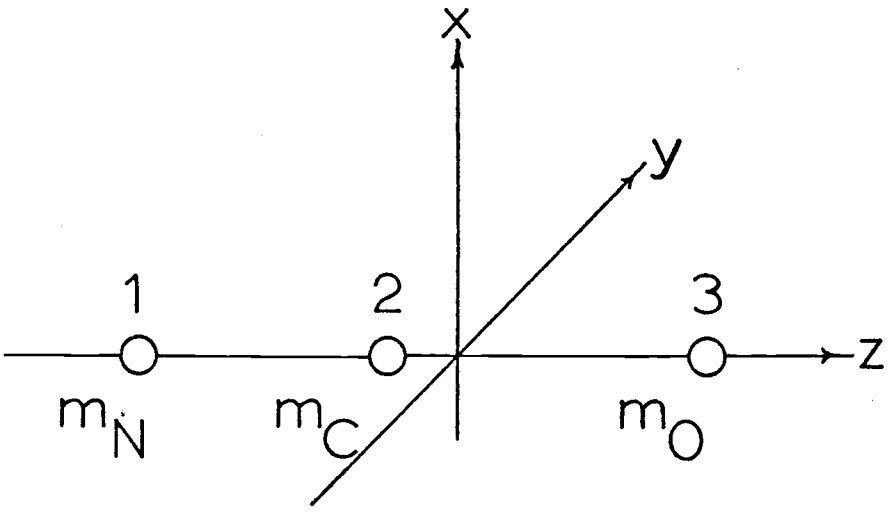

Figure 2-1. The cyanate ion in a cartesian coordinate system.

To describe the motion of three nuclei in cartesian coordinates, we need nine coordinates, three for each nucleus. Since we are interested in the vibrational motion, we are not concerned with translation of the system as a whole. The translation can be easily described by three coordinates of the center of mass. This introduces the condition that:

$$\sum_{i=1}^{N} m_i x_i = \sum_{i=1}^{N} m_i y_i = \sum_{i=1}^{N} m_i z_i = 0 \qquad (2\text{-}1)$$

Figure 2-1 shows the coordinate axis at the center of mass. The rotation, or orientation of the linear system in space, may be described by two of the nine coordinates. For infinitesimal changes, the conservation of momentum gives rise to (95,p.31):

$$\sum_{i=1}^{3} m_i z_i \Delta y_i = \sum_{i=1}^{3} m_i z_i \Delta x_i = 0 \qquad (2\text{-}2)$$

where z_i is the equilibrium position along the z-axis. Thus we are left with (3N-5) or four coordinates with which to describe the

vibrational motion of the ion. The number of vibrational degrees of freedom tells us the number of different "normal" modes of vibration.

Normal coordinates are obtained from cartesian coordinates by a linear transformation.

$$\text{(cartesian) } q_i = \sum_1^{3N} \ell_{ik} Q_k \quad \text{(normal)} \tag{2-3}$$

They have the property that:

$$\sum_1^{3N} q_i^2 = \sum_i \sum_k \sum_\ell \ell_{ik} \ell_{i\ell} Q_k Q_\ell = \Sigma Q_k^2 . \tag{2-4}$$

This ortho-normal condition is useful because in the treatment of harmonic motions, the squares of the coordinates are used extensively whereas the cross-terms only present complications.

Particles carrying out simple harmonic motion have displacements of the form:

$$x = \dot{x} \cos (2\pi\nu t + \phi) .$$

The corresponding acceleration is $\ddot{x} = -4 (\pi\nu)^2 x$ and the force is $F = m\ddot{x} = -4\pi^2 m\nu^2 x$. The restoring force for any simple harmonic motion of frequency, ν, is proportional to the displacement. This force is the negative derivative of the potential energy with respect to the displacement, $V = 2\pi^2\nu^2 m x^2$. When particles are executing harmonic motions, the potential function may be expressed as a power series expansion in the form:

$$2V = 2V_o + 2 \sum_{i=1}^{3N} (\partial V/\partial q_i)_o \, q_i + \sum_{i,j=1}^{3N} (\partial^2 V/\partial q_i \, \partial q_j)_o \, q_i q_j + \text{cubic + quartic + higher terms} \tag{2-5}$$

If the equilibrium position is chosen as being at zero potential, then the first term vanishes. This condition also implies, that the potential energy is at a minimum and thus the linear terms vanish as the partials evaluated at equilibrium are zero. And so equation 2-5 becomes:

$$2V = \sum_{i,j} k_{ij} q_i q_j + \text{cubic} + \text{quartic} + \ldots \quad . \tag{2-6}$$

For sufficiently small amplitudes, the cubic and higher terms can be neglected. More will be said about these terms later when anharmonicity is considered.

The kinetic energy is usually written in the form:

$$2T + \sum_{i} m_i \dot{q}_i^2 \quad . \tag{2-7}$$

If the q's in equation 2-3 to 2-7 are cartesians, then they are numbered consecutively according to the following scheme:

$$\begin{array}{lll} q_1 = x_1 & q_4 = x_2 & q_7 = x_3 \\ q_2 = y_1 & q_5 = y_2 & q_8 = y_3 \\ q_3 = z_1 & q_6 = z_2 & q_9 = z_3 \end{array} \quad .$$

Nielsen (63,p.160) has used a potential function of the form (see Figure 2-1):

$$2V = \sum_{i=1}^{3} \sum_{j=1}^{3} k_{ij} q_i q_j + k_4 (x^2 + y^2) ;$$

$$\text{where: } q_1 = z_2 - z_1 , \; q_2 = z_3 - z_2 , \; q_3 = z_3 - z_1 , \tag{2-8}$$

to arrive at:

$$2T = \dot{Q}_1^2 + (\dot{Q}_{21}^2 + \dot{Q}_{22}^2) + \dot{Q}_3^2$$

$$2V = k_1' Q_1^2 + k_2' (Q_{21}^2 + Q_{22}^2) + k_3' Q_3^2 \qquad (2\text{-}9)$$

in which the k's are shown in Appendix One, and are very complicated combinations of the masses and quadratic potential constants.

The frequencies of the normal modes are given by $\omega_i = (1/2\pi)\sqrt{k_i}$. The normal coordinates Q_1 and Q_3 are linear combinations of the valence bond distances (see Appendix One) and $Q_{21}^2 + Q_{22}^2$ are due to motions out of the axis of the ion.

From this brief excursion into the normal coordinate analysis of a linear cyanate ion, it is readily apparent that any complicated vibrational motion is resolvable into three fundamental frequencies. Two of them are due to stretches, and a degenerate bending motion. These are depicted in Figure 2-2.

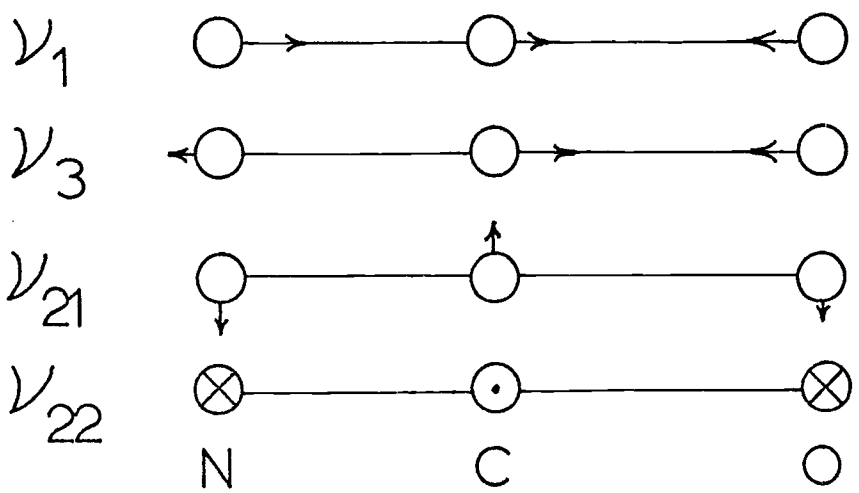

Figure 2-2. Normal Vibrational Modes for Cyanate.

It is also apparent that the potential constants in equation 2-9 are complicated functions of the potential constants which are seen to depend upon isotopic substitutions. Thus if we can

reduce our anharmonic oscillator to harmonic (zero order) frequencies for several isotopic species, it should be possible to calculate the quadratic potential constants in equations 2-8 and 2-9. We shall continue the discussion now, introducing wave mechanics utilizing equation 2-9.

The vibrational wave equation for our molecule has the following form (75, p. 67ff):

$$-(1/2)\hbar^2 \sum_{k=1}^{3n-5} (\partial^2\Psi_v/\partial Q_k^2) + (1/2) \sum_{k=1}^{3n-5} k_k' Q_k^2 \Psi_v = W_v\Psi_v; \quad (2\text{-}10)$$

where:

$$\Psi_v = \Psi_{(Q_1)} \Psi_{(Q_{21})} \Psi_{(Q_{22})} \Psi_{(Q_3)} \text{ ; and}$$

$$W_v = W_{(Q_1)} + W_{(Q_{21} + Q_{22})} + W_{(Q_3)} . \quad (2\text{-}11)$$

If equation 2-11 is accurate, then we can write:

$$-(1/2)\hbar^2[\partial^2\Psi_{(Q_k)}/\partial Q_k^2] + (1/2) k_k' Q_k^2 \Psi_{(Q_k)} = W_{(Q_k)}\Psi_{(Q_k)}. \quad (2\text{-}12)$$

Equation 2-12 is the differential equation for the harmonic oscillator which is treated in just about every quantum-mechanics text. The energy levels for this model have been found to be:

$$W_k = (v_k + d/2)\, h\omega_i, \quad (2\text{-}13)$$

where $v_k = 0,1,2,\ldots$, $i = 1,2,\ldots 3n-5$, $\Psi_{(Q_1)}$ and $\Psi_{(Q_3)}$ are Hermite polynomials, the doubly degenerate Ψ involving Q_{21} and Q_{22} are Laguerre polynomials, and d is the degeneracy of the k^{th} level. Unfortunately most molecules are not simple harmonic oscillators and the higher order terms in the potential function (equation 2-5) must be considered.

The potential function must be invariant to symmetry operations. Due to the axial symmetry of the cyanate ion, the cubic and quartic terms must be even functions of Q_{21} and Q_{22}. This requirement simplifies the number of cubic and quartic terms

contributing to the potential energy which is shown below:

$$V(\text{cubic}) = k_{111}Q_1^3 + k_{333}Q_3^3 + k_{122}Q_1(Q_{21}^2 + Q_{22}^2) + k_{113}Q_1^2Q_3 + k_{223}(Q_{21}^2 + Q_{22}^2)Q_3 + k_{133}Q_1Q_3^2 \qquad (2\text{-}14)$$

$$V(\text{quartic}) = k_{1111}Q_1^4 + k_{2222}(Q_{21}^2 + Q_{22}^2)^2 + k_{3333}Q_3^4 + k_{1223}Q_1(Q_{21}^2 + Q_{22}^2)Q_3 + k_{2233}(Q_{21}^2 + Q_{22}^2)Q_3^2 + k_{1133}Q_1^2Q_3^2 + k_{1122}Q_1^2(Q_{21}^2 + Q_{22}^2) + k_{1333}Q_1Q_3^3 + k_{3111}Q_3Q_1^3 \quad . \qquad (2\text{-}15)$$

The displacements within a molecule are assumed small, then in the power series potential expansion, the quadratic terms are large with respect to the cubic and quartic terms. For this reason, a common practice is to utilize the cubic and quartic terms in a first- and second-order perturbation treatment (75, p.151-177). This results in an energy expression of the form W = W(harmonic) + W(anharmonic), where the energy for the k^{th} level is desired and W(harmonic) is equation 2-13.

Inclusion of the cubic and quartic terms in the first-order perturbation treatment produces equations of the form:

$$W_k' = \int \Psi_{k(Q_k)} \; H_i' \; \Psi^*_{k(Q_k)} \; d\tau \; , \qquad (2\text{-}16)$$

where W_k' is the perturbation energy, H_i' is the perturbing potential, and the $\Psi_{(Q_k)}$ are the harmonic oscillator functions associated with Q_k . These integrals can be summarized (using equations 2-14 and 2-15) in the following format:

$$W_k' = \sum_{rst}^{333} k_{rst} \int \Psi_k \, Q_r Q_s Q_t \, \Psi_k^* \, d\tau + \sum_{rstu}^{3333} k_{rstu} \int \Psi_k Q_r Q_s Q_t Q_u \, \Psi_k^* \, d\tau \qquad (2\text{-}17)$$

Remembering that $\Psi_k = \Psi_{(Q_1)}\Psi_{(Q_3)}\Psi_{(Q_{21} + Q_{22})}$, then the

only non-vanishing integrals are (95, p.290-291):

$$\int \Psi_k Q_i^4 \Psi_k^* d\tau = (3\hbar^2/8\omega_i^2)[(v_i + 1/2)^2 + 1/4], \quad i = 1,3;$$
$$\int \Psi_k Q_i^2 Q_j^2 \Psi_k^* d\tau = (\hbar^2/4\omega_i\omega_j)[(v_i + 1/2)(v_j + 1/2)], \quad i=1, \ j=3;$$
$$\int \Psi_k Q_i^4 \Psi_k^* d\tau = (\hbar^2/8\omega_i^2)[3(v_i + 1)^2 + (1 - \ell^2)], \quad i = 2;$$
$$\int \Psi_k Q_i^2 Q_j^2 \Psi_k^* d\tau = (\hbar^2/4\omega_i\omega_j)[(v_i + 1/2)(v_j + 1)], \quad i=1,3 \ , \ j=2. \tag{2-18}$$

The result of the application of the second-order perturbation treatment gives energy corrections of the form:

$$W_k'' = \sum_{k' \neq k} [\int \Psi_k H' \Psi_k^* d\tau \int \Psi_k H' \Psi_k^* d\tau / (E_{k'}^o - E_k^o)]. \tag{2-19}$$

Nielsen (64) has shown that the evaluation of all these terms results in quadratic functions of $(v_i + d_i/2)$. Thus to a satisfactory degree of approximation, we can utilize an equation of the form given below to represent the vibrational energy of a molecule such as cyanate ion:

$$W = \sum_1^3 \omega_k(v_k + d_k/2) + \sum_{11}^{33} x_{k\ell} (v_\ell + d_\ell/2)(v_k + d_k/2) + g_{22}\ell^2, \tag{2-20}$$

where $v = 0,1,2,\ldots$, $\ell = 0,1,\ldots$, ω_k and $x_{\ell k}$ are called spectroscopic constants-the former are harmonic frequencies and the latter are anharmonicity constants. The energy equation may be fitted to the data by appropriate refinement techniques, and is commonly expanded with the zero level energies subtracted to give the following equation representing the observed transition in cm^{-1}:

$$[G_{v_1v_2v_3} - G_{000}] = \omega_1^o v_1 + \omega_2^o v_2 + \omega_3^o v_3 + x_{11}v_1^2 + x_{22}v_2^2 + x_{33}v_3^2 + x_{12}v_1v_2 + x_{13}v_1v_3 + x_{23}v_2v_3 + g_{22}\ell_2^2 \ . \tag{2-21}$$

Where the zero order harmonic frequencies, ω_k, are determined using the relations below:

$$\omega_k = \omega_k^{\circ} - x_{kk}d_k - (1/2) \sum_{k' \neq k} x_{kk'}d_{k'} \cdot \qquad (2\text{-}22)$$

The d_k is the degeneracy associated with the k^{th} mode, and v is a vibrational quantum number.

The anharmonicity constants can be related to the cubic and quartic coordinate potential constants. Nielsen's (63,64) results are shown in Appendix One.

The arguments thus far presented are adequate to describe the linear triatomic molecule in an isolated environment. We shall now consider effects on the cyanate's vibrational spectra caused by cyanate impurity in alkali halide lattices. Thus far all resonance interactions have been neglected. These will be dealt with in the chapter on Fermi resonance.

In the "isolated model" situation, the triatomic molecule is assumed free of external forces. After making corrections for Fermi interactions, Maki and Decius (56) found that the wealth of observed frequencies could be fitted to equation 2-21 with high degrees of agreement. This points to the likelihood that the external field of the crystal matrix is symmetrically disposed toward the impurity ion, with little dynamic coupling. This argument is supported by the observation that the doubly degenerate ν_2 is not split by the alkali halide environment. A similiar situation has been shown to exist for azide ion (N_3^-) by Turrell and Bryant (7). From steric considerations, the 111 (body diagonal) direction which has C_{3_v} symmetry seems intuitively preferable to the 100 direction which has C_{4_v} symmetry (19,p.2180). The overtone levels should provide the answer. $2\nu_2^{\ell}$ generates symmetry species $A_1(\ell=0)$ and E ($\ell=2$) for C_{3_v} species and A_1 ($\ell=0$), and B_1+B_2 for C_{4_v}. The selection rules permit the transition to both components in the

C_{3_v} case, but only the A_1 species in the C_{4_v} case. A transition to the 02^20 from the ground state has not been observed. The selection rule $\Delta\ell = 0, \pm 1$ for linear molecules has not been violated. While the lack of the 02^20 transition could be evidence for the C_{4_v} orientation, the C_{3_v} is preferred.

TABLE 2-1. CYANATE ION FUNDAMENTALS IN ALKALI HALIDE LATTICES.[-1]

Mode	KCl (3.14)		KBr (3.29)		KI (3.53)	
(cm^{-1})	NCO^-	$N^{13}CO^-$	NCO^-	$N^{13}CO^-$	NCO^-	$N^{13}CO^-$
ν_2^1	631.00	613.20	629.40	612.20	628.0	609.95
ν_1	1210.7	1195.2	1205.50	1191.0	1200.8	
$2\nu_2$	1297.3	1277.4	1292.60	1272.5	1288.0	1266.6
ν_3	2181.80	2124.70	2169.60	2112.80	2155.8	2099.05

When the cyanate is dissolved in the alkali melt which is subsequently crystalized, it is essentially isolated from other cyanate ions. In addition, it has been shown that the effect of neighboring cyanate ions is manifest not in observable frequency shifts of the fundamentals but in appearance of satellite peaks about the fundamental. Various concentrations of cyanate doped alkali halide crystals have produced no observable shift in fundamental frequencies. The intensities of these satellites have been found to be roughly quadraticly dependent upon concentration (19,p.2183) and the origin of the satellite shift is concluded to be site effect rather than a dynamic coupling.

-1 ν_1^o is not observed directly because of Fermi resonance. Values reported here were a result of this work (except for the KI frequencies (54). The lattice dimension "a" is shown in parentheses in Angstroms.

Table 2-1 shows the effect of changing lattices upon the various frequencies of the cyanate ion. It is seen, that as expected, the bending mode is least affected and the asymmetric stretch, ν_3 is shifted the most. The frequencies are seen to decrease as the lattice dimensions increase. Table 2-2 shows how the valence force constants change with lattice change.

TABLE 2-2. VALENCE FORCE CONSTANT CHANGE WITH CHANGE HOST LATTICE (84,p.21).

Constant	KCl	KBr	KI
f_{NC} (md/Å)	15.42	15.28	15.14
f_{CO} (md/Å)	11.46	11.34	11.21
f_{NC-CO} (md/Å)	1.15	1.16	1.18
f_{α} (10^{-11}erg/rad^2)	0.740	0.735	0.732

Long range forces operating on the impurity ion must be considered in assessing lattice effects on the frequencies of the cyanate ion. Since the inclusion of dilute cyanate ion in the crystal lattice at halide sites produces no large distortions of its cubic symmetry, ion-dipole interaction and other lower order interaction terms in the intermolecular potential energy vanish (by symmetry). The dipole-induced dipole term will have the most significant effect on vibrational frequency. The other long range effects, such as van der Waals and London (dispersion) forces do not give rise to as great a second derivative with respect to the normal coordinate as does the electrostatic term. Maki and Decius (56, p.781) have shown quantitatively that these forces do not contribute to an increase in frequency as the lattice dimensions decrease. The repulsive forces between the neighboring halide electron cloud and the cyanate ion cloud will affect the force

constants which in turn affect the frequency(see Table 2-2). Temperature effects on observed frequencies support this view. The frequency of ν_3 increases about one wave number for each 100°K reduction in temperature (56, p.781) and the lattice dimension decreases.

This chapter has attempted to show a good approximate model for the cyanate ion in an alkali halide lattice can be thought of as a linear triatomic gas in an approximate non-interacting medium. This enables us to adopt equation 2-21 as a vibrational energy equation. By its application to the observable frequencies of NCO^-, we may deduce the anharmonicity constants. Through this process the spectra of cyanate ion may be described. This treatment does suffer from the fallacy that the combination bands between ν_3 and lattice modes are observed in KBr and KI matrices and can not be predicted by our approximation. Other limitations of equation 2-21 will be discussed in Chapter Seven. We shall now proceed with a discussion of Fermi resonance.

CHAPTER 3

FERMI RESONANCE

BACKGROUND

A common occurrence in the vibrational spectra of triatomic molecules is the phenomenon of Fermi resonance. This particular type of "accidental" degeneracy was first brought to light during Raman work on carbon dioxide by Fermi in 1931 (26,p.250-259). Fermi presented arguments using resonance between two quanta of bending and one quantum of symmetric stretching vibration to explain the two strong Raman lines at 1388 cm^{-1} and 1285 cm^{-1} where only one strong band would have been expected. The latter was to have been attributed to the symmetric stretching mode.

Further work by Adel and Dennison (2,p.716-723) and later by Dennison (21,p.175-214) has provided more thorough elucidation of this phenomenon. Dennison's treatment is most commonly used in the literature as a basis for describing Fermi resonance as work on carbon dioxide continues. Amat and Pimbert (3,p.278-290), using the high resolution data of Courtoy (12) have further presented enlightening contributions to the description of Fermi resonance effects on rotational constants and band assignments. Further works by Gordon and McCubbin (28,p.137-154), Berney and Eggers (5), and Pariseau, Suzuki and Overend (73) demonstrated that the final word on Fermi resonance in carbon dioxide has yet to be said.

The Fermi resonance of N_2O has also been studied extensively. The variation of results obtained by Rao and Nielsen (80,p.1147-1152) as compared with Mantz, et al. (57,p.513-530) and Suzuki (89, p.54-73) clearly demonstrates the sensitivity of resonance to experimental results and isotopic substitution.

Carbon dioxide and nitrous oxide have been mentioned above because they are isoelectronic with cyanate ion which also exhibits strong Fermi resonance. Fermi resonance in the cyanate ion vibrational spectrum was first observed using infrared spectroscopy by Maki and Decius (55,56). Maki's original work (54,p.35-40) was extended by Decius and Gordon (18,p.1286-1288) and Schettino and Hisatune (84). These researchers studied cyanate ion in an alkali halide crystal environment. Dixon (22,p.258-260, and 23,p.165-192) has studied the free radical cyanate "gas" produced by flash photolysis of HCNO in various inert gas matrices. Recently, Milligan and Jacox (61) have extended this free radical cyanate study. Their observations on the cyanate radical were directly made with infrared and ultraviolet spectrometers.

FERMI RESONANCE THEORY

The following treatment parallels that originally given by Dennison as generalized by H. Nielsen (64,p.126-129) and simplified by Herzberg (33,p.215-217).

Fermi resonance occurs in polyatomic molecules when vibrational levels have nearly equal energy. This "accidental degeneracy" can also be thought of as an interaction or coupling of normal modes or mixing of states. Physically, this results in spectral bands separated by greater energy than would be predicted from zero order normal frequencies. This perturbation of energy levels is usually attributed to the anharmonic terms in the potential energy expansion which couple the normal coordinates and contribute significantly to the potential function.

The magnitude of the interaction depends upon the unperturbed energy difference and upon the matrix element describing the interaction, H_{ni}:

$$H_{ni} = \int \Psi_n^{o} W_{ni} \Psi_i^{o*} d\tau \qquad (3\text{-}1)$$

where W_{ni} represents the anharmonic terms coupling the Ψ_v^o's which are the zero order harmonic oscillator combination wave functions describing the two interacting levels. An important consequence of this approach is that the Ψ_v^o's must be of the same symmetry to make the integral non-vanishing because W_{ni} must be totally symmetric. Thus only vibrational levels of the same symmetry species can perturb one another causing Fermi resonance.

A resonable approximation of the magnitude of the energy shift can be calculated from the secular determinant of the form:

$$\begin{vmatrix} \nu_n^{o} - W & H_{ni} \\ H_{ni} & \nu_i^{o} - W \end{vmatrix} = 0 \qquad (3\text{-}2)$$

which is a description of the phenomenom depicted in Figure 3-1.

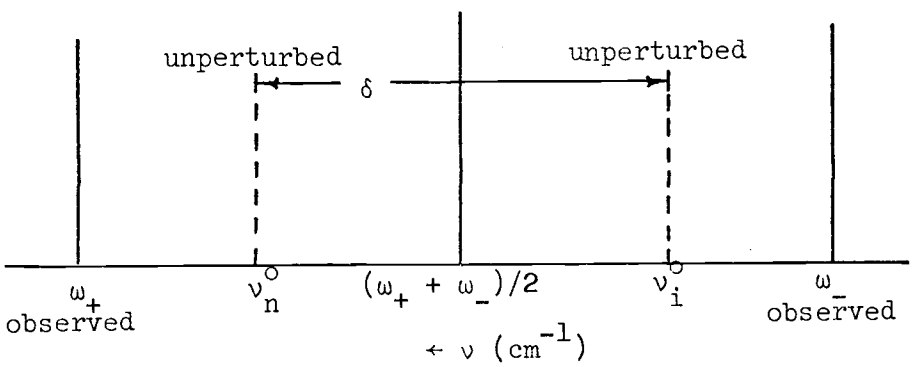

Figure 3-1. Diagram of Fermi resonance.

The resulting energies upon solution of equation 3-2 are:

$$\omega_{\pm} = [(\nu_n^{o} + \nu_i^{o})/2] \pm [\, 4|H_{ni}|^2 + (\nu_n^{o} - \nu_i^{o})^2]^{1/2}/2$$

$$\omega_{\pm} = \overline{\nu}^{o}_{ni} \pm (1/2)[4|H_{ni}|^2 + \delta^2]^{1/2}, \text{ or}$$

$$\omega_{\pm} = \overline{\nu}^{o}_{ni} \pm (1/2)\,\Delta\ . \qquad (3\text{-}3)$$

The eigenvalues of the W_{ni} states are represented as mixtures of the unperturbed eigenfunctions, Ψ_1^o and Ψ_2^o:

$$\Psi_+ = c_1\Psi_1^o + c_2\Psi_2^o\ , \text{ and } \quad \Psi_- = c_2\Psi_1^o - c_1\Psi_2^o\ , \text{ where}$$

$$c_1 = \left(\frac{\Delta + \delta}{2\Delta}\right)^{1/2}\ , \text{ and } \quad c_2 = \left(\frac{\Delta - \delta}{2\Delta}\right)^{1/2} \qquad (3\text{-}4)$$

From equation 3-4 it can be seen that: if $\delta = 0$, $c_1 = c_2$ and the states are equally mixed; and, if δ is very large, $c_1 \to 1$, and $c_2 \to 0$, and the resonance disappears.

Up to this point we have centered our discussion on the Fermi diad. The arguments above are commonly extended to higher multiplets. These will be discussed in the section on Fermi resonance in the cyanate ion.

The intensity of a spectroscopic transition, I_{ni}, is dependent upon a population factor, a frequency factor, and the square of the appropriate transition moment (22, p.259). Discounting all factors except the transition moment, we may write:

$$I_{ni} \propto [\int \Psi_n\, f(q_1 q_2 \ldots)\, \Psi_i^*\, d\tau\ ]^2 \qquad (3\text{-}5)$$

Then if two bands occur from a common unperturbed energy level, Ψ_{000}, the intensities can be expressed using equation 3-4 in the following way:

$$I_n \propto [c_1 \int \Psi_n f(q_1 q_2 \ldots) \Psi^*_{000} \, d\tau - c_2 \int \Psi_i f(q_1 q_2 \ldots) \Psi^*_{000} \, d\tau]^2$$

$$I_i \propto [c_2 \int \Psi_n f(q_1 q_2 \ldots) \Psi^*_{000} \, d\tau + c_1 \int \Psi_i f(q_1 q_2 \ldots) \Psi^*_{000} \, d\tau]^2$$

with the same constants of proportionality, or

$$I_n \propto [c_1(I^o_{no}) - c_2(I^o_{io})]^2, \text{ and}$$

$$I_i \propto [c_2(I^o_{no}) + c_1(I^o_{io})]^2. \qquad (3\text{-}6)$$

If the transition from o → n has negligible intensity compared with o → i, then equations in 3-6 taken as ratios yield:

$$\frac{I_n}{I_i} = \frac{c_2^2}{c_1^2} = \frac{\Delta - \delta}{2\Delta} \frac{2\Delta}{\Delta + \delta} = \frac{\Delta - \delta}{\Delta + \delta} \qquad (3\text{-}7)$$

This, perhaps oversimplified argument shows that even when one of the diad member intensity is expected to be small, it still contributes considerably to the intensity of a given member of the diad. More generally, if the o → n integral has a value μ times the o → i integral, the ratio of the observed fundamental's intensities becomes:

$$I_n / I_i = [(c_1\mu - c_2)/(c_2\mu + c_1)]^2. \qquad (3\text{-}8)$$

The H_{ni} term in equation 3-2 has been evaluated by Maki and Decius(56, p.778) for the diad and is given below:

$$W_{v_1 v_2^{\ell} v_3;\ v_1-1,\ v_2^{\ell}+2,\ v_3} = k_{122} \int \Psi_n Q_1 Q_2^2 \Psi_i^* \, d\tau$$

$$= (\hbar^3/64\omega_1\omega_2^2)^{1/2} k_{122} \sqrt{v_1} [(v_2 + 2)^2 - \ell^2]^{1/2} . \qquad (3\text{-}9)$$

where k_{122} is the potential energy constant and Ψ_α are harmonic oscillator wave functions. For the triad, a similar operation shows that equation 3-9 gives the off-diagonal terms, and all other off-diagonal terms vanish.

Throughout the above treatment we have neglected a possible coupling of the asymmetric stretch with the bending overtone. Such an interaction is permitted since Q_3 belongs to a symmetric species. Inclusion of the cubic terms of the type $k_{322} Q_3 Q_2^2$ in the calculation constitutes a refinement of the resonance description. Lide (48,p.451) points out that the $00^0 1$ level, which is connected through the k_{322} potential constant, should be included in secular equation of the type:

$$\begin{vmatrix} \nu_n^{\,o} - \omega & H_{ni} & 0 \\ H_{ni} & \nu_i - \omega & H_{ij} \\ 0 & H_{ij} & \nu_j^{\,o} - \omega \end{vmatrix} = 0. \qquad (3\text{-}10)$$

However it can be shown that owing to the large energy separation (usually 1000 cm^{-1}) between the ($02^0 0$, $10^0 0$) level and the $00^0 1$ level, the H_{ij} do not enter into calculation significantly. This suggests that equation 3-10 should not be significant for diad type resonances. In the normal coordinate potential function developed previously, the Fermi resonance coupling constant, k_{122} does include a contribution from both the internal coordinate constants K_{122} and K_{322}. Reichman and Overend have demonstrated this point analytically (83,p.1527). The method presented in Chapter Seven for handling the k_{322} effects on the diad resonance, treats its minor effect on the ω_1 on ω_3 (harmonic frequencies) as a perturbation. The k_{322} term is significant when higher multiplets are analyzed and is usually considered explicitly.

FERMI RESONANCE IN THE CYANATE ION

Fermi resonance occurs in the cyanate ion between the overtones of the bending vibration and the stretching modes. As in carbon dioxide and nitrous oxide, there is a very close resonance between energy levels 10^00 and 02^00 since $2\nu_2^o$ happens to be nearly equal to ν_1^o. Depending upon the isotopic constitution of the cyanate ion, and the alkali halide matrix in which it is studied, the doubly degenerate bending vibration, ν_2, is observed between 600 and 635 cm^{-1} and the symmetric stretch fundamental, ν_1^o, which, because of the strong Fermi interaction, is not observed directly and is located between 1150 and 1300 cm^{-1}.

As the result of this close resonance, there are perturbations between certain higher vibrational levels (e.g. 10^01 and 02^01 levels). Fermi resonance is also observed between combination and overtone bands producing multiplets (e.g. 04^00, 12^00, 20^00) and from thermally excited states (e.g. transition from $01^10 \rightarrow \{03^10, 11^10\}$ levels).

TABLE 3-1. FERMI MULTIPLETS AND NORMAL CYANATE ION IN KBR.

Initial State	Multiplet State	Observed Frequencies (cm^{-1})
02^20	$\{11^10, 03^10\}$ diad	557.9, 679.6
01^10	$\{10^00, 02^00\}$ diad	576.3, 663.4
00^00	$\{10^00, 02^00\}$ diad	1205.5, 1292.6
01^10	$\{11^10, 03^10\}$ diad	1188.1, 1309.1
02^20	$\{12^20, 04^20\}$ diad	1175.5, 1320.4
00^00	$\{10^01, 02^01\}$ diad	3355.0, 3442.2
01^10	$\{11^11, 03^11\}$ diad	3325.7
00^00	$\{20^00, 12^00, 04^00\}$ triad	2392.9, 2487.3, 2602.5
01^10	$\{21^10, 13^10, 05^10\}$ triad	2628.3
00^00	$\{04^01, 12^01, 20^01\}$ triad	4524.5, 4623.0, 4737.5
00^00	$\{30^00, 22^00, 14^00, 06^00\}$ tetrad	3893, 3781.6, 3674.2, 3562.8
01^10	$\{03^10, 11^10\}$ diad	1817.2, 1938.6

Fermi resonance affects most of the bands observed for any given isotopic species of cyanate ion. Table 3-1 shows Fermi multiplets which Decius, et al. observed for $^{14}N^{12}C^{16}O^-$ cyanate ion in KBr. (19, 56) There are only seven transitions not involved directly in this phenomenon which have been observed. These are listed in Table 3-2.

TABLE 3-2. NON-FERMI BANDS FOR NORMAL CYANATE ION IN KBR[-2]

Initial State	Final State	Frequency (cm^{-1})
00^00	01^10	629.4
00^00	00^01	2169.6
00^00	01^11	2788.1
01^10	02^21	2776.6
01^10	01^11	2158.6
02^20	02^21	2147.9
00^00	00^02	4318

[-2] All of the frequencies listed in this table were observed by Maki and Decius (56, p.774) except for the last entry which was discovered during this research.

CHAPTER 4

THE ISOTOPE EFFECT

Cyanate ion, with the atoms $^{14}N^{12}C^{16}O$, has received the most attention studied in KBr matrices. In addition to the vibrational spectrum of this "normal" form, several peaks attributed to other isotopes have been observed. The abundance of ^{13}C isotope in naturally occuring carbon is about 1.11%, that of ^{15}N isotope in nitrogen is 0.37%, and of ^{18}O in oxygen is 0.20%. In Table 4-1, the fundamental frequencies attributed to these substitutions in cyanate ion (in KBr) are shown. The frequency values shown were determined in this work; those having an asterisk were also observed by Maki and Decius (56). Their assignments have been confirmed with one exception in this work.[-3] The most striking frequency shift occurs when the heavier ^{13}C is substituted into cyanate. The most apparent observation is that if the mass is increased, the frequency of the mode decreases as would be expected from a harmonic-like vibration. The mathematical relationships are however, involved, as we shall see.

[-3] The referenced work mistakenly assigned a peak at 1188.9 cm^{-1} to $^{15}N^{12}C^{16}O$. Enrichment studies in this work have demonstrated the $^{15}N^{12}C^{16}O$ peak in that region to be at 1191.28 cm^{-1}.

TABLE 4-1. VIBRATIONAL FUNDAMENTALS OF ISOTOPIC FORMS OF CYANATE ION IN KBR.[-4]

Cyanate Ion					
N	C	O^-	$\{\nu_1, 2\nu_2\}(cm^{-1})$	$\nu_2(cm^{-1})$	$\nu_3\ (cm^{-1})$
14	12	16	1205.47, 1292.57	629.40	2169.60
14	13	16	1191.00, 1271.10*	611.9*	2112.74*
15	12	16	1191.28, 1282.33*	625.87*	2153.00*
15	13	16	1180.02, 1259.70	608.95	2094.76*
14	12	18	1176.37, 1272.95	624.72*	2161.66*
14	13	18	1166.5, 1247.59	607.8	2104.33

THE ISOTOPE EFFECT

In the theoretical treatment thus far, it has been demonstrated that the coefficients of the normal coordinates contain mass weighting, and that the Q's are complicated combinations of the intermolecular displacements. It is usually assumed that isotopic molecules have the same electronic structure for a given electronic level. This suggests, that to a very high order of approximation,[-5] the potential function governing the vibrational motion of the nucleii should be the same for different isotopic polyatomic species (33, p.227). The mass differences are manifested by changes in vibrational frequencies.

A meaningful method of describing these effects is complicated in the normal coordinate scheme, as those force constants are not easily relatable to atom-atom interactions. For this reason external symmetry coordinates will be introduced. (For a description of these coordinates, see reference 95,p.113ff.)

[-4] Isotopic peaks observed by Maki (54) and confirmed by enrichment studies in this paper are followed by an asterisk.

[-5] These approximations really depend on the Born-Oppenheimer separation of electronic and nuclear coordinates. The force constants are theoretically dependent on the equations for electronic motion involving charges and geometry of the nucleii only.

In terms of these coordinates, S_k, and their conjugate momenta P_k the kinetic energy, T, and the potential energy, V, are:

$$T = 1/2 \sum_k G_{kk} P_k^2 \quad \text{and} \quad V = 1/2 \sum_{kl} F_{kl} S_k S_l \quad . \tag{4-1}$$

The F_{kl} and G_{kk} are the matrix elements of the F and G matrices with the G matrix in diagonal form, each diagonal being the reciprocal mass, μ_k, of one atom of a single equivalent set. If this holds, then:

$$\det FG = |F| \prod_k \mu_k = \prod_k \lambda_k \quad ; \tag{4-2}$$

where λ_k are equal to $4\pi^2 c^2 \omega_k^2$. The F matrix is invariant to isotopic effects, then:

$$\frac{\prod_i \mu_i}{\prod_i \mu_i^*} = \frac{\prod_i \lambda_i}{\prod_i \lambda_i^*} = \frac{\prod_i \omega_i^2}{\prod_i (\omega_i^*)^2} = \frac{\prod_i m_i^*}{\prod_i m_i} \quad , \tag{4-3}$$

where the (*) designates the istopicly substituted species. This result holds if the symmetry species contain no translation or rotation. Our external symmetry coordinates contain these motions which make some of the λ_i=0. To overcome this problem, we assume that weak forces convert translation and rotation to low frequency oscillations. As these forces vanish under which conditions, internal mode couplings vanish, the ratio for the rotational and translational frequencies is given by:

$$\frac{\omega_{tr}^*}{\omega_{tr}} = \left(\frac{M}{M^*} \right)^{1/2} \quad , \quad \text{and} \quad \frac{\omega_{rot}}{\omega_{rot}^*} = \left(\frac{I}{I^*} \right)^{1/2}, \tag{4-4}$$

where I is the equilibrium moment of inertia with respect to a principle axis of rotation associated with the motion(species) under consideration (62, p.456), and M is the total mass of the molecule. Substituting the results of equation 4-4 into equation 4-3 for the vibrational and rotational frequencies, gives the following equation:

$$\prod_{k=1}^{3n-6(5)} \frac{\omega_k^*}{\omega_k} = \prod_{i}^{3n} \left(\frac{m_i}{m_i^*}\right)^{1/2} \left(\frac{M^*}{M}\right)^{\alpha/2} \left(\frac{I_x^* I_y^* I_z^*}{I_x I_y I_z}\right)^{\beta/2},$$

which is the Redlich-Teller Frequency Product Rule(95, p.183). For a linear molecule, this equation becomes:

$$\prod_{k=1}^{3n-5} \frac{\omega_k^*}{\omega_k} = \prod_{i}^{3n} \left(\frac{m_i}{m_i^*}\right)^{1/2} \left(\frac{M^*}{M}\right)^{\alpha/2} \left(\frac{I^*}{I}\right)^{\beta/2} . \qquad (4\text{-}5)$$

In a linear molecule, $I_x = I_y$ and I_z doesn't exist. In equation 4-5, α and β are 1 or 0 depending upon whether or not the rotation belongs to the symmetry type frequency product under consideration. This rule holds for modes of the same symmetry type. The Product Rule will theoretically hold rigorously for observed frequencies of infinitesimal displacement, but anharmonicity makes it only approximate for a given molecule (as higher than quadratic terms in the potential energy must be considered). In cyanate ion, isotopic substitution does not change the molecular symmetry, and approximate calculations based on this rule are relatively simple and should be quite accurate for cyanate fundamentals. In the linear XYZ molecule, the stretches are Σ(symmetry), and the bending mode is a Π species.

The product rule applicable to the Σ fundamentals is given by equation 4-6.

$$\frac{\omega_1^*\omega_3^*}{\omega_1\omega_3} = \left[\left(\frac{m_x m_y m_z}{m_x^* m_y^* m_z^*}\right)\left(\frac{M^*}{M}\right)\right]^{1/2} \qquad (4\text{-}6)$$

The α in equation 1-5 for $C_{\infty v}$ (see Appendix Three) is equal to one because the T_z (translation) belongs to the Σ species while the $\beta = 0$, because I_z doesn't exist. The Πvibrations obey the relationship:

$$\frac{\omega_2^*}{\omega_2} = \left[(m_x m_y m_z / m_x^* m_y^* m_z^*)(M^*/M)(I^*/I)\right]^{1/2}. \qquad (4\text{-}7)$$

Here it is seen that $\alpha = \beta = 1$. This occurs because $T_x = T_y$, and $R_x = R_y$ are degenerate modes and are only counted once as only a single non-genuine frequency may contribute to the product.

The linear XYZ molecule isotopic relations can be derived in another interesting and equivalent manner, without assuming the non-genuine vanishing normal frequencies. The G matrix for this molecule, in internal coordinates is(15, 25):

$$G = \begin{bmatrix} \mu_x + \mu_y & -\mu_y & 00 \\ -\mu_y & \mu_y + \mu_z & 00 \\ 00 & 00 & (1/r_{xy}^2)\mu_x + (1/r_{yz}^2)\mu_z + (r_{xy}^{-1} + r_{yz}^{-1})^2\mu_y \end{bmatrix}$$

Then applying the process outlined by equation 4-2 (and assuming the corresponding F matrix to be invarient), we get two factored equations:

$$\det FG = |F|\,[\mu_x\mu_y + \mu_y\mu_z + \mu_z\mu_x] = \prod_i \omega^2_k \quad , \text{ and}$$

$$\det FG = |F|[(1/r_{xy}^2)\mu_x + (1/r_{yz}^2)\mu_z + (r_{xy}^{-1} + r_{yz}^{-1})^2\mu_y] = \Pi\omega_k' \cdot$$

Forming the appropriate ratio yields

$$(\omega_1^*\omega_3^*/\omega_1\omega_3) = [(\mu_x^*\mu_y^* + \mu_y^*\mu_z^* + \mu_x^*\mu_z^*)/(\mu_x\mu_y + \mu_y\mu_z + \mu_x\mu_z)]^{1/2}$$

for the two Σ species, and

$$\omega_2^*/\omega_2 = \{[\mu_z^* + \rho^2\mu_x^* + \mu_y^*(1 + \rho)^2]/[\mu_z + \rho^2\mu_x + \mu_y(1+ \rho)^2]\}^{1/2}$$

for the bend. In these formulas $\mu_i = m_i^{-1}$ and $\rho = r_{xy}/r_{yz}$. These latter two equations developed above are exactly equivalent to equations 4-6 and 4-7. Although the equations are strictly rigorous for zero-order harmonic frequencies, they apply to the observed fundamentals for cyanate ion to within 0.5 cm^{-1}, as will be demonstrated in Chapter Six. We should also be able to predict the direction of the deviation when the observed ν_i^o are used. For a heavier isotope, the anharmonicity constants, x_{ij}^*, are smaller than the x_{ij}, and thus $\omega_i^* - \nu_i^*$ is less than $\omega_i - \nu_i$. Then the product $\prod_i \nu_i^* / \prod_i \nu_i$ should be greater than the right hand side of equation 4-3.

Darling and Dennison(14) found that the anharmonicity constants could be related by the expression:

$$x_{ij}^* = (\omega_i^*\omega_j^* / \omega_i\omega_j)\, x_{ij} \qquad (4\text{-}8)$$

to a good approximation. This latter expression is empirical but very accurate. Another empirical isotope rule, proposed by Noether(65), suggests the following relationship:

$$\frac{\nu_k(xy^*z)}{\nu_k(xyz)} = \frac{\nu_k(xy^*z)}{\nu_k(xyz^*)} \qquad (4\text{-}9)$$

which should prove useful for the disubstituted cyanate fundamentals. Now let us turn from isotope frequency effects to intensity phenomena.

The intensity of the infrared transition depends on the change in dipole moment, $\vec{\mu}$, with respect to the normal coordinate associated with the mode of the vibration under consideration. An integrated intensity for the k^{th} fundamental can be expressed as:

$I_k \propto (\partial\vec{\mu}/\partial Q_k)_o(\partial\vec{\mu}/\partial Q_{k'})_o$, which can be transformed to

symmetry coordinates ($S_k = \Sigma L_{k'k} Q_k$) to the form:

$$I_k \propto \sum_{k'} \sum_{k''} (\partial\vec{\mu}/\partial S_{k'})(\partial\vec{\mu}/\partial S_{k''}) L_{k'k} L_{k''k} \quad . \qquad (4\text{-}10)$$

These transformation coefficients are related to the G matrix (95, p.191-192) which are in turn related to the masses of the atoms. Thus for a given change in isotope in a polyatomic molecule, the intensity of a transition should change also. This assumes that the dipole moment changes. Figure 4-1 shows a view of the bending mode of cyanate ion demonstrating this.

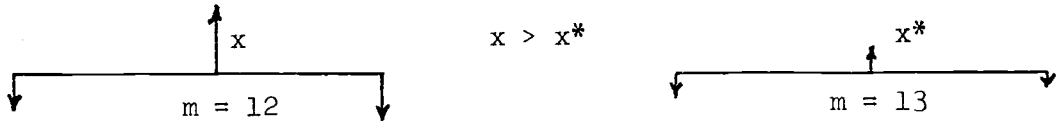

Figure 4-1. Schematic ν_2 representation of the dipole moment change of ^{12}C versus ^{13}C cyanate ion.

The amplitude of vibration for the heavier analogue will be less, hence the dipole moment will be smaller, and change less for the Q associated with the mode. This will be reflected in a decrease in intensity for bands involving the heavier isotope. This simple minded analogy is in agreement with the sum rule that $\Sigma I_k/\lambda_k$ is invariant for isotopic vibrations provided that the symmetry species over which the summation of intensities is carried out is not the same as that of any rotation of the molecule which moves the permanent dipole moment (13).

As a conclusion to this section, the isotope effect and Fermi resonance will be discussed. Maki and Decius (56) found the ^{13}C isotope effect on the Fermi splitting constant "b" ($k_{122}/\sqrt{2}$) to be -15%. Although the theory for unsymmetrical linear triatomic molecules is more complicated than for CO_2-like structures, it is expected that "b", which is proportioned to the coefficient of the cubic term $Q_1(Q_{21}+Q_{22})^2$ in the normal coordinate potential function, will be proportional to $G_1^{1/2}\ G_2$ in the G matrix. In CO_2, theory predicts a 3% decrease in "b" with ^{13}C atom substitution. Amat and Pimbert (3) suggested that the root of the problem was the assignment of $\nu_1^{\circ} > 2\nu_2^{\circ}$. The CO_2 problem was resolved with $2\nu_2^{\circ} > \nu_1^{\circ}$. The same has resulted for cyanate, if the higher member of the doublet is regarded as having mostly $2\nu_2^{\circ}$ character. As a result of the present study, the following results were obtained using rough data only (18).

Using the equations developed in the Fermi resonance section (equations 3-4 to 3-8) the coefficients of the functions:

$$\Psi_+ = c_1\Psi_1 + c_2\Psi_2 \qquad \text{and} \qquad \Psi_- = \pm(c_2\Psi_1 - c_1\Psi_2) \tag{4-11}$$

were calculated. Then the intensity ratios should be:

$$(I_+/I_-) = [(c_1 + c_2\mu)/(c_2 - c_1\mu)]^2, \text{ where } \mu = \mu_{000\rightarrow020}/\mu_{000\rightarrow100}. \quad (4\text{-}12)$$

TABLE 4-2. FREQUENCIES AND INTENSITIES OF INFRARED ABSORPTIONS OF CYANATE ION IN KBR AT LIQUID NITROGEN TEMPERATURE.

	$^{14}N^{12}C^{16}O^-$	$^{14}N^{13}C^{16}O^-$	$^{15}N^{12}C^{16}O^-$	$^{14}N^{12}C^{18}O^-$
ν_+	1293 (0.57)	1272 (0.69)	1282 (0.52)	1275 (0.44)
ν_-	1206 (0.43)	1191 (0.31)	1191 (0.48)	1176 (0.56)
$2\nu_2^{\circ}$	1260	1226	1253	1250
ν_1°	1239	1237	1220	1201
b	59.7	56.7	59.9	60.8

The ν_+ and ν_- are observables. The ν_1° and $2\nu_2^{\circ}$ were calculated using the harmonic approximation. The relative absorbances are shown in parentheses. Using the "b" of Table 4-2 and the relative absorbances, Table 4-3 is constructed, which is valid if $\mu \simeq 0.20$.

TABLE 4-3. MIXING OF STATES AND INTENSITIES FOR THE CYANATE ION FERMI DOUBLET FUNDAMENTAL IN KBR.

Parameter	$^{14}N^{12}C^{16}O^-$	$^{14}N^{13}C^{16}O^-$	$^{15}N^{12}C^{16}O^-$	$^{14}N^{12}C^{18}O^-$
c_1	0.62	0.75	0.56	0.50
c_2	0.79	0.66	0.83	0.86
$(I_+/I_-)_{calc}$	1.36	2.3	1.0	0.78
$(I_+/I_-)_{Obs}$	1.33 ± 0.1	2.2 ± 0.2	1.1 ± 0.1	0.8 ± 0.2

Hence, by using intensity data in consonance with Fermi resonance vibrational theory and isotopic substitution, an apparent anomaly was resolved.

Isotopic data also finds use in determining potential constants, as more fundamental frequencies lessen the need for simplifiying assumptions.

This section has presented basic concepts in the use of isotopic substitution in studying the cyanate ion. It has shown how assignments have been confirmed by enrichment studies and how basic structures can be elucidated using isotopes.

CHAPTER 5

EXPERIMENTAL

This chapter is divided into five sections and presents the experimental techniques and methods used during this research. After a few introductory remarks on the high temperature chemistry of the cyanate ion, the isotopic cyanate ion prepartions will be presented and discussed. Two basic techniques were utilized to prepare cyanate ion solid solutions in KCl and KBr. These will be discussed in the sections on pressed disk techniques and single crystal growth. The following section will briefly deal with the infrared instruments used to obtain the vibrational spectra of cyanate ion. The concluding section will briefly discuss calibration and error analysis.

It has been our experience that past cyanate chemical research has been deficient in presenting sufficient experimental detail to facilitate easy and consistent reproduction of results. With this in mind, this experimental section will attempt to provide all relevant data available.

BACKGROUND

The high temperature chemistry of cyanate has not been studied to any great extent. Hofmann, et al.(36, p.204-212) studied metal catalyzed oxidations of potassium cyanate in air at 400°C. These studies revealed that catalytic activity increased through the series Cu < Ni < Ag and that moist air increased the oxidation rate. Cyanate was found to react with water vapor to produce carbonate and ammonia gas. The ammonia reacted further to form nitrate ion. Maki (54, p.61-62) found that platinum could catalyze cyanate decomposition in KBr and KCl melts by atmospheric oxidation. He also

noted that the heavy metals in porcelain glaze acted in a similiar manner but at a reduced rate. Maki and Decius (56,p.773) observed carbonate, bicarbonate and nitrite as decomposition products at these temperatures. However Schettino and Hisatsune (84,p.13)reported large quantities of nitrate, and smaller amounts of nitrite, and carbon being produced when alkali halide pressed disks containing cyanate were heated slightly above 500°C for more than six hours in vacuo. Both of the above observations were encountered during this research, however, the production of impurities was desired to be minimal; hence conditions which would minimize carbonate, nitrate, bicarbonate, nitrite and carbon were utilized.

Cyanate has been found to undergo reduction to cyanide at high temperatures. Porterin's results (78,p.308-310) suggested that this reaction should be important at the temperatures used in this research. In contradiction to his indications, this reduction to cyanide was not encountered to any significant extent. Cyanate was quite commonly prepared via atmospheric oxidation of cyanide at many different atmospheric partial pressures of oxygen. Cyanate was heated in vacuo to ca 500°C with no increase in cyanide. And, cyanate was incorporated into alkali halides at their melting points under inert atmosphere with no significant production of alkali cyanide. The oxidative decomposition of cyanate is thus considered to be the dominant concern in the experimental procedures which will now be introduced.

ISOTOPIC CYANATE PREPARATIONS

The literature contains many methods by which alkali cyanates may be prepared. Haley and Lambooy (30,p.2926) obtained quantitative conversion of KCN to KNCO by aqueous alkaline oxidation with $KMNO_4$. Smith and Yates (87,p.6084) performed a similiar oxidation in cupric hydroxide. Waddington (91,p.2500) reacted anhydrous alkali bicarbonate with urea at elevated temperatures to obtain

cyanate. Dupree and Lindsey (24) have patented a process for obtaining metal cyanates by direct reaction of the respective metal with urea at temperatures above urea's melting point. Maki prepared cyanate (54,p.63-64) using a method devised by Cook and Robinson (11,p.1001-1005) in which cyanogen chloride is bubbled through alcoholic alkali hydroxide solutions, viz:

$$CNCl + KOH \rightarrow KNCO + KCl \qquad (5\text{-}1)$$

Maki (54,p.63) also demonstrated that cyanate could be prepared in closed tube oxidations of cyanide using lead dioxide at elevated temperatures. This result was also experienced by Wang and Fleischer (93,p.3874) during their tracer studies on ^{18}O in Ag_2O. Schettino and Hisatsune's cyanate preparations (84) utilized a solid state reaction between ammonium and carbonate ions to produce cyanates. Their procedures will be discussed in Chapter Eight.

In order to study the vibrational spectrum of cyanates, it is desirous to obtain cyanates as free from other impurities as possible. Aqueous methods are disadvantageous due to the presence of hydrolytic contamination products such as bicarbonate, carbonate, carbonate and ammonium ion (54,p.65). Prolonged high temperature preparations are not recommended due to cyanate decomposition and contamination by nitrates and nitrites (78).

Maki (54,p.64,65) found that cyanate is completely oxidized to carbonate and nitrite during single crystal growth in air. This led him to prepare cyanate by introducing cyanide into the alkali halide melt. He was compelled to grow these cyanate doped crystals quickly because of the rapid decomposition of the cyanate by the same atmospheric oxidation that produced it. His experiences suggested to us that direct atmospheric oxidation of isotopic cyanides should be feasible. The method also promised to be quick

and economical as only a few milligrams of isotopicly enriched cyanide needed to be used.

Preparation of Cyanate Enriched in Carbon-13 or Nitrogen-15.

Isomet Corporation 97 atom-percent nitrogen -15 enriched KCN and Eastman Kodak 61.9 atom-percent carbon -13 enriched KCN were used without further purification. Their infrared spectra did not show the presence of carbonate, bicarbonate or nitrite contamination nor any other contamination. The desired alkali halide salt was placed in a 1.9 cm (i.d.) X8cm vycor test tube and flushed with dry nitrogen with mild heating. The isotopic cyanide was quickly weighed and placed in a warm stoppered vial. Usually 0.5 weight percent (15 to 25mg) of cyanide was employed. When higher quantities of cyanate were desired, the nitrogen which served to dilute the atmospheric oxygen and hence retard the oxidation, was dispenced with, and a higher proportion of isotopic cyanide was used. In both cases, precautions were taken to exclude moisture, which promotes decomposition.

The salt was melted over a Fisher burner in a vycor tube. Upon removal of the flame, the cyanide was dumped in and the mass swirled quickly until the melt solidified. After the mass was cool, it was chipped out and ready for further alkali halide dilution or could be pressed into a pellet without further ado.

The cyanate prepared in this manner was always contaminated to some extent with carbonate, bicarbonate, unoxidized cyanide, and nitrite ion. However it was found that these contaminants with the exception of cyanide did not present any difficulty in the single crystal growing process which will be presented later in this chapter .

It was found that the level of contamination could be minimized by careful manipulation of the temperature and atmospheric

exposure of the melt. The procedure outlined above represents the most successful method. The contaminants, with the exception of the cyanide ion rarely appeared in single crystal doped with cyanate prepared in this fashion.

Preparation of Oxygen-18 Enriched Potassium Cyanate.

It was desired to prepare oxygen 18 enriched cyanate by the simplest and most expeditious means possible. It has previously been shown that cyanate could be produced by atmospheric oxidation of KCN. An inexpensive form of oxygen 18 enriched oxygen is the gas. Thus direct oxidation of the KCN in oxygen was studied and the results of this work are reported below. No attempt was made to determine the exact kinetics of the reaction, however a certain qualitative picture was obtained. The heterogeneous oxidation here reported does not preclude quantitative analysis but the study was not pursued to that extent.

Mallinckrodt (#6881) analytical grade potassium cyanide was used without further purification. Infrared analysis showed no detectable carbonate contamination. NCG-USP-grade oxygen of better than 99% purity by mass spectrometric analysis and YEDA (Rehovoth, Isreal) 93.5 atom-percent isotope eighteen enriched oxygen (batch #1841) were used in the oxidations.

The apparatus shown in Figure 5-1 was used after being out-gassed for a minimum of sixteen hours between runs.

Into a clean, dry, 12mm (i.d.) x30mm pyrex tube (Figure 5-1, H) was placed a charge of 7.8 to 15.4 millimoles KCN. The tube was placed in the apparatus and out-gassed at ca.100°-200°C for at least 15 hours. Bulb A was filled with four millimoles of oxygen, and isolated from the system.

The temperature of the tube was brought up to about 470°C in vacuo and held for at least 20 minutes or until the pressure in the

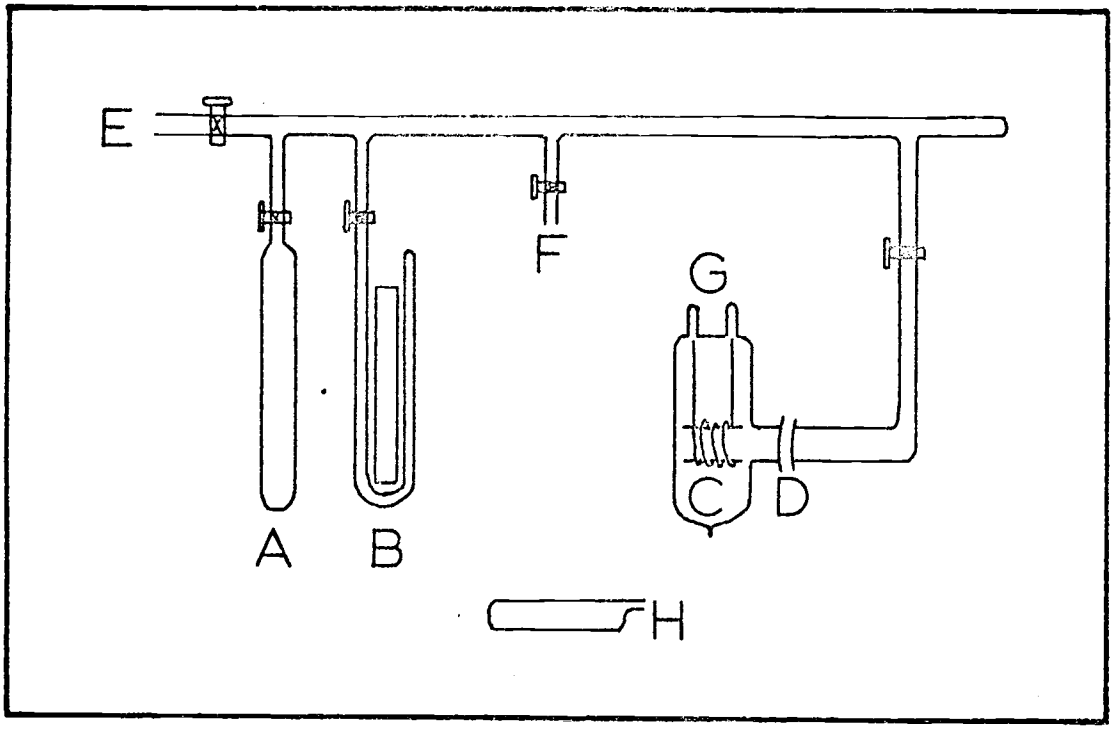

Figure 5-1. Reaction apparatus.

Bulb A is a 103ml volume. B is a manometer. C is the furnace constructed from a 100 watt Mazda airway beacon. The side arm is 35mm in diameter, and the total volume (including the side arm) is 500ml. The 35 ohm nichrome coil is wrapped around a 19mm vycor tube wrapped with asbestos. D is a 35/25 S_J ball and socket joint. E goes to the vacuum system. F is an accessory outlet used for mass spectrometric sampling. G are the electrical heater terminals; amperage to the furnace is regulated by a variac. H shows the reaction vessel which contains the reaction's solid, (not to scale).

system was undetectable; then the system was isolated from the pump. At this time oxygen was allowed to expand from bulb A into the system and the reaction commenced. Figure 5-2 shows a typical reaction curve using the above procedure.

The pressure drop in the system indicates that the reaction proceeds smoothly at the suggested temperature. Initially the cyanide is solid; as the reaction proceeds, a liquid phase forms after 300-500 minutes, and the tube contains melt. This is presumably a solution of cyanate, cyanide, and carbonate, the cyanide being in excess. The reaction will not go below 450°C to any detectable extent. Figure 5-2 shows a typical reaction curve demonstrating that the initial uptake of oxygen was rapid.

Analysis of the gas left in the system after the reaction was complete by mass spectrometric techniques, demonstrates beyond any doubt that carbon dioxide and nitrogen are produced in equimolar quantities. Infrared analysis shows that the production of carbonate is greater as higher reaction temperatures are used. From semi-quantitative intensity work it was found that roughly 20-30 percent of the solid reaction product is carbonate. Figure 5-3 shows the results of mass spectrometric analysis for the unreacted $^{18}O_2$ as the reaction shown in Figure 5-2 proceeded. Also, no species other than carbonate, cyanide and cyanate were detected in the product. A separate experiment showed that cyanate, at the temperature of the reaction and in the absence of oxygen did not decompose to any appreciable extent.

The reaction exhibits the following stoichiometry based upon the above observations:

$$2\ KCN + O_2 = 2\ KNCO \qquad (5\text{-}2)$$

$$4\ KNCO + 3\ O_2 = 2\ N_2 + 2\ CO_2 + 2\ K_2CO_3 \qquad (5\text{-}3)$$

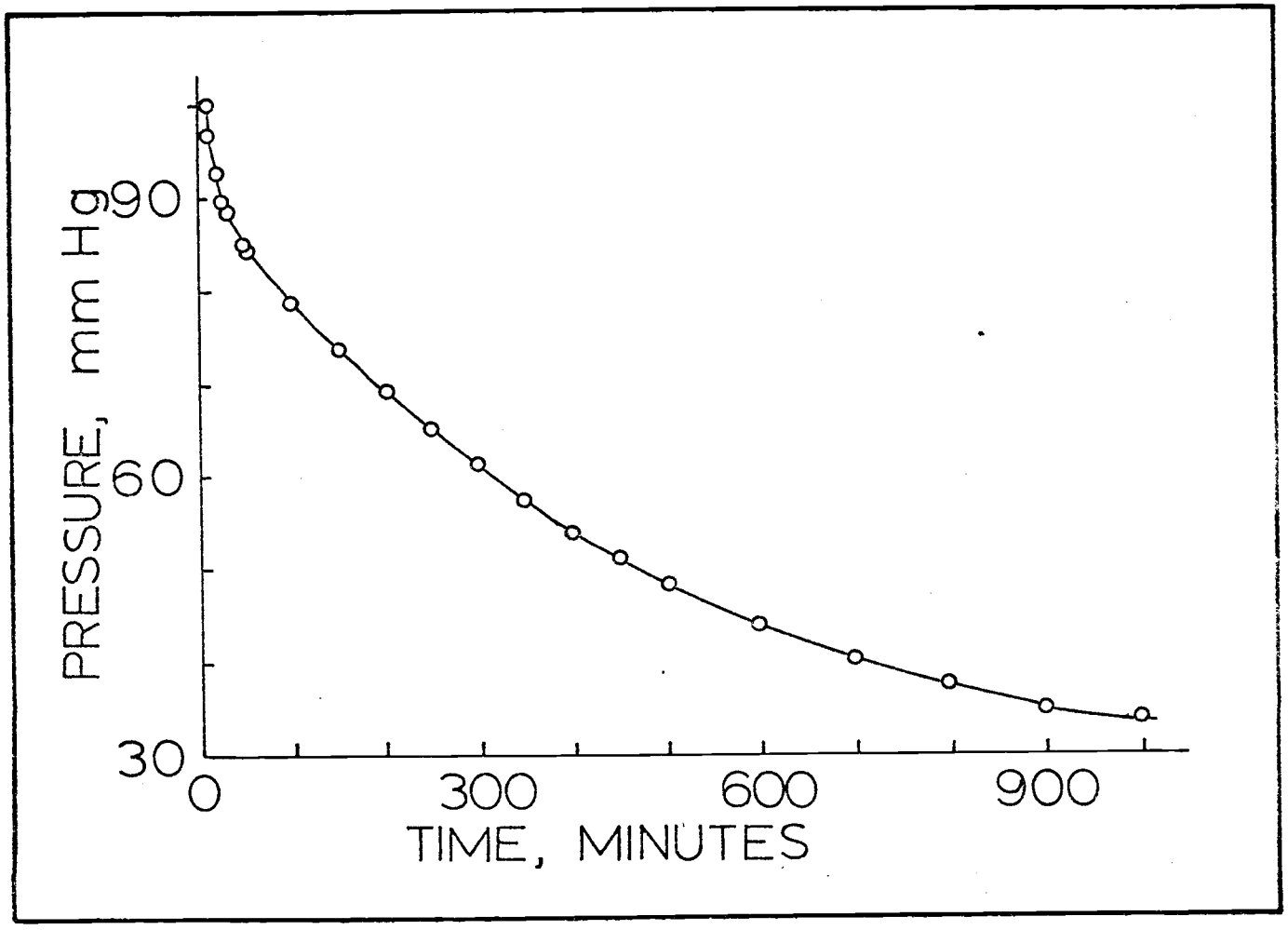

Figure 5-2. Typical Reaction Curve.

The ordinate is scaled to the total systemic pressure.

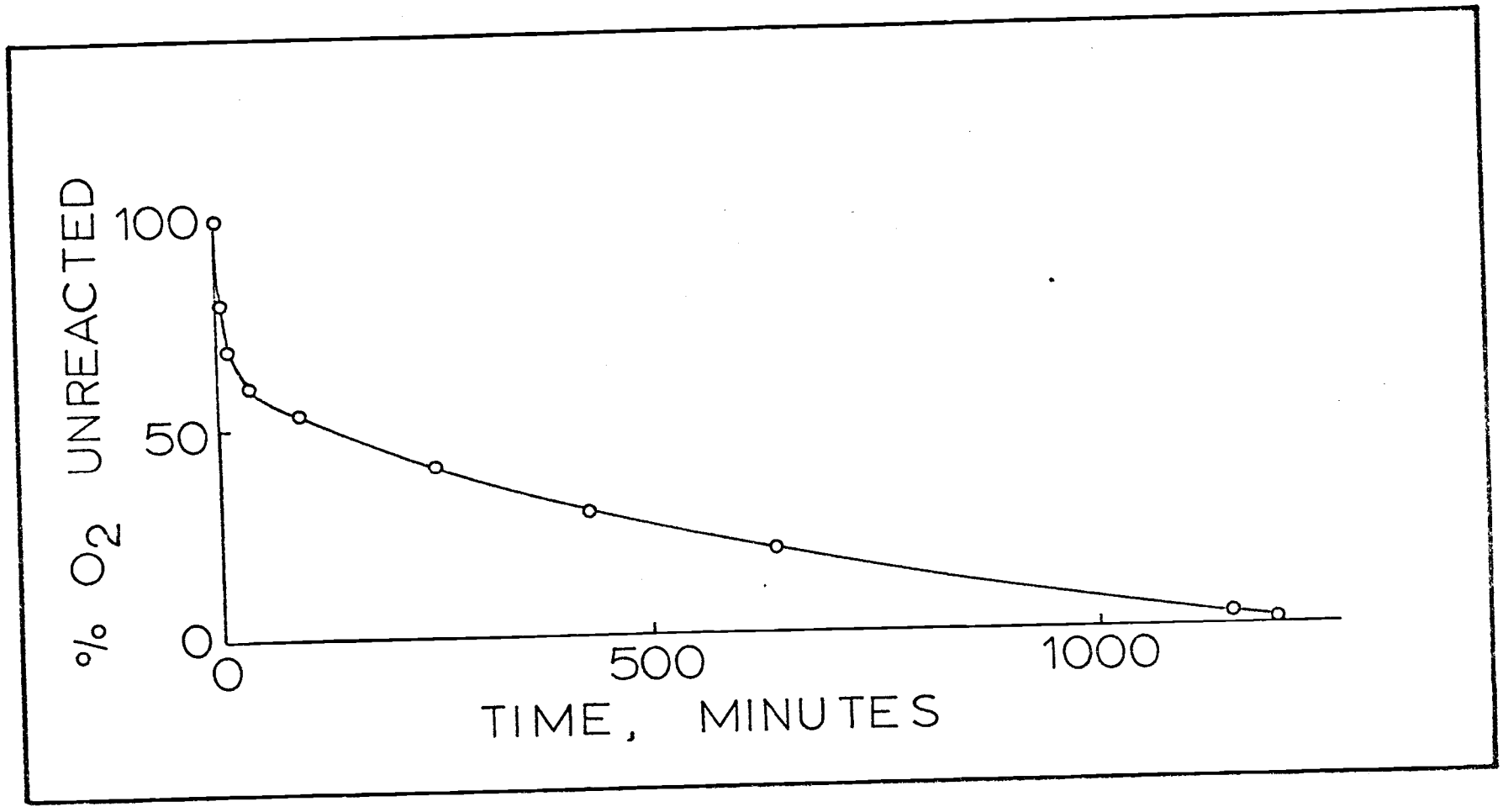

Figure 5-3. Percent oxygen unreacted versus time for the reaction shown in Figure 5-2, as determined by mass spectrometric analysis.

The reactions (equations 5-2 and 5-3) are consecutive only because the cyanate must be formed so that the decomposition via oxidation can proceed. Once some cyanate is present, then there is a competition for the oxygen beginning after about 10 to 15 minutes as shown in Figures 5-2 and 5-3. The oxidative decomposition is a complicated reaction sequence which is variously effected by the conditions; at the conditions suggested, the cyanate formation appears to be maximized and the temperature seems to be the most important single factor.

The products from the 93.5 atom-percent ^{18}O-enriched cyanate preparation were only 40-50% enriched in oxygen-18. This can be easily seen in Figure 5-4 if one compares the relative intensities of the 14 13 16 and 14 13 18 peaks at 2124 and 2116 cm^{-1}, respectively. The apparatus had previously been used to perform the preparation using oxygen-16. It appears that some sort of exchange reaction takes place between the oxygen on the nichrome and the $^{18}O_2$ used in the isotope preparation. The result was severe isotopic dilution of the ^{18}O-enriched cyanate. Although precautions were taken to minimize the product's contact with atmospheric oxygen and water vapor, it is possible that an oxygen exchange reaction could have also contributed to the dilution by atmospheric oxygen sources. The infrared spectrum shown in Figure 5-4, clearly demonstrates this result.

THE PRESSED DISK TECHNIQUE

A very useful technique of preparing solids for infrared study is the pressed disk or pellet method (79, p.148-153). Simply described, the procedure consists of intimately mixing the dry and finely divided potassium halide with the sample of interest,

and then pressing the mass into a clear pellet. Variations on this theme are employed to obtain the desired results. The pressed disk method is useful when: (a) the sample is present in limited quantity, (b) the use of infrared inactive solvents is not feasible, (c) rapid qualitative or semi-quantitative analysis is the objective, (d) the use of mulls is impractical. Since cyanate ion solid solution spectra are desired, it should be possible to do this with pellets (1). Improvement of this technique constitutes a minor development of this work. Pellets and mulls are both useful when one desires to study strongly absorbing molecules.

Potassium chloride used in pellet preparation was obtained from single crystals grown from the melt. The dry chloride was freshly ground before each preparation in a 50°C mullite mortar. The Harshaw infrared quality powered potassium bromide was stored in a heated and dry atmosphere.

The pellet press, milling capsule and balls, mortar and pestle were kept scrupulously clean and were stored in a 110°C drying oven when not in use. The pressing faces of the die and anvil were kept highly polished with a jewelers cloth impregnated with cerium oxide rouge; isopropyl alcohol was used as a polishing lubricant.

A normal charge of between 250 to 300 mg of KBr or KCl was quickly weighed and placed in the hot mullite mortar. Less than 0.75 weight percent cyanate sample was then added. The two ingrediants were ground thoroughly for five to ten minutes. The mix was then milled in a standard ball mill for 15 to 20 minutes. The powder was quickly transferred to the warm press and evenly distributed between the anvil and die by tamping the press on a table top and then rotating the plunger in one direction for 10 to 15 revolutions. The press was placed in a Carver Lab Press (#17585) and evacuated. Good quality, one centimeter diameter pellets were obtained when pressures between 6000 and 8000 psi were employed

for ten to fifteen minutes. Gentle removal of the pellet was accomplished by inverting the press and carefully pushing out the pellet using the force of the hydraulic press until a soft click was heard, signaling the release of the disk.

The best pellets were obtained when: (a) the KBr or KCl was moisture-free, (b) the grinding and milling procedure produced powder which had the consistancy of talc; (c) the sample concentration was below one percent; (d) the initial KBr or KCl powder charge was between 200 to 250 mg: (e) the milled powder was evenly distributed in the press; and (f) the pressing faces were freshly polished and the press very clean and dry.

It must be borne in mind that the pellet technique was employed with a view both to preparing solid solutions of cyanate ion in KBr and KCl and for the rapid identification of isotopic cyanate ion effects and isotopic peak assignments. Pellets prepared in the above manner only gave solid solution spectra directly when less than 0.5 weight percent cyanate was used. The technique (above) was also used for semi-quantitative analysis of contaminants which occured during various states of isotopic cyanate preparation; carbonate ion concentration could easily be estimated at 1414 cm^{-1} (KBr) using Beer's Law (79,p.152). Once the best isotopic cyanate samples were obtained, more intense solid solution spectra were desired. Increased milling times and higher pressures helped but for the more subtle features of the cyanate spectrum, the aforementioned concentrations were not adequate.

SOLID SOLUTION OF CYANATE ION IN PELLETS

Many methods of obtaining solid solution spectra from pellets have been successful to some extent (1,p.1104). Successive grinding and repressing is probably the least extreme procedure but the loss of sample and the tedium as well as the high probability of

outside contamination make this method suspect. Subjecting a 1.5 weight percent cyanate ion doped pellet to temperatures near the melting point of KBr or KCl in a closed system for six to nine hours did yield a solid solution pellet; but it had impaired optical properties due to decomposition and heavy metal contamination of the pellet.

The decomposition of the cyanate due to high temperatures and the chemical and catalytic activity of metal molecules (derived from the milling and pressing operations) contributed to these results. Some pellets were allowed to sit in a controlled atmosphere at 230°C for 3 to 4 weeks with no significant increase in solid solution infrared absorptions.

Pellets with less than 0.5 weight percent cyanate gave good solid solution properties. Most 250-300 mg pellets were one centimeter in diameter and 0.7 mm thick. Thus pellets up to seven millimeters thick were prepared; the expectation being that the increased path length would enhance the weaker features of the cyanate spectrum. Visible clarity of the pellet was good in most cases, the critical factors in their preparation being higher pressures (8000-10,000 psi) and even powder distribution in the press. The major drawback was the energy loss due to internal reflection (58) in the thicker pellets which necessitated wide slits and high gains, thus resulting in high noise and loss of resolution and thus defeating this whole approach to a large extent. The following procedure eliminated most of the difficulties alluded to above.

Small crystals of the alkali halide were placed in a 19mm (i.d.) X 6cm vycor test tube. The salt was melted in a stream of nitrogen gas over a Fisher burner. The cyanate dopant was quickly added to the molten salt as it was being removed from the flame but still in the nitrogen stream. The tube was swirled and inclined so that the cooling process was hastened. Best results were obtained with one to two gram potassium halide batches. The cool mass

was chipped out and a pellet subsequently prepared. With dopant concentrations exceeding two-weight-percent, remelting was necessary and further decomposition did result. When cyanide was the dopant, the nitrogen was discontinued during the addition of the dopant to the melt.

Figures 5-4 and 5-5 illustrate the results and usefulness of the pellet techniques discussed in the two preceding sections. Figure 5-5 shows the spectral region where $2\nu_2^o$, ν_1^o, Fermi resonant diad occurs. Figure 5-5(a) shows a 300 mg KBr pellet containing about two milligrams of an approximately two percent ^{18}O-enriched cyanate sample. The sharpness of the peaks as well as their location indicates that most all the cyanate is in solid solution. The two strong absorbances at 1205 and 1293 cm^{-1} are due to the 14 12 16 cyanate ν_1, $2\nu_2$ fundamental transition. The bands at 1187 and 1308 cm^{-1} are due to the excited $01^10 \rightarrow \{11^10, 03^10\}$ transition. The other two absorbances at 1176 and 1273 cm^{-1} are the fundamental ν_1, $2\nu_2$ transitions attributed to the 14 12 18 cyanate ion species. This is confirmed in Figures 5-5(b) and 5-5(c), where the ^{18}O- enrichment was increased to about 40 percent. In Figure 5-5(b), about 20-30 mg of ^{18}O-enriched cyanate sample was pelleted with 300 mg of KBr. The resulting pellet had good optical properties but a significant portion of the cyanate was not in solid solution. The normal KNCO peaks at ca. 1300 and 1210 cm^{-1} and the $KNC^{18}O$ peak at ca. 1190 and 1283 cm^{-1} support this conclusion. When the pellet was carefully remelted and repelleted, the spectra in Figure 5-5(c) was obtained. While more of the cyanate had gone into solution, the shoulder on the 1205 cm^{-1} absorbance and the strong peak at 1300 cm^{-1} still indicate the presence of the KNCO lattice. A by-product of this procedure was the appearance of the 14 12 18 $01^10 \rightarrow \{11^10, 03^10\}$ absorbances at 1160 and 1290 cm^{-1}.

Decomposition products from the cyanate preparations could easily be identified in the infrared spectra of the pressed disk.

Figure 5-4

Asymmetric stretch fundamentals of O^{18}
enriched cyanate in a KCl pellet.

The isotopic cyanate ions are in solid solution. The upper spectra was taken at ca. 100°K and shows the fundamentals clearly distinguished from the hot bands structures evident in the lower 300° K spectra. The success of the cooling procedure is evidenced by the absence of the 14 12 18 01^10 to 01^11 transition at 2162 cm^{-1} in the lower spectra. The cyanate concentration is about 0.8 weight percent.

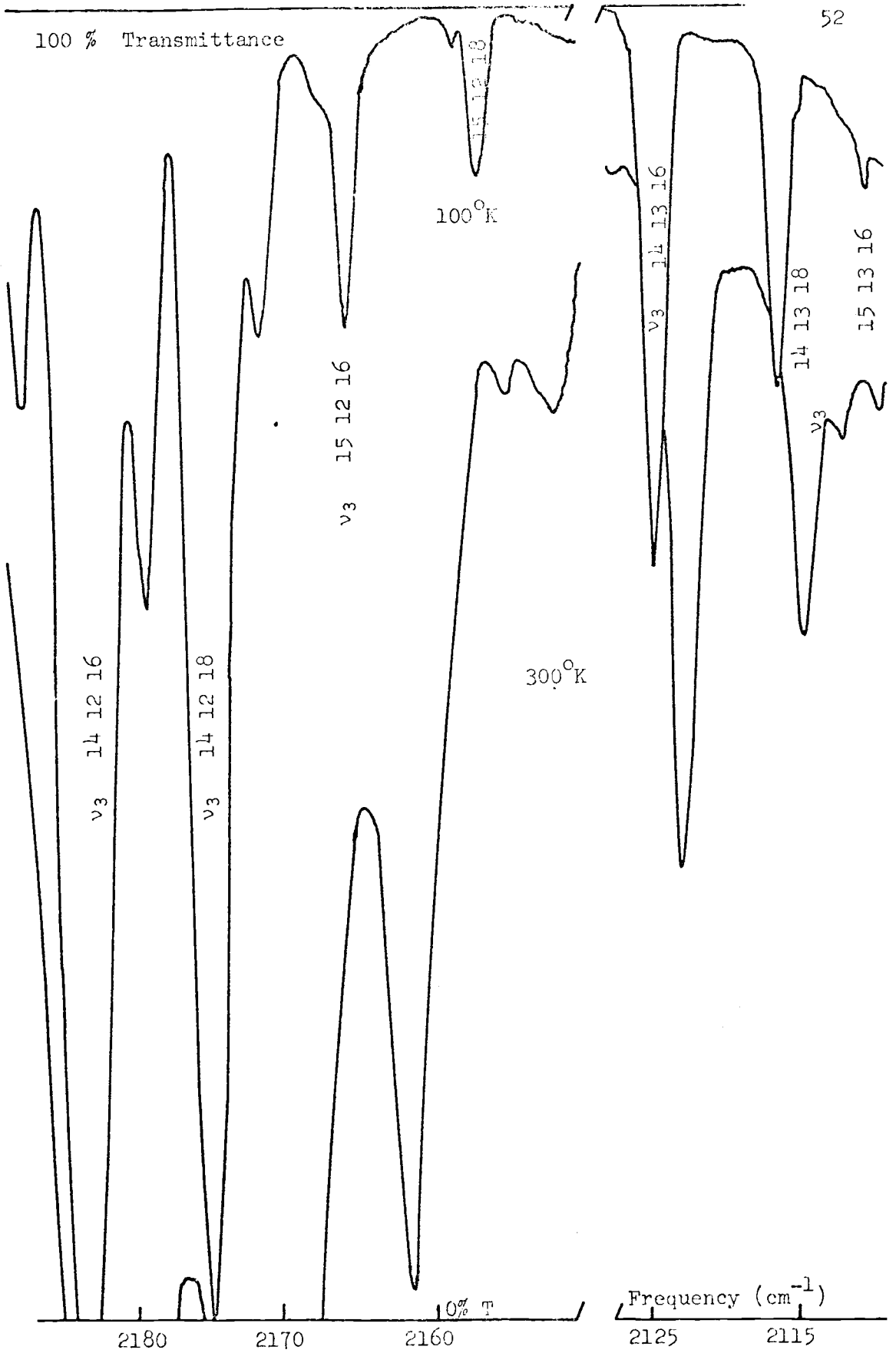
100 % Transmittance
100°K
300°K
ν_3 14 12 16
ν_3 14 12 18
ν_3 15 12 16
15 13 18
ν_3 14 13 16
14 13 18
ν_3
15 13 16
0% T
2180
2170
2160
2125
2115
Frequency (cm^{-1})

Figure 5-5

Cyanate ion impurity spectra in a KBr pellet showing the Fermi fundamental for a:

(a) Less than 0.5 weight-percent cyanate ion concentration, less than ten atom-percent ^{18}O-enriched;

(b) One to two weight-percent cyanate ion concentration about 40 atom-percent ^{18}O-enriched;

(c) One to two weight-percent cyanate ion concentration about 40 atom-percent ^{18}O-enriched after remelting and repressing.

All of the pellets were one centimeter in diameter by 0.7 mm thick.

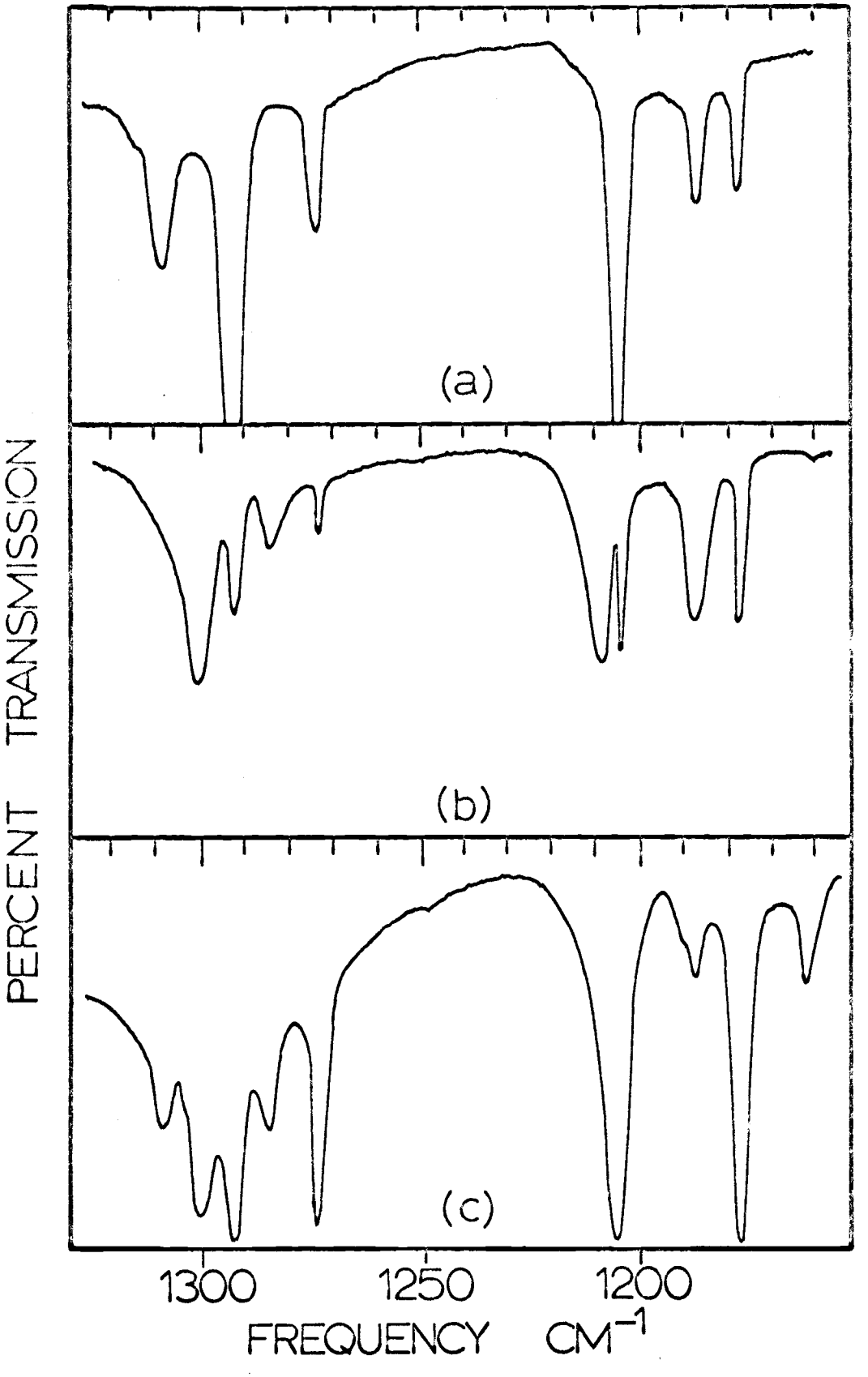
PERCENT TRANSMISSION
(a)
(b)
(c)
1300
1250
1200
FREQUENCY CM^{-1}

The most significant contaminants encountered in this technique are shown in Table 5-1 for KBr. Potassium chloride was not used extensively to make pellets, hence, the impurity ion frequencies in KCl are not shown. KCl and KBr pellets were used to confirm isotopic assignments.

This method was employed extensively in this work. Many obscure features of the cyanate spectrum were uncovered and assigned. However, complete solution of all the dopant was very rarely obtained and never realized when the dopant concentrations exceeded two-weight percent. It was found that the cyanate ion solid solution spectra deteriorated with time except those very dilute in dopant or those which have been remelted. This effect was even more pronounced in KCl. The question of cyanate affinity for halide sites will be left to future studies and will not be pursued further in this text.

Weak features, such as the $01^10 \rightarrow 02^21$ cyanate energy transition could not be definitely located using the pellet method as the energy loss and isotopic complications, which necessitated high resolution and low noise levels, were not facilitated using the pressed disks. A further complication was the presence of contaminants in the disks which obscured detail.

TABLE 5-1. IMPURITY ION CONTAMINANTS IN KBR.

A. Nitrite Ion Frequencies:

Frequency (cm^{-1})	Intensity (relative)	Description (band shape)
840	medium	sharp
1270	very strong	very broad
1375	very strong	very broad
2095	weak	medium
2425	medium	sharp
2550	medium	broad
2760	medium	sharp

TABLE 5-1 CONTINUED.

b. Carbonate Ion Frequencies:

Frequency cm^{-1}	Intensity (relative)	Description (band shape)
883	medium	sharp
1414	very strong	medium
1460	medium	sharp

c. Cyanide Ion Frequencies:

1952	weak	sharp
2070.4	very strong	broad with sharp maximum
2025	weak	$^{12}C^{15}N$ sharp
2035	very strong	$^{12}C^{15}N$ broad with sharp maximum

SINGLE CRYSTAL GROWTH

The process of growing crystals is amenable to scientific logic but largely implemented by trial and error in the laboratory. Lawson and Nielson (47) have expounded at great length on the "art" alone. Growth of single crystals from the fused salt has been analyzed by Holmes (37) and many of his techniques proved invaluable to this work. The general technique employed in this work is commonly known as the Kyropoulos method (45, 59).

The Kyropoulos method consists of rotating a continously cooled seed crystal in the fused salt and gradually pulling the melt away from the growing crystal. The melt is maintained a few degrees above its melting point. When it is desired to add dopant, such as cyanate ion, this should be done after initial growth has begun.

The apparatus which was used to grow single crystals during this study has been described by Holmes (37,p.18-28). It had the

advantage over previous cyanate doped single crystal growing procedures (54,p.66) that one could control the atmosphere over the melt.

Prepurified research grade argon, 99.998% minimum purity was passed through porous copper wire at 400°C to remove residual oxygen. Purified hydrogen chloride (or hydrogen bromide) was passed through a tube of freshly activated silica gel to remove any moisture present. Positive pressure and a closed system was maintained in the system by using a bubbler filled with Shell Ondina oil.

The starting materials used in the crystal growth were either J. T. Baker Co. or Matheson-Coleman-Bell Co. reagent-grade potassium chloride and Harshaw Chemical Co. infrared quality potassium bromide powder. These halide salts were used without further purification except as noted below. Pellets of the salts showed no infrared activity between 500 and 4000 wave numbers when appropriate precautions were taken to insure the absence of water vapor.

A normal charge of from 40 to 60 grams of alkali halide was weighed directly into a fused quartz crucible (General Electric Co. catalog #QC-20A1); the crucible was then placed in the apparatus which was subsequently evacuated and heated to about 120°C ("30" on all variac dials). The water coolant in the seed-bearing cold finger and in the upper heat shield was started. The internal pressure at this point had to be below five microns or the procedure was terminated; after the initial drying phase, the systemic pressure was typically below two microns. Twenty-four hours later, the oven temperature was raised to around 400°C ("60" on all variac dials) as the pumping was continued. After four hours, the pump was cut out of the system and the prepurified argon was bled in until a positive pressure of from one to two Torr was achieved. Then the argon was shut off and the hydrogen chloride (hydrogen bromide

in the case of a potassium bromide charge) purge was begun. The oven temperature was raised in order to melt the salt during the purge; the melting process usually took about one hour. The lower furnace coil was used to control the temperature during growth as the upper and door coils were implemented to reduce heat loss. When the salt became melted, the KCl (HBr) purge was discontinued and the argon purge restarted. Typical purge rates were from three to ten liters per hour. The melt was allowed to sit while the argon displaced the hydrogen halide gas; 15 to 20 minutes later, the dopant was placed in the doping spoon and rapidly introduced into the system.

After reducing the amperage in the lower furnace coil, the seed was manually lowered into the surface of the melt and rotation of the cold finger was begun. If the temperature of the melt was about 10°C higher than its melting point, rounding of the seed contours indicated that it was melting back as shown in Figure 5-6 (b). When this occured the seed was manually raised until only its tip was in contact with the surface as depicted in Figure 5-6 (c). As downward growth began, the seed was again raised as before. This procedure removed carbonaceous deposits and other surface crystallite contaminants which accumulate on the melt surface during the drying and purge phases (see Figure 5-6 (d)). This manipulation of the seed also contributed to the production of a more perfect crystal which is evidenced by fewer grain boundaries and better cleavage properties.

Ideally, the crystals were permitted to grow down as far as possible before the oven supporting table was mechanically lowered. Common lowering rates were between one to two centimeters per hour; slower at first, then increasing in rate, as the crystal growth progressed. The growth rate was controlled by "artful" manipulation of lower furnace coils and the speed of the crystal "pulling". Figure 5-6 (e) depicts crystal growth proceding properly. The most

Figure 5-6

Steps in single crystal growing.

(a) Shows approximate seed crystal and crucible size.

(b) Immerse seed until it begins to melt back.

(c) Manual manipulation to clear contaminants.

(d) Growing down.

(e) Shows point at which pulling is begun in earnest.

(f) Finished boule.

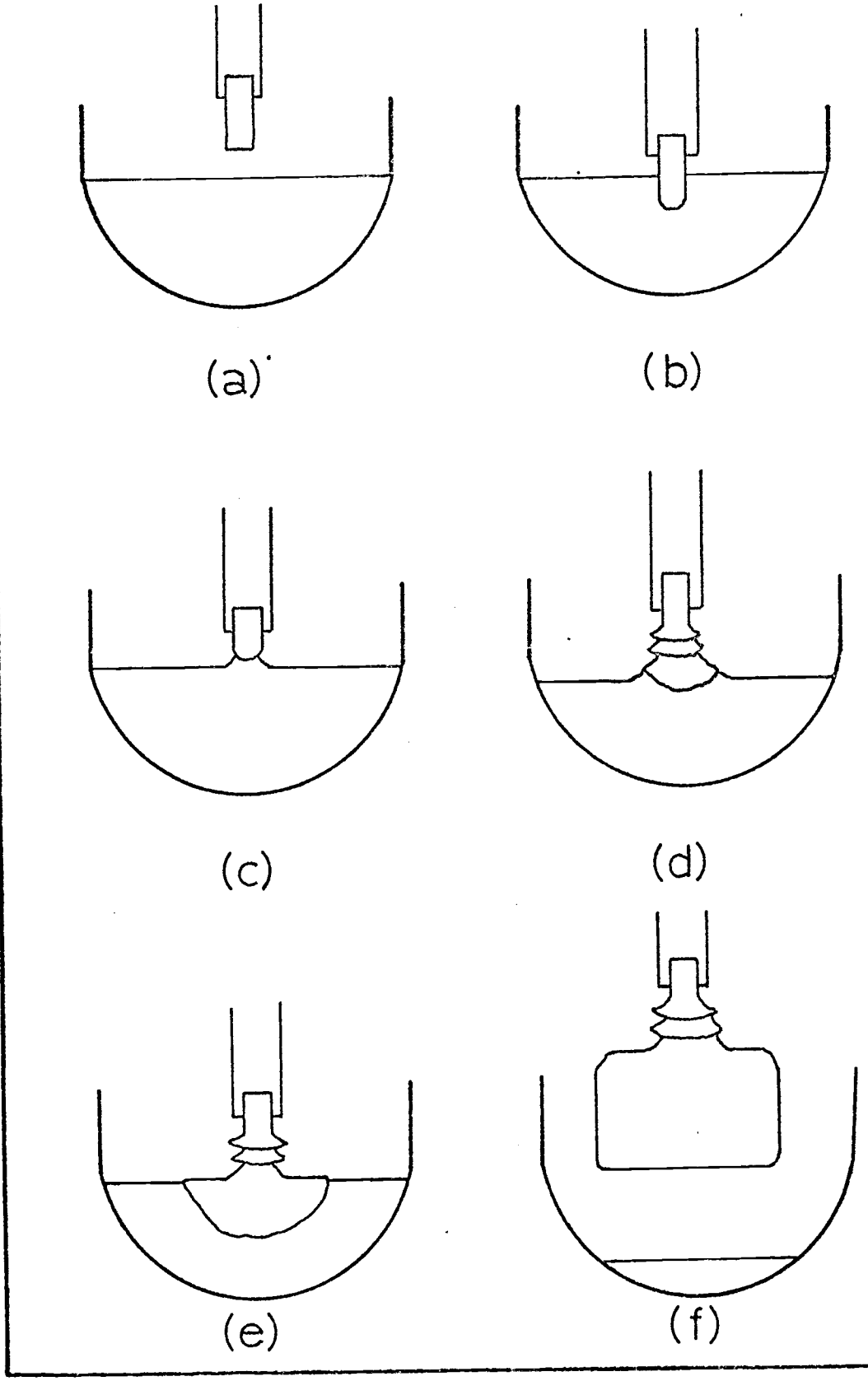
(a)
(b)
(c)
(d)
(e)
(f)

common problem encountered was that the crystal would grow out too fast, as the melt temperature dropped too low; this contributed to polycrystallinity and uncontrolable growth, and usually resulted in the necessity of remelting the whole mass. It was noted that the presence of dopant substantially affected the temperature conditions of the melt; the variation of concentration (as was the case with cyanate, due to decomposition and varying degrees of impurity incorporation in the lattice) in the melt also presented problems which were overcome only by trial and error.

Doping of the molten salt could be done at any point during the growth process. However, it was found that for cyanate, the best method of addition was continuously for about 30 to 45 minutes during the initial "growing-down" (see Figure 5-6 (d)) phase of the process. This specification is set because in the initial phases, the impurities on the surface of the melt catalyze decomposition and the molten salt temperature is higher. Addition of the dopant at too late a time presents a high probability of polycrystallinity. Since the dopant is added via an internal spoon, tardy addition was found to decrease the amount of material reaching the melt; this becomes an important consideration when one is either working with rare and expensive isotopic material, or is interested in analytical quantities, or both. A further advantage of early doping with cyanate is that the cyanate-halide solution equilibrium quickly becomes established and more uniform doping is thereby facilitated. Also the development of bubbles is reduced.

Returning to the methodology, when the crystal was large enough, contact was manually broken and the oven shut down (see Figure 5-6 (f)). The crucible and crystal were usually removed from six to ten hours later. During the growing period, constant supervision and adjusting of the conditions were necessary. The actual growth time usually ran three to six hours.

Several minor difficulties were encountered. In most instances, when the drying time was shortened, etching of the quartz crucible resulted. While no detectable hydroxyl infrared absorptions were in evidence, metaborate ion was observed to some degree in all crystals. When etching was more severe, the metaborate infrared absorptions were stronger.

TABLE 5-2. SOME METABORATE ION FREQUENCIES[-6]

	KBr		KCl	
Band	$^{10}BO_2^-$	$^{11}BO_2^-$	$^{10}BO_2^-$	$^{11}BO_2^-$
ν_2	609.54	588.64	610.69	589.74
ν_3	2029.0	1958.4	2043.6	1972.8
$\nu_1+\nu_3$	3095.4	3022.3	3116.9	3042.0

The uniformity of the cyanate dispersion in the alkali halide crystal lattice is open to question. Generally, the cyanate concentration was slightly greater in the portion of the crystal which grew during the doping operation. However, cyanate ion occured in all regions of a given single crystal. In crystals which had high doping levels, growth did not proceed as smoothly as those whose dopant levels were low. Dopant concentration gradients presented no problem to the infrared viewing of the sample because the crystals were physically oriented to minimize gradient effects.

There exists a real solubility equilibrium between cyanate ion in solid and molten alkali halide which is different for each alkali halide. When five to six weight percent dopant was added to the melt, vigorous bubbling and a clouded solution resulted.

[-6] These frequencies were supplied by Dr. J. C. Decius from a yet unpublished work on Metaborate Ion, June 15, 1966.

This was allowed to sit for ten to fifteen minutes, during which time the solution cleared. The crystal growth was then started and allowed to proceed until about one-third of the total charge weight was crystal. At this point the crystal growth had to be terminated as the bubbles forming around the growing boule caused to much disruption; forced growth after this point always resulted in a randomly oriented polycrystalline mass. The decomposition products did not interfere with the infrared spectrum to any detectable extent.

Apparently the cyanate in the melt is concentrated by the removal of the halide salt in forming the crystal. The excess cyanate then decomposes. The solubility of the cyanate ion in the crystal appears to be a function of the initial cyanate ion concentration evidenced by the fact that all residues contained a higher concentration of cyanate (and decomposition products) than did the respective crystals. There exists a limit to the cyanate concentration in the crystal. This was found to be greater for KBr than KCl.

Previous investigations encountered difficulties due to cyanate decomposition (54,p.58-61) in air grown crystals. This problem was eliminated using the aforementioned procedure except as stated above. The Bridgeman method (54,p.61) was attempted but yielded polycrystalline results. The atmosphere controled Kyropoulos method facilitated purification of the isotopic cyanate preparations; the crystal picked up only cyanate, cyanide and metaborate in infrared detectable amounts whereas pellets prepared using the same dopants showed significant quantities of carbonate, nitrate, and nitrite ion. These contaminants were also found in the unused melt.

INSTRUMENTAL

All spectral data obtained between 800 and 4000 wave numbers were derived from a Beckman IR-7 recording spectrometer. Those results reported between 400 and 800 wave numbers were obtained from a Beckman IR-11 recording spectrometer. Both instruments employ optical mull techniques in the double beam mode. Both instruments were constantly flushed with dry air produced by either a Beckman Dual Air Dryer (#45170) or by a Gilbarco Heatless Dryer (Gilbert and Barker Mfg. Co. Applied Pneumatics Div., West Springfield Mass., Model HF211A112). Spectral data from 4000 to 5000 wave numbers was obtained using a modified Perkin Elmer Model E-1 Monochromator which was located in the Spectroscopy Laboratory at the University of Minnesota. This instrument was operated in the double pass, single beam mode with a Nerst glower source. It was equipped with a two inch square (576 lines/mm) grating mounted in a 50cm Ebert-system. A thirteen cycle chopper was utilized. The output of the thermocouple detector was fed into a voltage divider scale expansion circuit to provide a 1X to 20X (absorbance) scale expansion. The signal to noise ratio was essentially proportional to the squareroot of the time constant, τ, and could be maximized by increasing τ, and increasing the mechanical slit width. The scale expansion feature was especially useful in finding $2\nu_3$ as shown in Figure 6-3. The E-1's accuracy was adjudged to be ± 0.6 cm^{-1} from 4000-5000 cm^{-1} and its repeatability was better than ± 0.1 cm^{-1}. Both the instrument and its sample compartment were continuously purged with dry nitrogen.

The Beckman IR-7 utilized a foreprism and grating type double monochromator giving dispersion capable of a resolution of 0.3 to 0.4 cm^{-1} throughout most of the NaCl foreprism range (42). The absolute frequency accuracy and reproducibility specified by specified by Beckman is presented in Table 5-3 (66,67).

TABLE 5-3. IR-7 SPECIFICATIONS (IN WAVE NUMBERS).

Order	First	Second	Third	Fourth
Range	650-1100	1100-2000	2000-2800	2800-4000cm^{-1}
Precision	±0.25	±0.25	±1.0	±1.0cm^{-1}
Accuracy	±0.5 (650)	±2.0 (1404)	±2.5 (2016)	±5.0 (4000)

Krueger has shown that the Beckman IR-7 is capable of higher precision and accuracy (42). This investigator has confirmed his claims, which are shown in Table 5-4.

TABLE 5-4 IR-7 PRECISION AND ACCURACY AFTER CALIBRATION (44).

Order	First	Second	Third	Fourth
Reproducibility	±0.02	±0.02	±0.06	±0.06
Accuracy	±0.035	±0.061	±0.086	±0.109

All of the above specifications apply when the spectral data is taken "off the frequency dial" of the instrument. Krueger's claims were made after calibrating his modified IR-7; claims made in his work were limited only by precision and systematic errors.

Even though the IR-7 and IR-11 are double beam instruments, the presence of strong carbon absorptions in the 660 and 2350 wave numbers region caused adverse effects due to low energy in these areas. The insertion of an ascarite column in the flushing lines partially reduced these problems but did not eliminate them.

The Beckman IR-11 uses single, filter/grating, monochromator and operating in the double beam mode utilizes the optical null principle. The source is a high pressure mercury arc and the detector is a diamond window Golay pneumatic device. A wave number accuracy of ±1.0 wave number through out its entire range (33 to 800 cm^{-1}) is claimed by Beckman. Many problems were solved with the calibration technique in this work.

High gains used during some phases of this work produced high noise levels. The noise levels in both instruments were effectively minimized by the installation of a 100 mfd filtering capacitor in the respective filtering circuits of both instruments and reducing the scanning speeds to the slowest possible. Speeds as slow as five minutes per wave number were attained. Resolution was also increased in many cases by narrowing the slits of both instruments from their "normal programmed" settings.

No attempt was made to calibrate the instruments, only the peaks were determined. The frequency dials were ignored. The abscissa of the Beckman instrument was found to be linear (or very close to linear) over wide ranges of chart distance; usually 50 to 100 wave numbers. Table 5-5 shows the calibration gases used in this work. The peaks were calibrated by locating them between two known peaks during a continuous scan and interpolating the corresponding distances to determine the sample peak's frequency.

The use of this procedure necessitates several precautions to insure maximum accuracy. The slowest scanning speeds were used to minimize the tracking error due to the difference in peak widths. Comparable gains were used for the same reason. Temperature effects were no problem because enough time was allowed so that the sample and calibrant would come to equilibrium with the instrument; temperature effects are very small and negligible when the precision is taken into account. At least six determinations were made for each peak, in some cases, as many as 25 were made. Distance measurements were made with an engineers' scale and facilitated through the use of a very fine writing pen. In most cases the average deviation from the mean was found to be about 0.05 cm^{-1} from 500 to 2000 wave numbers, and ca.0.085 to 0.2 from 2000 to 4000 cm^{-1}. Care was taken to insure that the calibration peaks were just as intense as the sample peaks to insure that pen wire effects were negated.

TABLE 5-5. GASES USED TO CALIBRATE CYANATE ION FREQUENCIES .

Calibration Gas	Region (cm^{-1})	Reference
water vapor	500 - 600	6
nitrous oxide	600 - 650	38
carbon dioxide	630 - 700	38
ammonia	1150 - 1212	38
methane	1247 - 1332	38
water vapor	1700 - 1900	38
carbon monoxide	2000 - 2250	38
carbon dioxide	2320 - 2380	38
hydrogen bromide	2380 - 2700	38
hydrogen chloride	2700 - 2900	38
hydrogen cyanide	3240 - 3360	38
water vapor	3360 - 3500	27
carbon dioxide	3500 - 3700	38
water vapor	3800 - 4000	38
carbon monoxide	4130 - 4340	38

The IUPAC Commission on Molecular Structure and Spectroscopy states that a spectrometer whose best resolution is ca. 0.3 wave numbers should be capable of at least ±0.06 cm^{-1} precision (32, p.537). Krueger shows that because of the distance the cam follower moves is not sufficiently large in the third and fourth orders, the precision in those regions is not that good (42).

The frequency data, which will be presented in Chapter Six, has the absolute accuracies specified in Table 5-6.

TABLE 5-6. ABSOLUTE ACCURACY OF REPORTED CYANATE ION FREQUENCY RESULTS.

Reported Value (cm^{-1})	Example (cm^{-1})	Absolute Accuracy (cm^{-1})
to 0.01	2181.88	better than ±0.20
to 0.1	3372.5	better than ±0.5
to 1	3949	better than ±5

The precision determinations for most of the reported values are listed in Tables 6-1 to 6-12. These are simple arithmetic mean values. The accuracies specified in Table 5-6 take into account reproducibility, peak resolution, line breadth, instruments capabilities, and temperature variation. All values reported in this thesis are at 300°K. The spectra presented in Figures 6-1 through 6-13 (except for Figure 6-3) are reproductions of "slowest speed" scans made at the programmed conditions built into the Beckman IR-7 and IR-11 recording spectrometers. Figure 6-3 was obtained using the Perkin-Elmer E-1 spectrometer.

CHAPTER 6

SPECTRAL ASSIGNMENTS

This chapter is devoted to the presentation of data observed during this research. Previous studies by Maki and Decius provided an abundance of vibrational bands for 14 12 16 cyanate ion in KBr and KI, but not much in KCl (54, 55, 56). Independent of this research, Schettino and Hisatsune reinvestigated their work and extended cyanate studies to 14 13 16, 14 12 18, 15 12 16, and 15 13 16 cyanate species in KCl, KBr and KI utilizing the pellet technique (84). Chapter Eight compares their work to ours. However, it should be pointed out at this time that our single crystal technique has permitted us to obtain more extensive data than they were able to observe, exemplified by our discovery of the $2\nu_3$ overtone.

Experimental work during this study concentrated on vibrational absorbance spectra in KCl, and isotopic enrichment studies in both KCl and KBr. The first two sections of this chapter will present data and assignment arguments for cyanate ion dissolved in KCl, and results obtained for various cyanate isotopes in KBr. The third section will summarize the spectral results. The concluding section will deal with isotopic product rule calculations based on the concepts presented in Chapter Four.

CYANATE ION IN POTASSIUM CHLORIDE

Harmonic theory suggests that the linear N-C-O ion should give three fundamental peaks corresponding to a N-C stretch at 2200 cm^{-1}, a C-O stretch around 1200 cm^{-1} and a doubly degenerate bend around 600 cm^{-1}. Figures 6-1 and 6-2 clearly indicate the presence of four fundamental-like vibrations at 631 cm^{-1}, 1206 cm^{-1}, 1297 cm^{-1} and 2180 cm^{-1}. The 2180 cm^{-1} is clearly due to the CN stretch and by

analogy to CO_2, designated ν_3, the asymmetric mode. Likewise the 631 cm^{-1} peak is the ν_2, or doubly degenerate bend. From knowledge of the likelihood of Fermi resonance, the two remaining bands are assigned to resonance between ν_1 and $2\nu_2^0$ ($\ell = 0$ for the Σ species, making it the same species as the ν_1 from symmetry considerations). The theory developed in Chapter Three also allows for the $2\nu_2^0$ overtones's intensity in the resonance to be enhanced by the coupling. The magnitude of the splitting indicates that fairly close resonance interaction is taking place in light of similiar effects observed in CO_2 and N_2O as mentioned in Chapter Three.

In assigning the multitude of bands, the convention of designating the transition $G_{(v_1v_2^{\ell}v_3)}-G_{(v_1'v_2'^{\ell}v_3')}$ will be written $v_1v_2^{\ell}v_3 \rightarrow v_1'v_2'^{\ell}v_3'$. Fermi resonance, which in effect mixes the states of the unperturbed levels, will be designated by the symbolism $v_1v_2^{\ell}v_3$ to $\{v_1'v_2'^{\ell}v_3', v_1''v_2''^{\ell}v_3''\}$. Since the quantum number ℓ may assume values:

$$\ell = V_2 \ldots V_2 - 4, V_2 - 2, 1 \text{ or } 0 \text{ and } \Delta\ell = \pm 1, 0 \qquad (6\text{-}1)$$

the number of allowed transitions is limited (33,p.379). Utilizing the criteria for Fermi resonance : (i) interacting levels be of the same symmetry; (ii) predicted unperturbed levels be nearly degenerate, then Table 6-1 through 6-5 shows the assignments. Figures 6-1, 6-2, and 6-3, show the normally abundant cyanate in a KCl environment at $300^{\circ}K$ and $100^{\circ}K$.

The ν_2 region is dominated by the 631.17 cm^{-1} bending transition. There are two strong hot bands at 579.65 cm^{-1} and 666.88 cm^{-1} which look like the Fermi diad in the 1200-1300 cm^{-1} region. The 01^10 level has the largest population other than the ground state, and the difference between the two bands is 87 cm^{-1} which is approximately the same separation between the 02^00-10^00 resonance. Hence the assignments $01^10 \rightarrow (100, 02^00)$ is made to this diad. The separation between

the weak features at 560.78 and 682.28 cm^{-1} is 121 cm^{-1}, which is the separation between the 11^10 and 03^10 levels observed in the ν_1 region of the spectrum. These peaks disappear quickly upon cooling and thus originate from the 02^20 excited level. The $01^10 \rightarrow 02^20$ transition should be fairly strong, but its frequency will occur around 631 cm^{-1} and will be masked by the ν_2 fundamental. Four lines can be predicted to originate from the 10^00, 02^00 levels, which should be appreciably populated at room temperature, at 526, 615, 647, and 735 cm^{-1}. The two extreme frequencies could not be located in the spectrum but the 647.71 cm^{-1} and the high frequency side of the ^{13}C-cyanate ν_2 peak indicated their presence. The 614 cm^{-1} peak is due to normally abundant $N^{13}CO^-$, and the weak shoulders on the low frequency side of the 631 cm^{-1} fundamental are due to ^{15}N and ^{18}O isotopes. The weak bands between 600 and 610 cm^{-1} that appear upon cooling are due to doubly substituted cyanate. The 590 cm^{-1} absorbance is due to metaborate ion which arrises as a minor impurity during the crystal growing process and is observed in practically all spectra shown in this section. Enrichment studies of the ν_2 region have confirmed these isotope assignments and can be seen by comparing Figures 6-4, 6-6, and 6-8.

The ν_1, $2\nu_2^o$, or symmetric stretch region between 1140 and 1330 cm^{-1}, at first glance appears quite complicated. At room temperature six absorbances are strongly apparent. The three most populated lower states at room temperature are the 00^00, 01^10 and 02^20. The latter level originates from the $01^10 \rightarrow 02^20$ transition; it is not an observable transition as it would fall under the band envelope of the $00^00 \rightarrow 01^10$ transition. These excited states each give rise to resonant doublets, $01^10 \rightarrow \{11^10, 03^10\}$ and $02^20 \rightarrow \{12^20, 04^20\}$, respectively. Both these pair of "hot bands" disappear upon cooling (to ca. 70^oK) revealing many other pairs of fundamental resonant diads. In Figure 6-1, the $01^10 \rightarrow \{11^10, 03^10\}$ hot bands are incompletely extinguished at 1192.4 and 1314.17 cm^{-1}. The lower

member of the $00^0 0 \rightarrow \{02^0 0, 10^0 0\}$ diad for ^{13}C and ^{15}N cyanate species are largely unresolved at 1196 cm^{-1} as are the upper members of the ^{13}C and ^{18}O species doublet at 1277 cm^{-1}. Enrichment studies shown in Figures 6-4, 6-6 and 6-8, clearly demonstrate this coincidence. The ^{18}O cyanate peak at 1181.5 cm^{-1} and the ^{15}N peak at 1286.8 cm^{-1} complete the mono-substituted cyanate set. The weak features at 1183 cm^{-1} and 1264 cm^{-1} are attributed to the $^{15}N^{13}CO^-$ species.

TABLE 6-1. ASSIGNMENTS FOR $^{14}N^{12}C^{16}O^-$ CYANATE VIBRATIONAL FREQUENCIES IN KCL.

Initial State	Final State	Observed Frequency (cm^{-1})	Precision ($\pm cm^{-1}$)
$00^0 0$	$01^1 0$	631.17	0.02
000	$10^0 0$	1210.59	0.04
	$02^0 0$	1297.40	0.04
000	$11^1 0$	1823.4	0.30
	$03^1 0$	1945.3	0.30
000	$00^0 1$	2181.88	0.10
	200	2402.88	0.15
000	$12^0 0$	2499.26	0.15
	$04^0 0$	2612.80	0.15
000	$01^1 1$	2801.72	0.08
000	$10^0 1$	3372.5	0.10
	$02^0 1$	3458.7	0.10
	$30^0 0$	3579.2	1.0
	$22^0 0$	3693.2	0.6
000	$14^0 0$	3798.3	0.6
	$06^0 0$	3949.	3.0
000	002	4341.8	0.4

TABLE 6-1. CONTINUED.

Initial State	Final State	Observed Frequency (cm^{-1})	Precision ($\pm$ cm^{-1})
	20^00^1	4544.4	0.5
00^00	12^00^1	4640.3	0.5
	04^00^1	4751.3	0.5
01^10	10^00	579.65	0.05
	02^00	666.88	0.07
01^10	11^10	1192.43	0.04
	03^10	1314.17	0.05
01^10	01^11	2170.57	0.05
	21^10		
01^10	13^10		
	05^10	2639.58	0.07
01^10	10^01	2740.88	0.02
	02^01	2827.01	0.04
01^10	02^21	2791.12	0.07
01^10	11^11	3342.4	0.2
	03^11	3462.5	0.4
02^20	11^10	560.78	0.09
	03^10	682.28	0.10
02^20	12^20	1178.68	0.05
	04^20	1326.22	0.07
02^20	02^21	2160.35	0.08

The region between 1330 and 2000 cm^{-1} has revealed only two weak features attributable to cyanate ion in all the isotopes studied. This was at 1823.2 and 1945.1 cm^{-1}. These bands did not extinguish upon cooling and hence were assigned to the $00^00 \rightarrow \{11^10, 03^10\}$ Fermi diad. The $^{11}BO_2^-$ peak was observed around 1970 cm^{-1}.

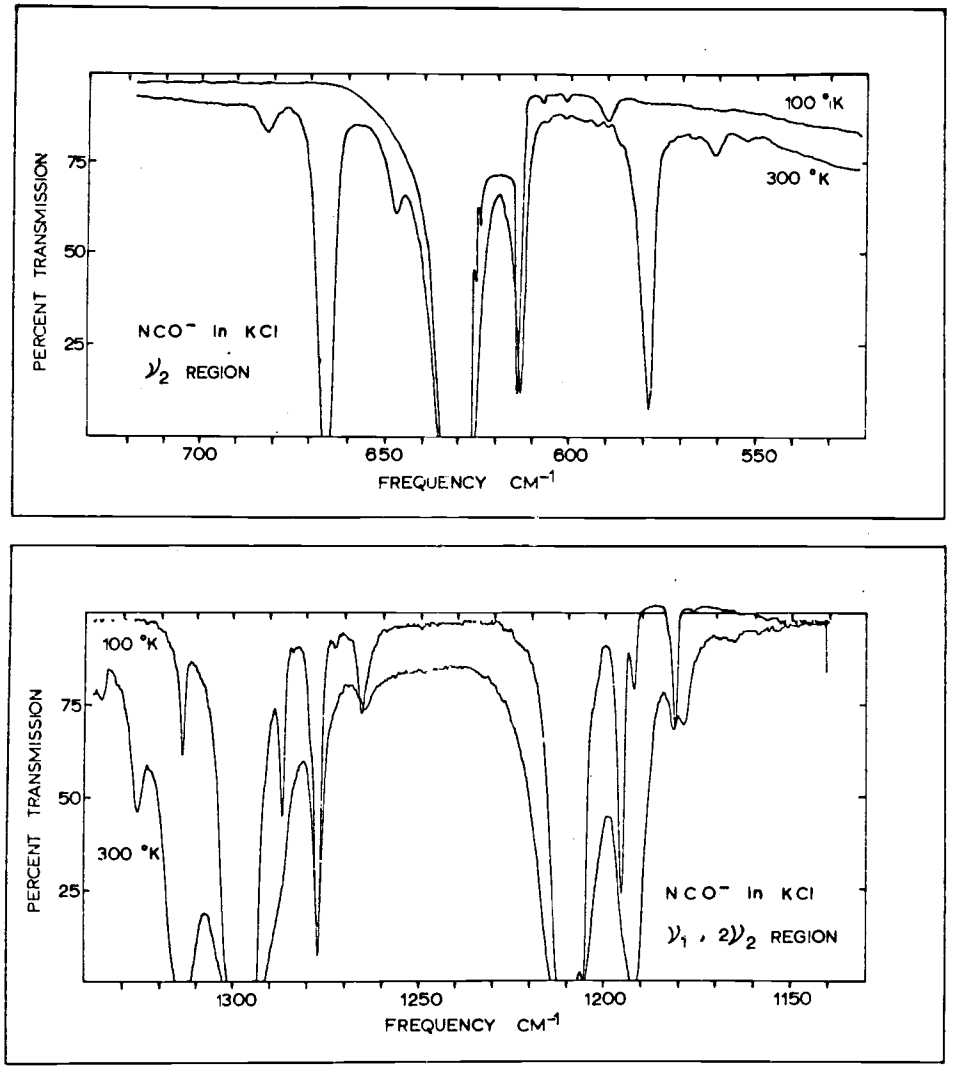

Figure 6-1

Infrared spectrum of a 5-6 weight-percent normal cyanate ion doped potassium chloride crystal at 100°K and 300°K. The upper figure shows the bending region. The lower figure depicts the Fermi doublet fundamental region.

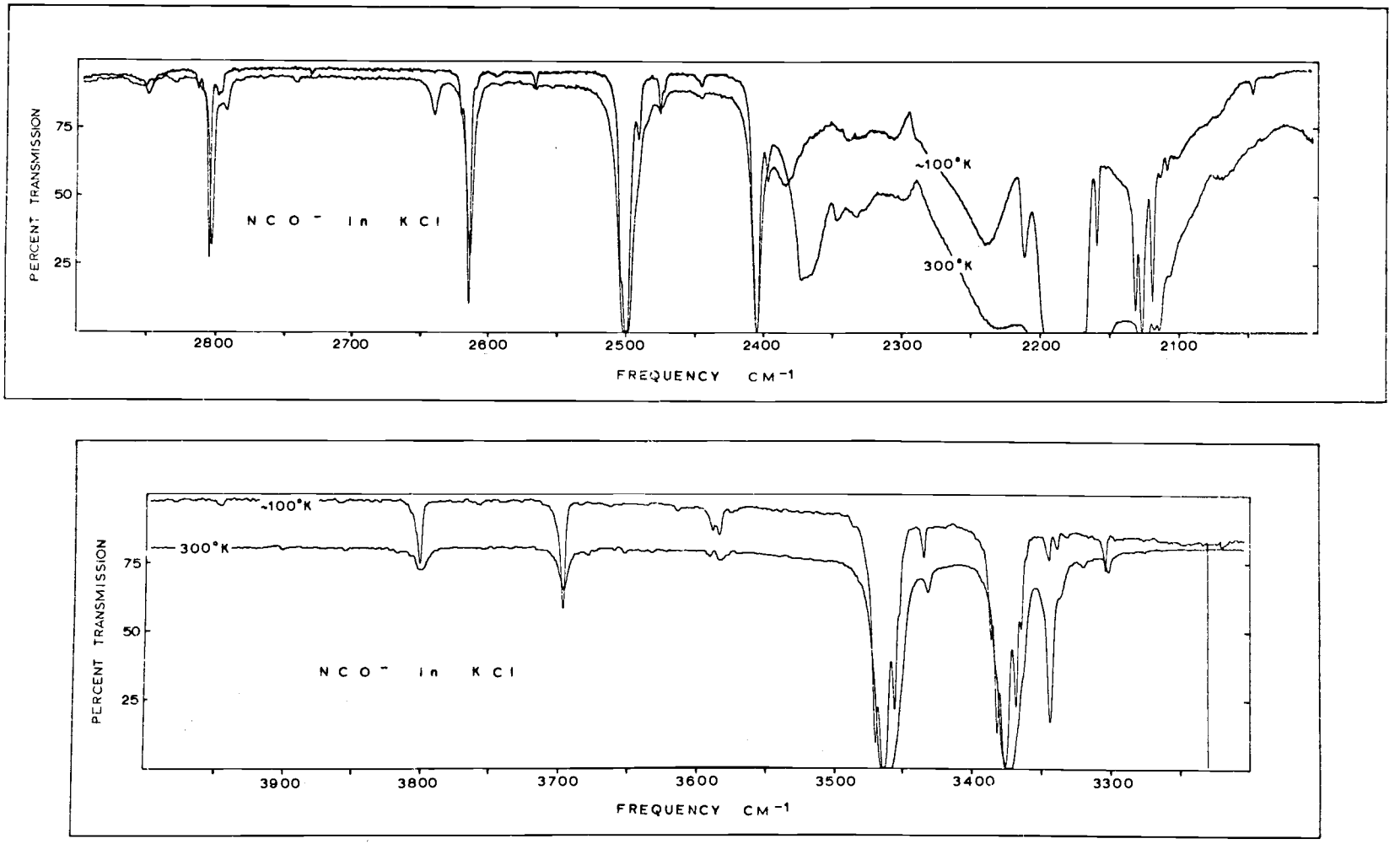

Figure 6-2. Infrared spectrum of a 5-6 weight-percent cyanate doped potassium chloride crystal at 100°K and 300°K from 2000 cm^{-1} to 4000 cm^{-1}.

The strongest fundamental absorbance in the cyanate ion spectrum is the asymmetric-like stretch, ν_3, at 2181.88 cm^{-1}. The ^{13}C isotope cyanate ν_3 at 2124 cm^{-1} is also readily determined, (see also Figure 5-4). In order to study the "hot" band structure and other detailed features, it was necessary to use a more dilute sample than shown in Figure 6-2, although the $^{15}NCO^-$, 000 → 001, transition is readily discernable at 2165.30 cm^{-1}. Upon doing this, bands which vanished upon cooling were found at 2170.50 cm^{-1} and 2160.35 cm^{-1}, corresponding to the $01^10 \rightarrow 01^11$ and $02^20 \rightarrow 02^21$ transitions respectively. The ^{18}O cyanate species was identified, after the "hot" bands were extinguished, at 2172.74 cm^{-1}, and confirmed as shown in Figure 6-7. In all of the cyanate spectra the ν_3 fundamental was accompanied by a series of nearly equally spaced lines on either side of it. These "satellite" lines did not vanish upon cooling and were found associated with combination bands involving the ν_3 mode. They are summarized in Table 6-6 and have been shown by Decius, et al. (19), to be concentration dependent, a result of localized vibrational interactions between neighboring cyanate ions.

A Fermi triplet occurs between 2350 cm^{-1} and 2650 cm^{-1}. This involves resonance between transitions 000 to (20^00, 12^00, 04^00) and accounts for the absorbances at 2402.88 cm^{-1}, 2499.26 cm^{-1} and 2612.80 cm^{-1}. A peak at 2639.58 cm^{-1} dissappears upon cooling and is attributed to the (01^10) to (21^10, 13^10, 05^10) triad. Satellite-like features are observed about these peaks upon cooling. In addition, isotope peaks due to ^{13}C and ^{15}N are weakly distinguishable (see Figures 6-9 and 6-7 and the footnote to Table 6-12).

The band at 2801.72 cm^{-1} arrises from combination of $\nu_2 + \nu_3$. Upon quenching the "hot" band corresponding to a $01^10 \rightarrow 02^21$ transition at 2791.12 cm^{-1}, satellites about the main peak are observed. In Figure 6-2, this effect can be detected although much stronger samples were utilized in the calibration phase of this study. These

stronger sample studies combined with enrichment studies pinpointed the $\nu_2 + \nu_3$ combination band in $^{15}NCO^-$ at 2781.01 cm^{-1} and that for $NC^{18}O^-$ at 2788.82 cm^{-1}. The $N^{13}CO^-$ $\nu_2 + \nu_3$ level can be observed at 2728.01 cm^{-1} upon cooling the crystal (see Figure 6-2). Two weak "hot" band-type peaks are barely evident in this combination region at 2740.88 cm^{-1} and 2827.01 cm^{-1}. They are due to the Fermi diad which results during the $01^10 \rightarrow \{10^01, 02^01\}$ transition. Substantuating this is their difference of 86.1 cm^{-1} which is the separation of the 10^00, 02^00 levels. This diad is observable in Figure 6-2.

The 3300 cm^{-1} to 3500 cm^{-1} region is dominated by strong combinations of the "fundamental Fermi diad" and the asymmetric stretch. The two main features for the "normal" cyanate occur strongly at 3372.5 cm^{-1} and 3458 cm^{-1}. These transitions whose difference is around 86 cm^{-1}, are assigned to the 10^01, 02^01 combination level and upon cooling yield satellite structures. The "hot" bands associated with the 01^10 to $\{11^11, 03^11\}$ transition are apparent at 3342.4 cm^{-1} and as a shoulder on the main peak at 3462.5 cm^{-1}. Their separation of about 120 cm^{-1} correlates with that observed for the corresponding diad in the symmetric stretch region.

The lower member of the $^{14}N^{13}C^{16}O^-$ combination diad is weakly observable at 3300.68 cm^{-1}. Its upper member at 3383 cm^{-1} is obscured by the breadth of the "normal" cyanate peak. Likewise the $^{15}N^{12}C^{16}O^-$ peak at 3430.52 cm^{-1} is readly seen, but its lower member at 3341 cm^{-1} is hidden by the normal cyanate's hot band. Upon cooling the crystal, the lower ^{15}N peak is indeed observed at 3341.40 cm^{-1} along with a member of the ^{18}O species diad at 3336.3 cm^{-1}. Cooling also sharpens the ^{13}C peak and the satellite structure on the main peaks can now be seen. All of these isotopic assignments have been confirmed by enrichment spectra. An interesting observation of this region is that even though the combination is with ν_3 fundamental, the Fermi resonance splitting

is little changed from that observed in the symmetric stretch region. This enhances the arguments against the k_{322} coupling constant playing a significant role in this resonance.

The region between 3500 cm^{-1} and 4000 cm^{-1} is difficult to study due to the noise limitations of the instrument and water vapor which absorbs strongly in this region. Three peaks can be readly seen at 3519.2 cm^{-1}, 3693.2 cm^{-1}, and 3798.3 cm^{-1}. Based on symmetry, and the fundamental frequencies, taken together with the strong Fermi resonances, one would expect the Fermi tetrad (30^00, 22^00, 14^00, 06^00) to be observed, albeit weakly due to the large quantum number change from the ground state. Upon cooling the sample, a very weak feature is detectable at 3949 cm^{-1}, and resonance calculations do indeed predict it to be in that region. The other weak feature at ca. 3680 cm^{-1} has not been assigned and may be an overtone of BO_2^-.

Prior to this investigation, the 00^00 to 00^02 transition had not been observed. The cyanate spectrum is similar to that of carbon dioxide where this transition is forbidden by symmetry. But owing to the asymmetry of the linear XYZ model, this transition is not forbidden and should occur for cyanate ion, albeit weakly. Using the scale expansion features of the spectrometer at the University of Minnesota, we were able to locate this very weak feature at 4341.8 cm^{-1} for 14 12 16 cyanate ion in KCl. $2\nu_3$ was seen for the first time when a three to five weight percent 15 12 16 cyanate ion doped KCl crystal was examined. The corresponding peak was then discovered in a similarly doped KBr crystal. From these two frequencies and the potential energy program (presented in Chapter Seven) the 4341 peak was predicted. The peak is shown in Figure 6-3. The $2\nu_3$ overtone is important in potential energy calculations and serves to determine the cubic normal coordinate constants involving the asymmetric vibrational mode.

Figure 6-3

Infrared spectrum of the resolvable weak features of a 5-6 weight-percent normal cyanate ion doped potassium chloride crystal above 4000 cm^{-1}. The $2\nu_3$ overtone spectrum shows the result of a ten-fold percent-transmission scale expansion. The combination Fermi triplet observed between 4530 cm^{-1} and 4760 cm^{-1} shows a similar five-fold expansion. The mechanical slit width was eight millimeters and the temperature was $300^{\circ}K$.

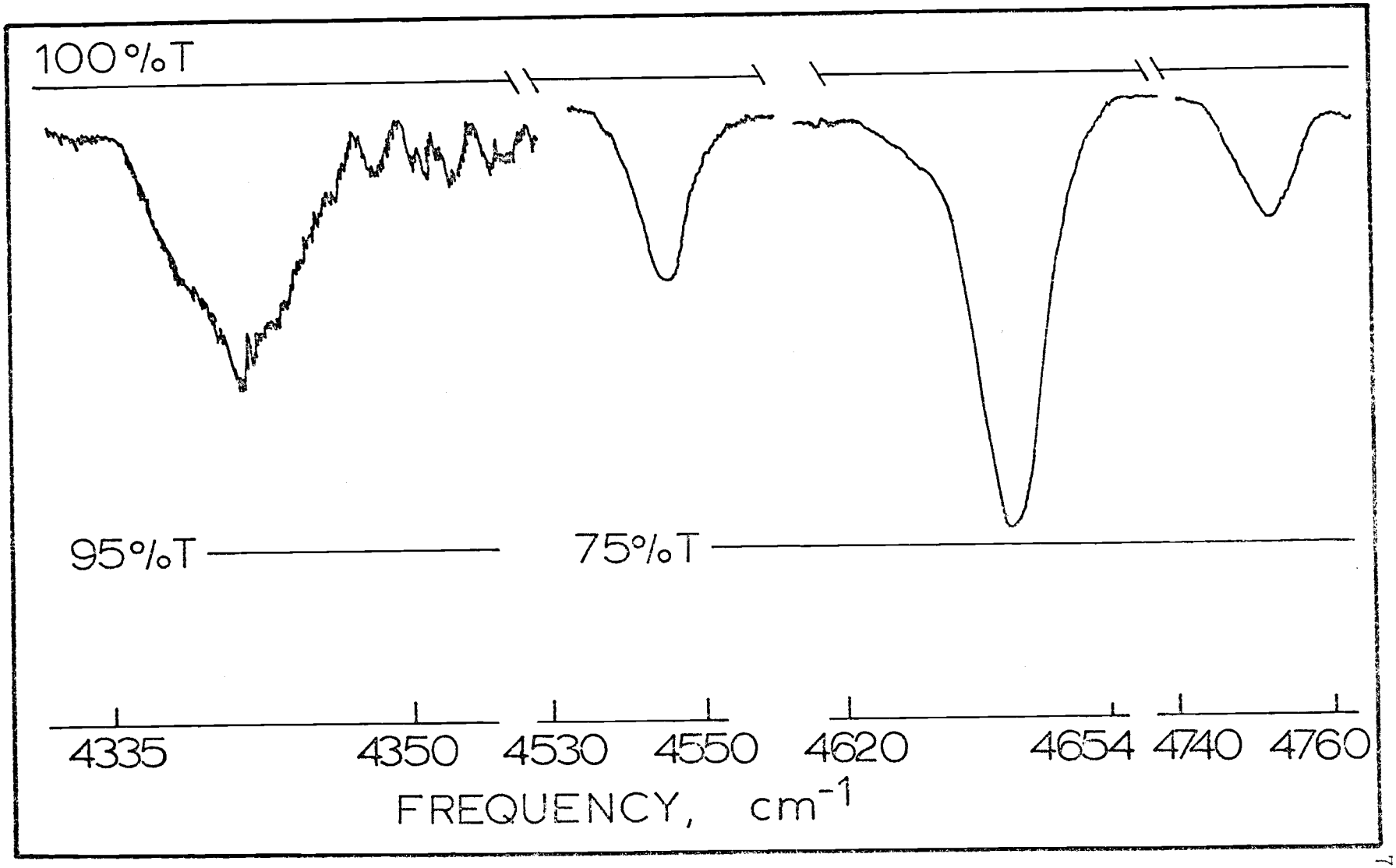
100%T
95%T
75%T
4335
4350
4530
4550
4620
4654
4740
4760
FREQUENCY, cm-1

Weak features observed between 4400 cm^{-1} and 4800 cm^{-1} were assigned to the $00^00 \rightarrow \{ 20^01, 12^01, 04^01\}$ triad. Figure 6-3 shows this triad. No effort was made to determine the exact frequency of these transitions. They are reported in Table 6-12 and the values given are accurate to within three cm^{-1} as dicussed in Chapter Five.

Most of the features of the cyanate spectrum have been explained above. However, impurities other than cyanate, lattice mode effects, and spurious absorbances due to water vapor and CO_2 have not been discussed. Table 5-1 and 5-2 lists other impurity ion frequencies which have been observed during this study in single crystals of KCl and KBr. In Figure 6-2, the broad feature ca. 2370 cm^{-1} is due to the CO_2 band in that region. Lattice effects with the asymmetric stretch are evidenced in Figure 6-2 by broad bands centered at 2240 cm^{-1}, the sharp (cooled)band at 2220 cm^{-1}, the broad band (obscured by ^{13}C absorbances) at ca. 2130 cm^{-1}, and the sharp band at 2050 cm^{-1}. These type bands have been adequately treated by previous investigators (55,56,84) and will not be discussed here.

The preceding arguments have been based on several concepts used by the spectroscopist in analyzing any detailed spectrum. Variables at his command fall into two general categories: (i) those which more affect the intensity of a given band and (ii) those which more affect the location of the band in the absorption spectrum of the impurity ion.

Increasing the concentration of the impurity ion in the medium enables one to distinguish weak features such as higher overtones and combination bands. This can be accomplished by increasing the pathlength;viz., growing longer crystals. Experiments have shown, that cyanate can only be dissolved in alkali halide, using the technique in Chapter Five, to about two-mole percent before decomposition causes the crystal to be non-singular and have bubbles

form in it. Both of these methods were used in this research. Due to the limited quantities of isotopic cyanate, however, highly concentrated cyanate samples of ^{13}C and ^{18}O were never achieved. Another concentration effect is to increase the band width with the accompanying complication that weak features in the fundamental regions are masked by the associated coupling of modes of nearly equal vibrational frequency.

This latter effect has been observed through the satellite lines of the ν_3 fundamental. Walnut (92,p.58-62) has shown that if the coupling is significant, a series of discrete lines will be observed as a result of neighbor ion interaction. Decius (16,p. 1290-1294) has observed this for nitrate and carbonate and has demonstrated that this effect is probable for cyanate (19,p.2183) in KBr. Generally, when the coupling constant is small, only line broadening results, as the effect is usually less than the resolution of the instrument. The net result is that line breadth increases; with the associated difficulty of ascertaining where the peak absorption is truly located. This has been a problem with the ν_2 $\{000 \rightarrow 01^10\}$ fundamental. Thus it can be said that varying the concentration not only affects the observed intensity of bands, but also the position or observed frequency.

Isotopic enrichment is a special category of concentration effect. In this study ^{13}C, ^{15}N and ^{18}O mono-substituted cyanate dopants were introduced into KCl and KBr. By comparing spectra, it was then possible to determine which line was due to the respective isotope. This effect can readily be seen by comparing the representative spectra accompanying this chapter. The assignments listed in the tables agreed very well with Redlich-Teller Product Rule calculations (see Tables 6-17 and 6-18). Qualitatively, heavier isotope substitution shift a given band to lower frequency in the order: 14 12 16>14 12 18>15 12 16>14 13 16.

Another tool at the spectroscopist's disposal is temperature. Maki studied cyanate's frequency change with temperature (54,p. 118-125). He found the shift to higher frequency as the temperature is lowered to be at most 1 cm^{-1} per 100°K for a given band. This result has been confirmed by Schettino and Hisatsune (84). In assigning peaks, the most significant change when lowering the crystal's temperature, is in the spectrum itself. Some peaks dissappear, others sharpen, and weak features become resolved, as the sample is cooled.

When the temperature is lowered, the equilibrium population of excited vibrational states will change. This is manifested in intensity changes in the vibrational spectrum. The Boltzman distribution law is given by:

$$N_u/N_\ell = (du/d\ell)\ \exp\{-(\nu_u - \nu_\ell)\ hc/kT\} \qquad (6\text{-}2)$$

where N_u/N_ℓ is the ratio of the population of the upper state (u) to the lower state (ℓ), d is the associated degeneracy, T the temperature, k the Boltzman constant, and "c" the speed of light. The intensity of any transition is dependent upon this factor. Table 6-15 gives calculated ratios useful in the analysis. The stronger most populated, excited state, in the cyanate spectrum is the ν_2^1 . Transitions from this level are temperature sensitive. This is even more pronounced for the 02^20 level transitions. Cooling the crystal easily distinguishes these bands. This effect can easily be observed in figures accompanying this section. When these "hot" bands are "quenched",weak features due to fundamental transitions of isotopic species become observable in the fundamental regions.

Another effect is the sharpening of absorptions at reduced temperatures, which at room temperature, are smeared out and diffuse. Striking examples of this combination band at~2560 cm^{-1}, the

peak at 3800 cm^{-1}, and the very weak feature at 3950 cm^{-1}, are just a few examples of this phenomenon. The $2\nu_3$ band in Figure 6-3 also shows this effect. In crystals, the occupants of the lattice undergo thermal vibrations about their equilibrium positions. This motion has an amplitude of ca. 0.03 Å (33,p.362) and is sufficient to vary the potential field on the cyanate ion. Thus different cyanate ions are found in slightly different lattice potentials due to thermal fluctuation of the lattice. As the crystal is cooled, the host mean square thermal amplitude decreases and the potential becomes more rigidly defined. Thus the absorption line becomes sharper, and their respective intensities are increased at the absorption peak and are less smeared out.

TABLE 6-15. RATIOS OF POPULATION IN EXCITED STATES (ABOVE $00^0 0$).

ν (cm^{-1})	100°K	300°K
90	0.50	0.64
630 (d=2)	0.091	0.10
1260 (d=2)	$< 10^{-5}$	0.0048
2170		$<10^{-6}$

Another contribution to line broadening is thought to arrise from librational motions of the polyatomic impurity (34). These pseudorotational motions contribute to line broadening at higher temperatures because their higher states are more highly populated. No attempt in this analysis will be made to assign librational peaks although they certainly contribute to the structure observed around the ν_3 fundamental (56,p.116).

Up to this point the discussion has concerned features observed when normal cyanate is introduced an an impurity in KCl. The following discusses isotopic cyanate ions introduced as dopants into KCl.

Table 6-2 and Figures 6-4 and 6-5 show a 97.3 atom-percent ^{15}N-enriched cyanate absorption spectrum. In the bend region, the asymmetry of the ^{15}N ν_2^1 is attributed to the 14 12 16 peak at 631 cm^{-1}. The presence of the strong feature at 590 cm^{-1} is due to the presence of $^{11}BO_2$ ion. The symmetric stretch region confirms 15 12 16 assignments in the normal cyanate spectra. Previous work (56) without the benefit of the ^{15}N-enrichment, had been confused over the assignment of the lower diad members of 15 12 16, 14 13 16 and 14 12 18 cyanate species. While ^{13}C studies had confirmed that the lower member of the species occured at 1195 cm^{-1}, the approximate coincidence of the ^{15}N member could not be conclusively demonstrated and the ^{18}O peak at 1181 cm^{-1} was mistakenly attributed to ^{15}N. Decius suspected this coincidence because of the anomalously higher relative intensity of the lower ^{13}C peak, as previously assigned, in normally occuring cyanate as compared with the ^{13}C enrichment studies (compare Figure 6-1 with Figure 6-8). And so the $00^00 \rightarrow \{10^00, 02^00\}$ transition is at 1196.44 cm^{-1} and 1286.85 cm^{-1} for 15 12 16 cyanate ion. The weak features at 1210 and 1297 cm^{-1} are due to 14 12 16 cyanate ion. The new features revealed by this enrichment are the 15 12 16 "hot" bands both from the 01^10 and 02^20 levels listed in Table 6-2. In addition, the doubly substituted 15 13 16 cyanate fundamentals at 1264.92 and 1183.71 cm^{-1} have been resolved. The upper member of the 15 12 18 diad occurs as a weak and sharp peak upon cooling at 1269.0 cm^{-1} but its lower member at 1167.5 is just barely resolved. Upon cooling the ^{15}N $01^10 \rightarrow \{03^10, 11^10\}$ hot bands at 1166.32 cm^{-1}, a fundamental-type absorption appears, it has been assigned to 15 12 18, and the one resolved at ca. 1193 cm^{-1} could be due to ^{13}C species. These could be satellite type peaks as they were not observed in every ^{15}N spectra and could be localized concentration effect. The di- and tri- substituted cyanate peaks are tabulated in Table 6-5.

Figure 6-5 shows the higher energy regions of the ^{15}N-enriched cyanate ion absorption spectrum. Assignments in these regions parallel those made for normal cyanate. Although many previously unobserved lines were uncovered, none were surprising. The ^{15}N-cyanide band at ca. 2040 cm^{-1} occurs as expected due to its incomplete oxidation to cyanate. $^{15}N^{13}C^{16}O^-$ and $^{15}N^{13}C^{18}O^-$ fundamentals were easily resolved and are listed in Table 6-5; the same situation applies to the $^{15}N^{12}C^{18}O^-$ ν_3 fundamental which occurs at 2156.4 cm^{-1}.

The regions above 3500 cm^{-1} are not shown because of the 15 12 16 cyanates' similarity to the normal cyanate spectra shown in Figure 6-3. These frequencies are listed in Table 6-2. As was noted earlier, the $2\nu_3$ band was first located in this isotopic cyanate in KCl and KBr. Apparently, the absolute intensity of the ^{15}N-cyanate $2\nu_3$ is greater that that of any other cyanate species. The 14 12 16 cyanate concentrations in KBr and KCl crystals, which were examined for $2\nu_3$, were higher but gave weaker $2\nu_3$ peaks. The reason for this is tied up in the mode's center of mass change effect on the molecule's dipole moment and mechanical-electrical anharmonicity. Further intensity studies in this area should provide a more detailed explanation of this phenomenon. It would also be interesting to examine the region above 6000 cm^{-1} for the $3\nu_3$ band.

Figures 6-6 and 6-7 show a 40 mole-percent ^{18}O-enriched cyanate spectrum. Although many ^{18}O-enriched samples were prepared, high concentration cyanate doped KCl single crystals were never achieved. As expected, the symmetric stretch region was most affected by ^{18}O substitution, and 14 13 18 and 15 12 18 cyanate peaks were only weakly observable. By studying the normal cyanate spectra (Figures 6-1 and 6-2) it was possible to discern those features due to 14 12 18 cyanate, and these are tabulated in Table 6-3.

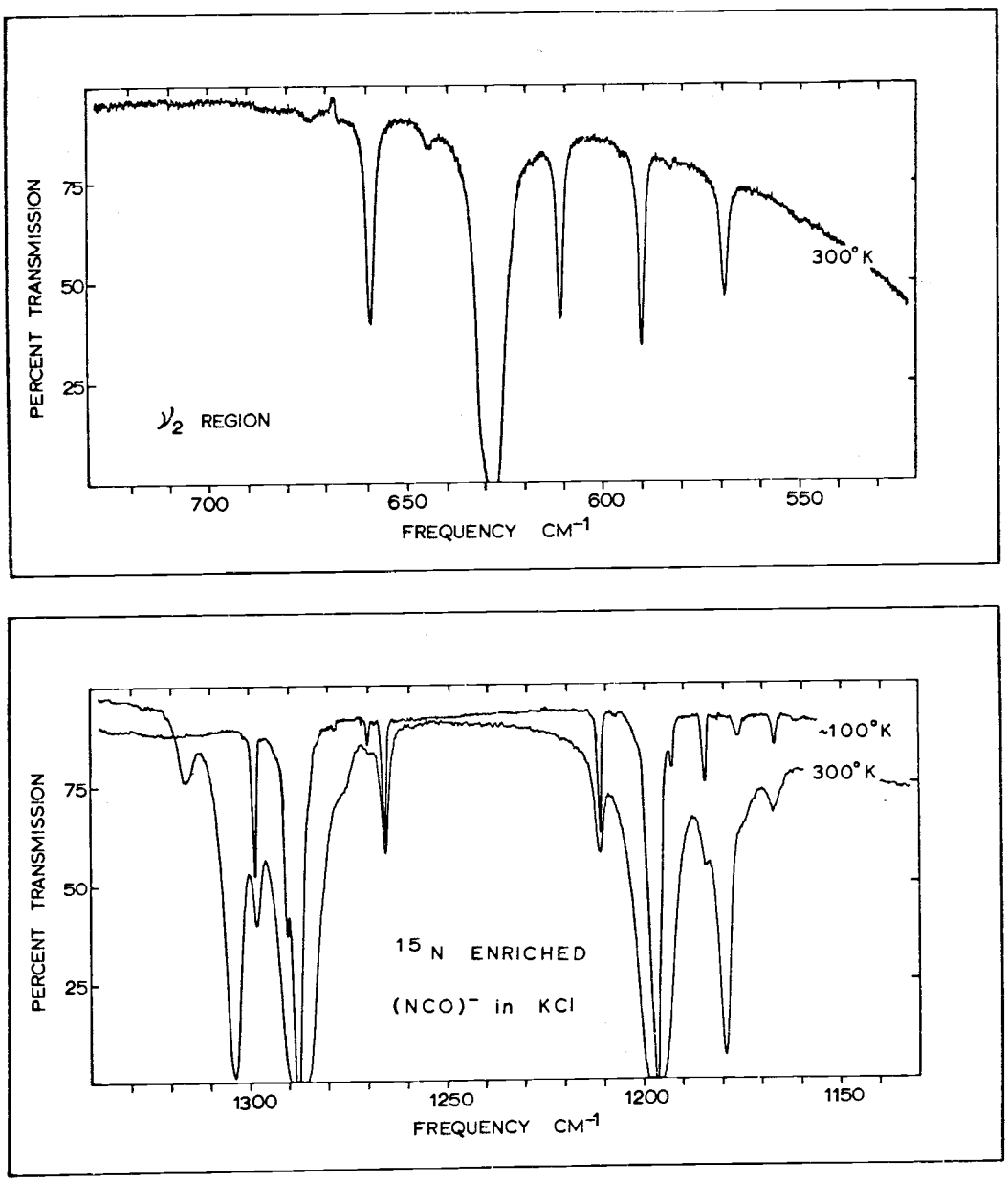

Figure 6-4. Infrared spectrum of a 97.3 atom-percent ^{15}N-enriched cyanate doped KCl crystal. The cyanate ion concentration is approximately 0.75 to 1.25 weight-percent. The upper figure shows the bending region and the lower figure shows the Fermi fundamental region.

Figure 6-5

Infrared spectrum of a 97.3 atom-percent 15-nitrogen enriched cyanate ion doped potassium chloride crystal showing the significant absorptions from 2000 cm^{-1} to 3500 cm^{-1} at 100°K and 300°K.

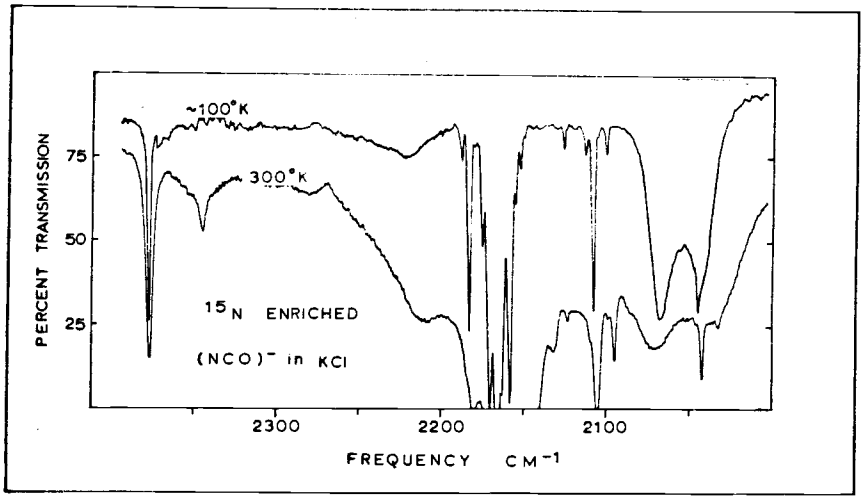
~100°K
300°K
^{15}N ENRICHED
(NCO)$^-$ in KCl
PERCENT TRANSMISSION
75
50
25
2300
2200
2100
FREQUENCY CM^{-1}

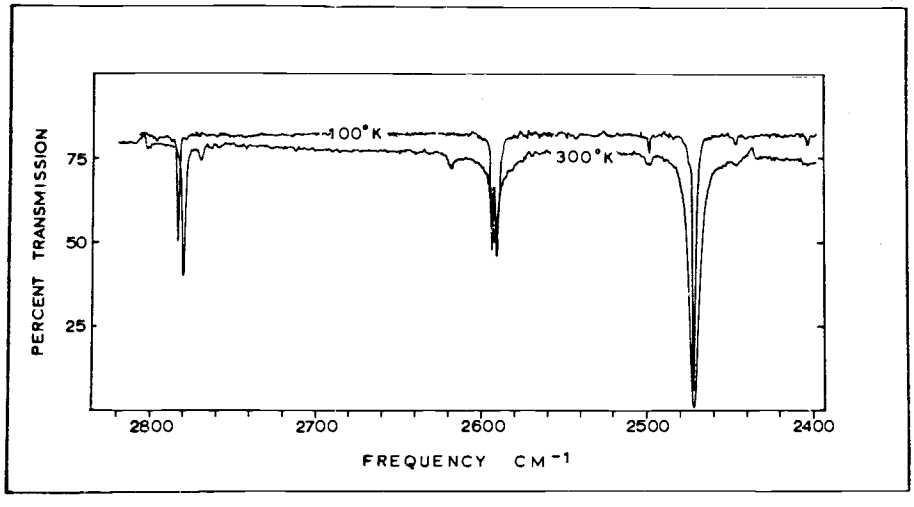
~100°K
300°K
PERCENT TRANSMISSION
75
50
25
2800
2700
2600
2500
2400
FREQUENCY CM^{-1}

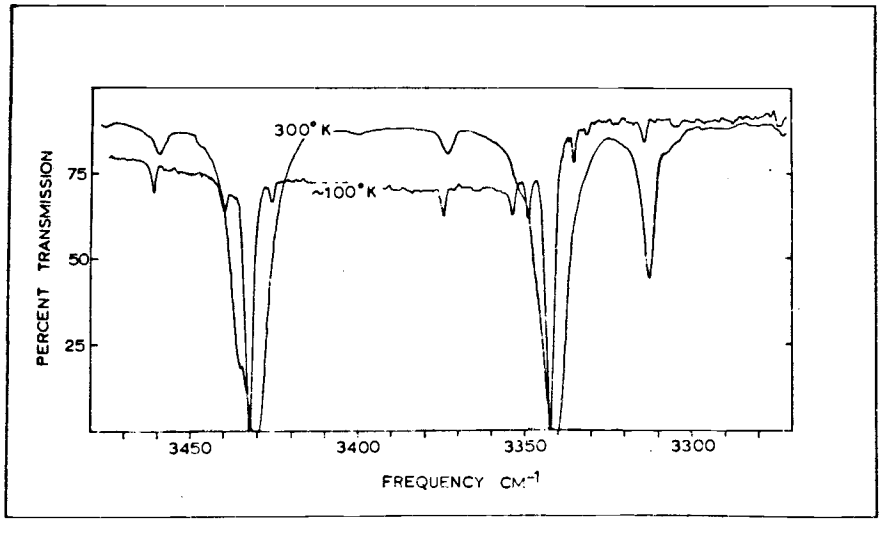
300°K
~100°K
PERCENT TRANSMISSION
75
50
25
3450
3400
3350
3300
FREQUENCY CM^{-1}

TABLE 6-2. ASSIGNMENTS FOR $^{15}N^{12}C^{16}O^-$ CYANATE VIBRATIONAL FREQUENCIES IN KCL.

Initial State	Final State	Observed Frequency(cm^{-1})	Precision ($\pm cm^{-1}$)
00^00	01^10	627.43	0.05
00^00	10^00	1196.44	0.05
	02^00	1286.85	0.05
00^00	00^01	2165.30	0.10
	20^00	2377.47	0.42
00^00	12^00	2471.81	0.22
	04^00	2593.60	0.60
00^00	10^01	3341.40	0.06
	02^01	3430.52	0.07
00^00	01^11	2781.01	0.06
	30^00	3583.0	
	22^00	3648.7	3.0
00^00	14^00	3760.0	3.0
	06^00	3917	
00^00	00^02	4306.95	0.03
	20^01	4502.0	2.0
00^00	12^01	4597.0	2.0
	04^01	4716.2	2.0
01^10	10^00	568.92	0.04
	02^00	659.35	0.05
01^10	11^10	1178.83	0.05
	03^10	1303.31	0.05
01^10	01^11	2153.94	0.14
01^10	02^21	2770.71	0.07
01^10	11^11	3312.7	0.2
	03^11	3435.3	0.4

TABLE 6-2. (Continued).

Initial State	Final State	Observed Frequency(cm^{-1})	Precision ($\pm$ cm^{-1})
02^20	11^10	551.0	0.2
	03^10	675.0	0.2
02^20	12^20	1315.33	0.07
	04^20	1166.32	0.05
02^20	02^21	2143.31	0.16

TABLE 6-3. ASSIGNMENTS FOR $^{14}N^{12}C^{18}O^-$ CYANATE VIBRATIONAL FREQUENCIES IN KCL.

00^00	01^10	626.25	0.08
00^00	10^00	1181.52	0.08
	02^00	1277.73	0.05
00^00	00^01	2172.74	0.06
	20^00	2350.66	0.14
00^00	12^00	2443.62	0.10
	04^00	2576.10	0.16
00^00	01^11	2788.82	0.08
00^00	10^01	3336.3	0.2
	02^01	3432.0	0.2
00^00	20^01 12^01 04^01	4578.0	2.0
01^10	10^00	556	(weak)
	02^00	651.45	0.04
01^10	11^10	1164.93	0.05
	03^10	1293.73	0.07
01^10	01^11	2161.6	0.1
01^10	11^11	3310.0	0.4
	03^11	3435.5	0.4

TABLE 6-3. (Continued).

Initial State	Final State	Observed Frequency(cm^{-1})	Precision (± cm^{-1})
01^10	02^21	2780	2.0
02^20	02^21	2149.5	0.1

TABLE 6-4. ASSIGNMENTS FOR $^{14}N^{13}C^{16}O^-$ CYANATE VIBRATIONAL FREQUENCIES IN KCL.

00^00	01^10	614.10	0.09
00^00	10^00	1195.18	0.04
	02^00	1277.43	0.04
00^00	00^01	2124.10	0.10
	20^00	2369.23	0.50
00^00	12^00	2473.93	0.05
	04^00	2565.16	0.05
00^00	01^11	2728.01	0.04
00^00	10^01	3300.68	0.20
	02^01	3383.08	0.20
	20^01	4453.0	3.0
00^00	12^01	4560.6	1.0
	04^01	4651.4	2.0
01^10	10^00	663.90	0.90
	02^00	581.32	0.04
01^10	11^10	1178.67	0.10
	03^10	1292.53	0.10
01^10	01^11	2113.6	0.10
01^10	02^21	2718.69	0.97

TABLE 6-4. (Continued).

Initial State	Final State	Observed Frequency(cm^{-1})	Precision ($\pm$ cm^{-1})
01^10	11^11	3273.8	0.4
	03^11	3363	0.3
02^20	02^21	2102.4	0.1

Figures 6-8 and 6-9 depict a 60 mole-percent ^{13}C-enriched cyanate spectrum in potassium chloride single crystal. The assignments for the $^{14}N^{13}C^{16}O^-$ species are listed in Table 6-4. While we were not able to locate $2\nu_3$ for either the 14 13 16 or the 14 12 18 cyanate species, the weak triplet above 4000 cm^{-1} was found at frequencies predicted by the potential energy calculations. In the 14 13 16 cyanate case, all three were located; however, in the 14 12 18 cyanate species, owing to the weaker dopant level, only the strongest band could be identified.

Table 6-5 lists bands assigned to di- and tri-substituted cyanate species in KCl. Table 6-6 lists fine structure detail in KCl which was discussed in the earlier sections of this chapter and includes the satellites observed about the isotopic peaks.

TABLE 6-5. OTHER ISOTOPIC CYANATE FREQUENCIES IN KCL.

Initial State	Final State	$^{15}N^{13}C^{16}O^-$	$^{15}N^{12}C^{18}O^-$	$^{14}N^{13}C^{18}O^-$	$^{15}N^{13}C^{18}O^-$
00^00	01^10	610.53±.04	624	609.8	606.5±.5
00^00	10^00	1183.71±.12	1167.5±1	1171.80±.10	
	02^00	1264.92±.07	1269.0±.5	1251.92±.14	
00^00	00^01	2106.86±.07	2156.4±.5	2116.60±.20	2097±2
01^10	01^11	2096.37±.11			
01^10	11^10	1166.3±.1			
	03^10	1280 ±1.0			

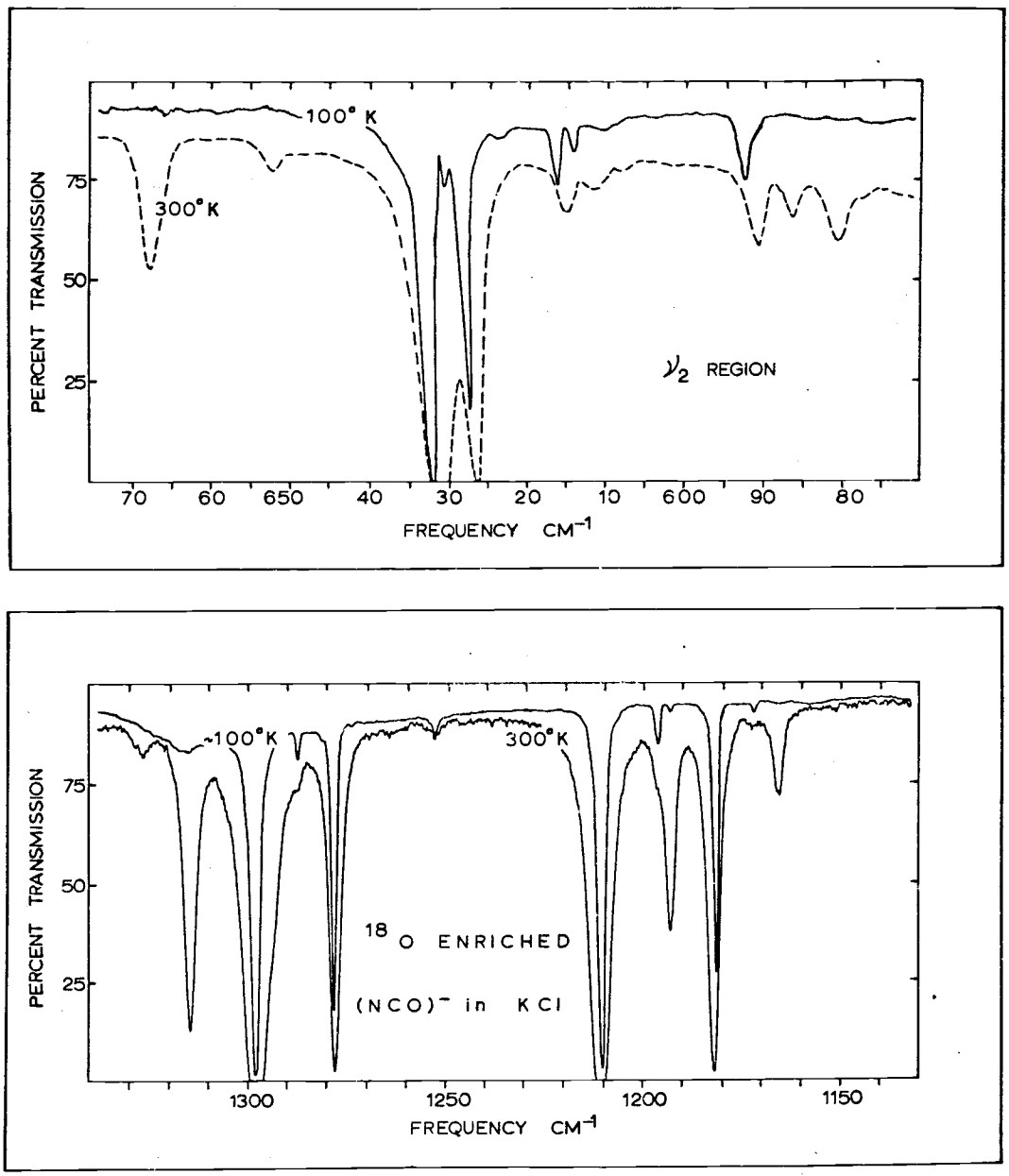

Figure 6-6. Infrared spectrum of an approximately 40 atom-percent ^{18}O-enriched cyanate ion doped KCl crystal. The doping level is between 0.5 and 1.0 weight-percent. The upper figures shows the bending region and the lower figure shows the Fermi fundamental region.

Figure 6-7

Infrared spectrum of an approximately 40 atom-percent 18-oxygen enriched cyanate ion doped potassium chloride crystal. These spectra show the resolvable features between 2000 cm^{-1} to 3500 cm^{-1} at 100°K and 300°K.

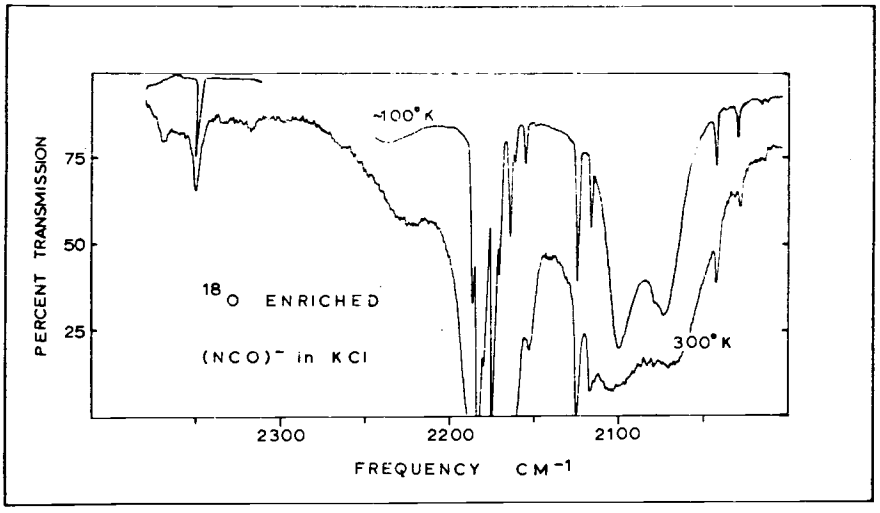
PERCENT TRANSMISSION
75
50
25
~100°K
^{18}O ENRICHED
$(NCO)^-$ in KCl
300°K
2300
2200
2100
FREQUENCY CM^{-1}

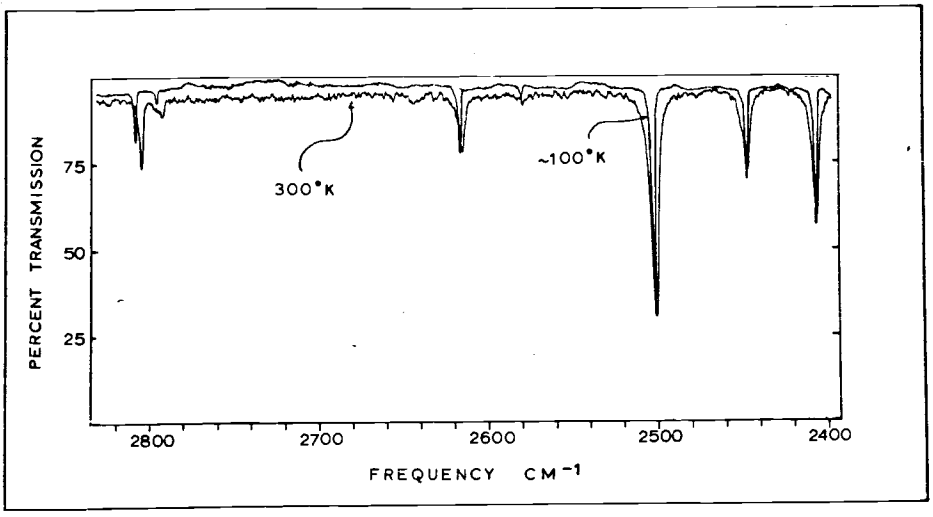
PERCENT TRANSMISSION
75
50
25
300°K
~100°K
2800
2700
2600
2500
2400
FREQUENCY CM^{-1}

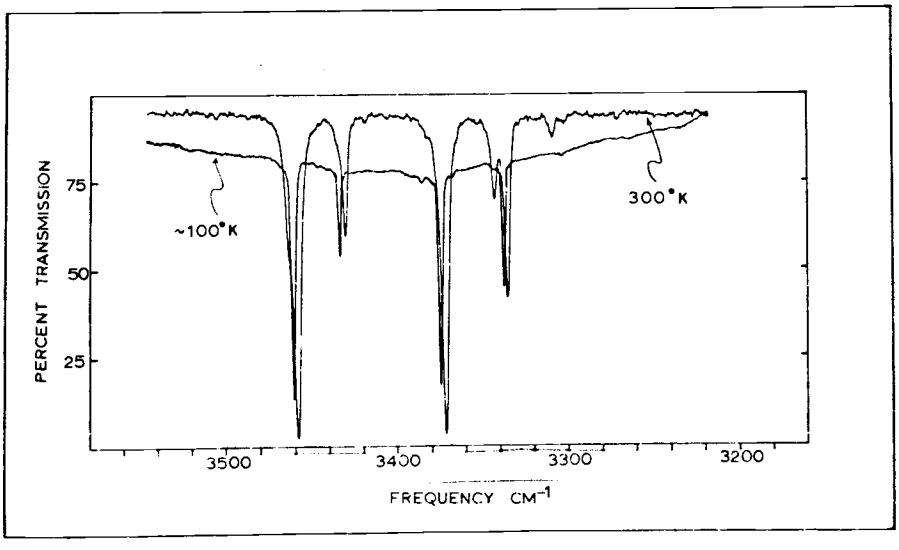
PERCENT TRANSMISSION
75
50
25
~100°K
300°K
3500
3400
3300
3200
FREQUENCY CM^{-1}

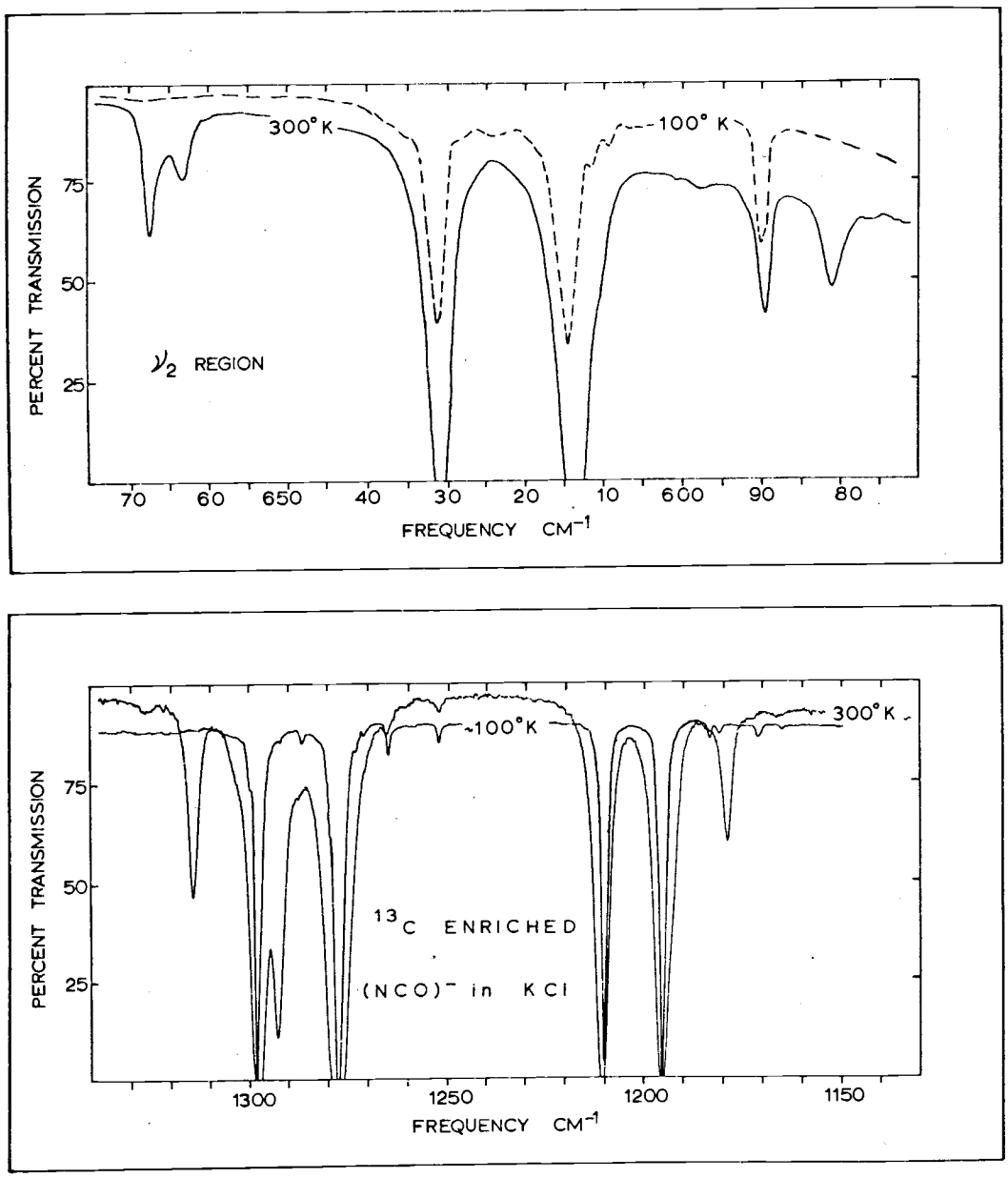

Figure 6-8. Infrared spectrum of a 60 atom-percent ^{13}C-enriched cyanate ion doped KCl crystal. The doping level is between one and two weight-percent. The upper figure shows the bending region and the lower figure depicts the Fermi fundamental region at 100°K and 300°K.

Figure 6-9

Infrared spectrum of a 60 atom-percent 13-carbon enriched cyanate ion doped potassium chloride crystal between 2000 cm^{-1} and 3500 cm^{-1}.

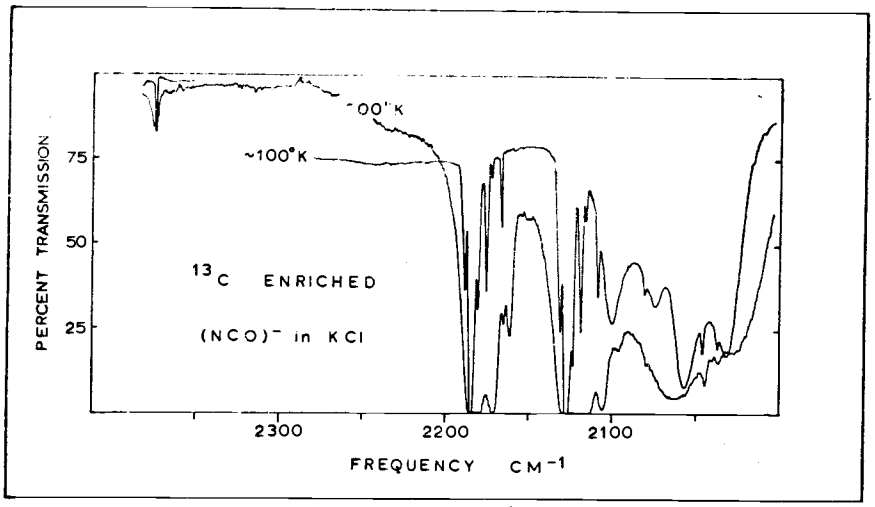
~100°K
PERCENT TRANSMISSION
75
50
25
^{13}C ENRICHED
(NCO)$^-$ in KCl
2300
2200
2100
FREQUENCY CM^{-1}

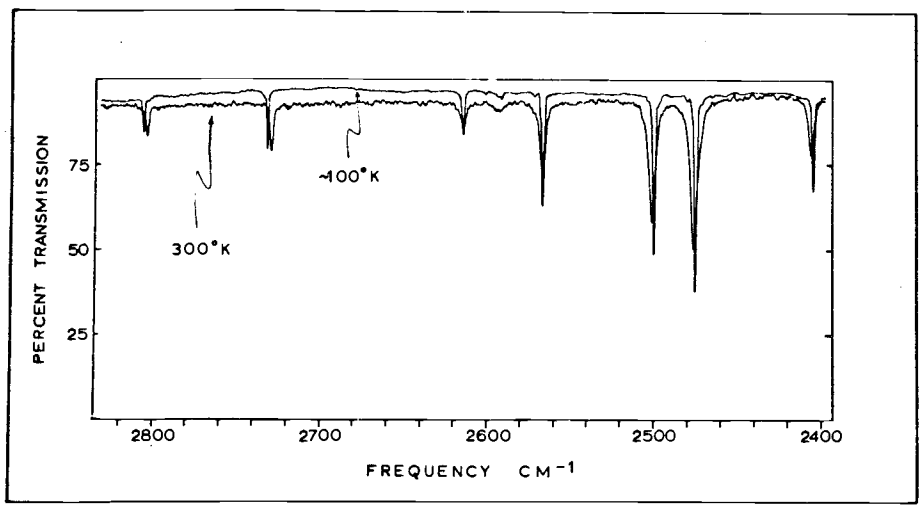
PERCENT TRANSMISSION
75
50
25
300°K
~100°K
2800
2700
2600
2500
2400
FREQUENCY CM^{-1}

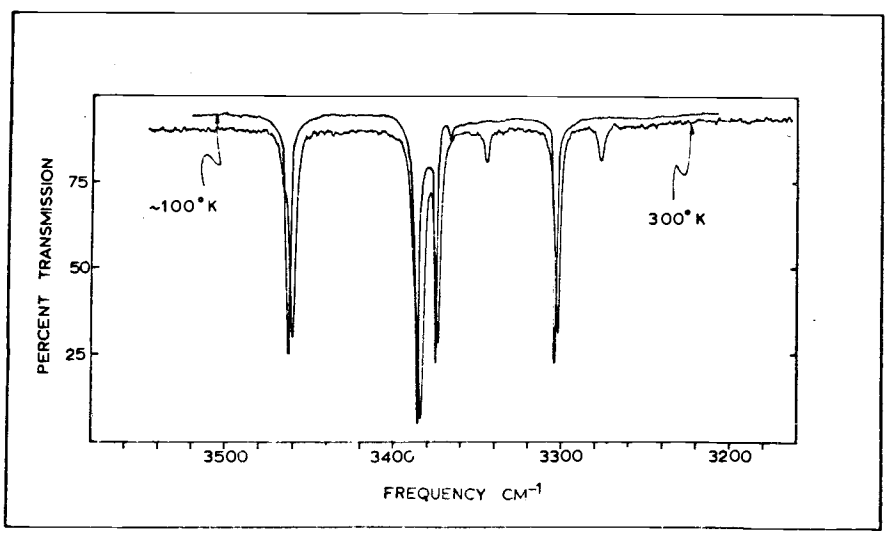
PERCENT TRANSMISSION
75
50
25
~100°K
300°K
3500
3400
3300
3200
FREQUENCY CM^{-1}

TABLE 6-6. FINE STRUCTURE DUE TO CYANATE ION IN KCL.

Main Peak(from the ground 00^00 level), Isotope, Frequency (cm^{-1})	Satellites, from Main Peak ($\pm cm^{-1}$)
00^01, $^{14}N^{12}C^{16}O^-$, 2181.88	-3.6, +4.4
01^11, $^{14}N^{12}C^{16}O^-$, 2801.72	-4.5, +7.5
10^01, $^{14}N^{12}C^{16}O^-$, 3372.5	-11.0, -7.6, +5.8, +11.0
02^01 3458.7	-10.6, -7.6, +6.2
00^01 $^{14}N^{13}C^{16}O^-$, 2124.10	-3.5, +4.4
00^01 $^{15}N^{12}C^{16}O^-$, 2165.30	-2.5
00^01 $^{14}N^{12}C^{18}O^-$, 2172.74	-2.9, +2.1
00^01 $^{14}N^{13}C^{18}O^-$, 2116.60	+2.5
20^00 2402.88	-3.3, +2.5
12^00 $^{14}N^{12}C^{16}O^-$, 2499.26	-4.0, +3.0
04^00 2612.80	-4.7, +3.8

CYANATE ION IN POTASSIUM BROMIDE

The infrared spectrum of the cyanate impurity ion in potassium bromide is almost the same as its spectrum in KCl except that all frequencies are lower. For this reason, only a brief discription of the major differences between the two will be mentioned here. Maki and Decius (56) have elucidated the normal cyanate spectra in KBr in great detail, and Maki (54) was able to observe the strongest 14 13 16 fundamentals in an enriched sample pellet. This research extends their work to enriched isotopic cyanate species in KBr single crystals.

The effect of changing lattices from KCl to KBr has been discussed in Chapter Two. It can be thought of as decreasing the pressure on the impurity ion as the lattice dimensions increase in KBr; the short range repulsive forces predominate. Slyhouse and Drickamer (85,p.1226-1227) studied the cyanate spectrum (mistakenly identified as cyanide) in a crystal lattice under high pressure.

This is exactly what is observed by changing lattices, as the KBr frequencies are lower for all the peaks of the cyanate impurity ions.

The frequency data listed in Table 6-7 tabulates absorption bands which were redetermined during this study. It will be noted that the ν_2 changes by two cm^{-1} while ν_3 changes by 12 cm^{-1} from KCl to KBr (refer to Table 6-1). The last column of the table shows the difference between Maki's data and that arrived at in this research. The blank entries show which bands were not observed by Maki.[-7] It was necessary to redetermine the normal cyanate data to provide an internally consistent set of frequencies from which anharmonicity and potential constants could be calculated. The spectrum of normal cyanate is not shown by itself because of its similarity to Figures 6-1, 6-2, and 6-3, however, it is present in Figures 6-12 and 6-13.

TABLE 6-7. ASSIGNMENTS FOR $^{14}N^{12}C^{16}O^-$ VIBRATIONAL FREQUENCIES IN KBR.

Initial State	Final State	Observed Frequency(cm^{-1})	Precision ($\pm$ cm-1)	Δ [-8] ($\pm$ cm^{-1})
00^00	01^10	629.40	0.05	0.0
00^00	10^00	1205.47	0.05	-0.0
	02^00	1292.57	0.05	-0.0
00^00	11^10	1817.10	0.05	
	03^10	1938.42	0.05	
00^00	00^01	2169.60	0.05	0.0

[-7] The majority of these were subsequently found by Decius, et al. (19, p.2181-2183).

[-8] Comparison with data of Maki and Decius (56, p.774). The Δ is calculated by subtracting the earlier data from that listed above.

TABLE 6-7. CONTINUED.

Initial State	Final State	Observed Frequency (cm^{-1})	Precision (±cm-1)	Δ^{-8} (± cm-1)
	20^00	2393.43	0.05	0.5
00^00	12^00	2487.82	0.06	0.5
	04^00	2603.61	0.06	1.1
00^00	01^11	2787.71	0.08	0.4
00^00	10^01	3354.69	0.07	0.3
	02^01	3440.68	0.05	1.3
	30^00	3563.6	0.4	
00^00	22^00	3675.6	0.4	
	14^00	3781.4	0.6	
	06^00			
00^00	00^02	4381	5.0	
	20^01	4523.2	2.0	
00^00	12^01	4617.5	1.0	
	04^01	4732.0	2.0	
01^10	10^00	576.05	0.05	1.7
	02^00	663.48	0.05	0.3
01^10	11^10	1187.52	0.05	0.6
	03^10	1308.85	0.05	0.4
01^10	01^11	2158.40	0.05	0.2
01^10	10^01	2725.44	0.05	0.4
	02^01	2811.73	0.07	1.3
01^10	02^21	2777.01	0.11	0.4
01^10	11^11	3325.9	0.10	0.2
	03^11	3446.73	0.08	
02^20	11^10	577.73	0.04	
	03^10	678.89	0.07	
02^20	12^20	1174.27	0.07	1.3
	04^20	1320.63	0.05	0.2
02^20	02^21	2148.02	0.05	0.1

The remaining data in this section show isotopic assignment information which parallels that found for KCl. Table 6-8 tabulates 15 12 16 data obtained from 97 mole-percent enriched sample depicted in Figures 6-10 and 6-11 (note the weak 14 12 16 ν_3 fundamental at 2169).

TABLE 6-8. ASSIGNMENTS FOR $^{15}N^{12}C^{16}O^-$ CYANATE VIBRATIONAL FREQUENCIES IN KBR.

Initial State	Final State	Observed Frequency (cm^{-1})	Precision ($\pm$ cm^{-1})
00^00	01^10	625.87	0.09
00^00	10^00	1191.28	0.05
	02^00	1282.33	0.05
00^00	00^01	2153.00	0.10
	20^00	2367.45	0.10
00^00	12^00	2461.28	0.10
	04^00	2584.36	0.12
00^00	01^11	2767.31	0.07
00^00	10^01	3324.00	0.08
	02^01	3414.05	0.10
	20^01	4479.9	1.0
00^00	12^01	4573.1	1.0
	04^01	4695.8	1.5
01^10	10^00	565.29	0.03
	02^00	656.23	0.04
01^10	11^10	1173.84	0.04
	03^10	1298.72	0.04
01^10	01^11	2141.46	0.10
01^10	02^21	2757.17	0.03
01^10	11^11	3296.4	0.2
	03^11	3420.5	0.3

TABLE 6-8. CONTINUED.

Initial State	Final State	Frequencies Observed (cm^{-1})	Precision ($\pm$ cm^{-1})
02^20	12^20	1161.51	0.05
	04^20	1310.25	0.05
02^20	02^21	2131.5	1.0
00^00	00^02	4282.87	0.03
00^00	30^00	3523.8	1.0
	22^00	3631.6	1.0
	14^00	3747.6	1.0
	06^00	3904	4.0

Table 6-9 shows data derived from ^{18}O-enriched cyanate both in pellets an ca. 20 mole percent ^{18}O-enriched cyanate doped crystals. The low enrichment level can easily be seen in Figures 6-12 and 6-13. In Figures 6-12, the $1^4\ 12\ 18$ ν_2 appears as a weakly resolved shoulder on the 629 cm^{-1} peak and its associated "hot" bands can not be distinguished at all. The resolution of the ^{13}C and ^{18}O Fermi doublet peaks at 1272 cm^{-1} is readily apparent.

TABLE 6-9. ASSIGNMENTS FOR $^{14}N^{12}C^{18}O^-$ CYANATE VIBRATIONAL FREQUENCIES IN KBR.

Initial State	Final State	Frequencies Observed (cm^{-1})	Percision ($\pm$ cm^{-1})
00^00	01^10	624.72	0.07
00^00	10^00	1176.37	0.05
	02^00	1272.95	0.04
00^00	00^01	2161.66	0.10
	20^00	2340.78	0.5
00^00	12^00	2434.06	0.5
	04^00	2568.52	0.5
00^00	01^11	2775.62	0.1

TABLE 6-9. CONTINUED.

Initial State	Final State	Frequencies Observed (cm^{-1})	Precision ($\pm cm^{-1}$)
00^00	10^01	3319.2	0.2
	02^01	3414.7	0.2
00^00	20^01 12^01 04^01	4556.7	2.0
01^10	10^00	553.2	0.5
	02^00	648	1.0
01^10	11^10	1160.08	0.05
	03^10	1290	3.0
01^10	11^11	3293	1.0
	03^11	3418.5	1.0
02^20	02^21	2140.0.	0.3
10^00 02^00	11^10 03^10	634	1.0

The 14 13 16 enriched spectrum duplicates Figures 6-8 and 6-9 (KCl) and no concentration samples were prepared of this isotope in KBr. Table 6-10 presents the frequency data attributed to this isotopic species. Table 6-11 shows bands assigned to doubly substituted cyanates and one resolvable peak attributed to 15 13 18.
Some satellite structure was observed for cyanate samples in KBr but owing to the low cyanate doping level used in this environment, not many occured.

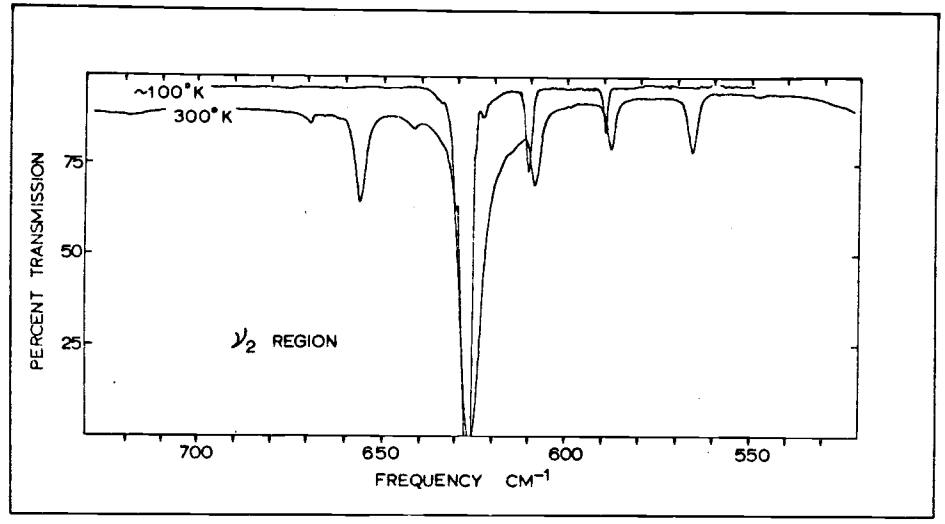

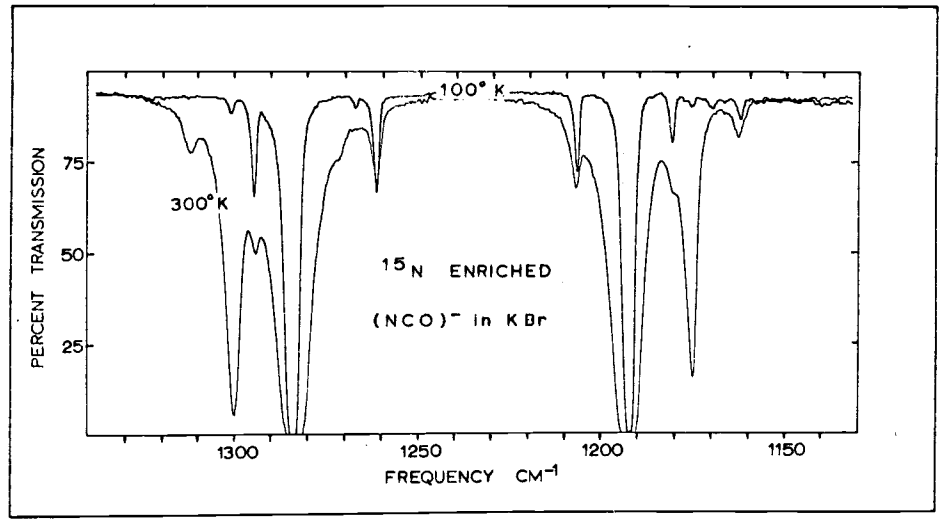

Figure 6-10

Infrared spectrum of a 97.3 atom-percent 15-nitrogen enriched cyanate ion in a potassium bromide crystal. The doping level is between one and two weight-percent.

Figure 6-11

Infrared spectrum of a 97.3 atom-percent 15-nitrogen enriched cyanate ion in a potassium bromide crystal between 2000 cm^{-1} and 3500 cm^{-1}.

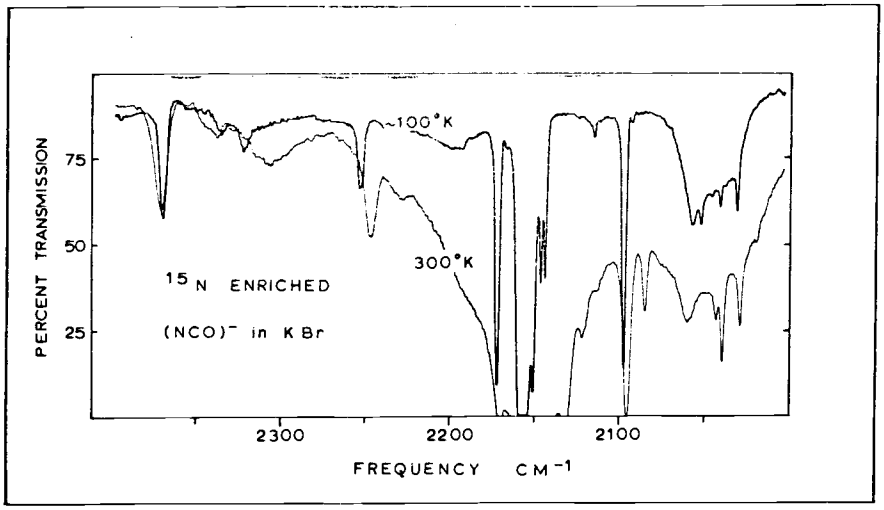
PERCENT TRANSMISSION
75
50
25
~100°K
300°K
^{15}N ENRICHED
(NCO)$^-$ in KBr
2300
2200
2100
FREQUENCY CM^{-1}

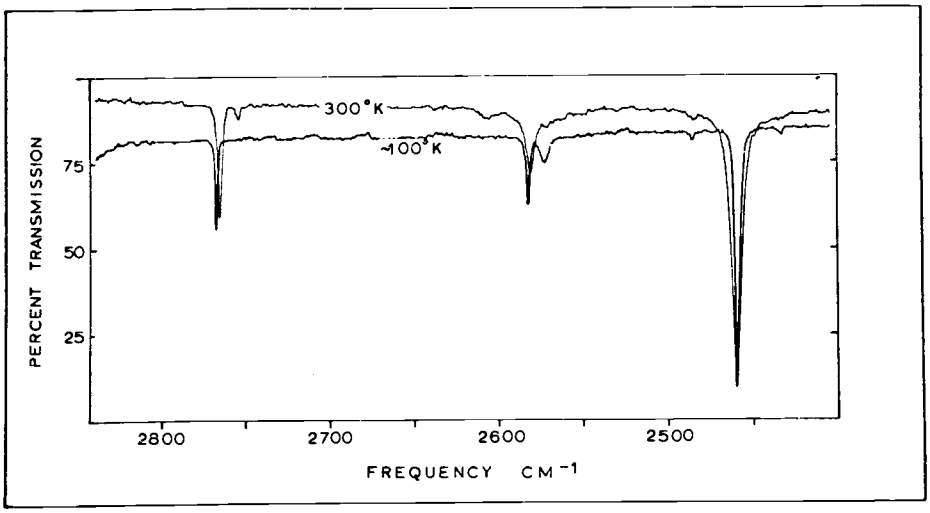
PERCENT TRANSMISSION
75
50
25
300°K
~100°K
2800
2700
2600
2500
FREQUENCY CM^{-1}

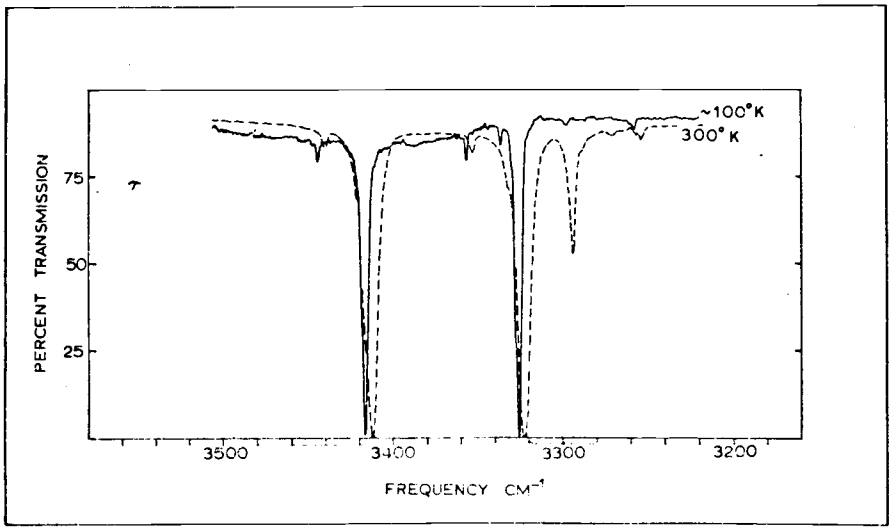
PERCENT TRANSMISSION
75
50
25
~100°K
300°K
3500
3400
3300
3200
FREQUENCY CM^{-1}

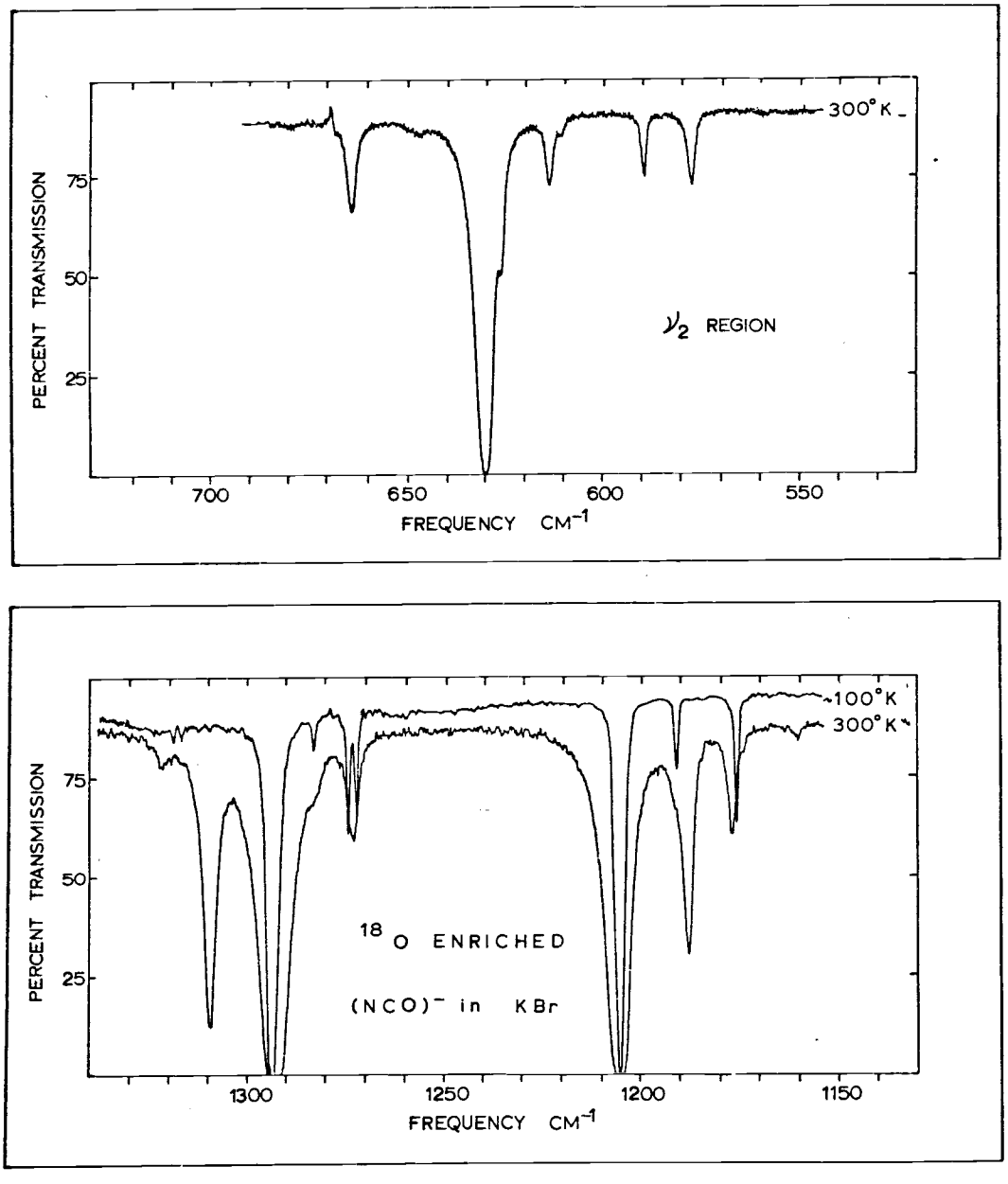

Figure 6-12. Infrared spectrum of a two to five atom-percent ^{18}O-enriched cyanate ion in a KBr crystal. The upper spectrum shows the bending region and the lower shows the Fermi fundamental region.

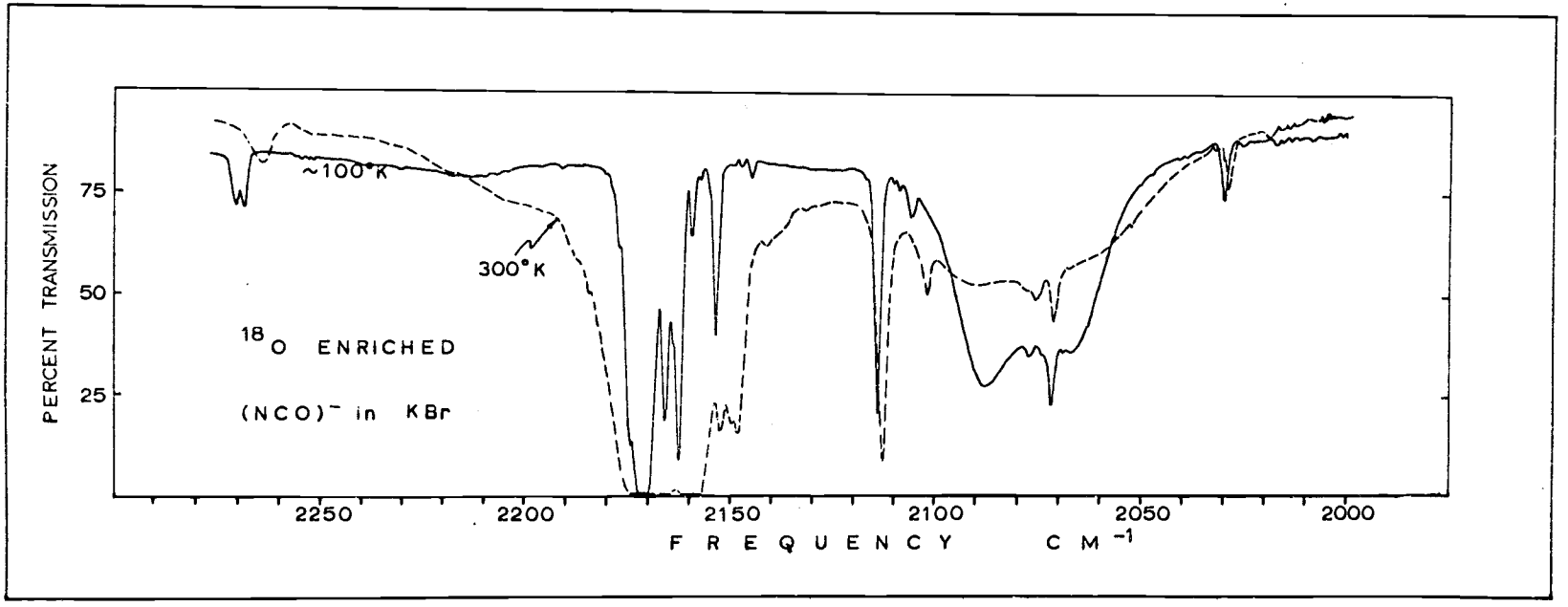

Figure 6-13

Infrared spectrum of a two to five atom-percent 18-oxygen enriched cyanate ion in a potassium bromide crystal. The doping level is less than two-weight percent. This figure shows the asymmetric stretch region between 2000 cm^{-1} and 2300 cm^{-1} at 100°K and 300°K.

TABLE 6-10. ASSIGNMENTS FOR $^{14}N^{13}C^{16}O^-$ CYANATE VIBRATION FREQUENCIES IN KBR.

Initial State	Final State	Observed Frequency (cm^{-1})	Precision ($\pm$ cm^{-1})
00^00	01^10	611.9	0.3
00^00	10^00	1191.00	0.05
	02^00	1271.10	0.03
00^00	00^01	2112.74	0.05
	20^00	2360.3	0.5
00^00	12^00	2462.2	0.5
	04^00	2553.9	0.5
00^00	01^11	2714.85	0.03
00^00	10^01	3283.72	0.20
	02^01	3363	1.0
01^10	11^10	1174.3	0.5
	03^10	1285.70	0.05
01^10	01^11	2102.07	0.2

TABLE 6-11. ASSIGNMENTS FOR OTHER ISOTOPIC CYANATES IN KBR.

Initial	Final	$^{15}N^{13}C^{16}O^-$	$^{15}N^{12}C^{18}O^-$	$^{14}N^{13}C^{18}O^-$	$^{15}N^{13}C^{18}O^-$
00^00	01^10	608.95±.07	618±1	607.8±.5	604.5±.07
00^00	100	1180.02±.07	1161±3	1166.5±.11	
	02^00	1259.70±.04	1265±2	1247.59±.10	
00^00	00^01	2094.76±.05	2144±4	2104.33±.05	
01^10	11^10	1162.2±.5			
	03^10				
01^10	01^11	2084.0±.1			

ASSIGNMENT SUMMARY

During this research well over 300 absorbance bands were studied. About 40 percent of them had never before been reported. Thus organizing the myriad of frequencies into a suitably intelligible format presents a problem. The first portion of this section will present the data summarized in two ways. The latter portion deals with the Redlich-Teller Product Rule and Noether's Rule calculations and their application to the data.

Table 6-12 lists cyanate bands by relative intensity in KCl and Table 6-13 presents the corresponding data in the KBr lattice. These two tables show how the various vibrational transitions are affected by monoisotopic substitution. The tables also show which isotopic peaks are to be expected when only a normal cyanate doped crystal is studied. If one compares Table 6-12 with 6-13, it is immediately apparent that the normal cyanate concentration was higher (in this study) in KCl because more isotopic peaks were observed. This was indeed the case. Table 6-12 does represent a crystal which is as saturated as the procedures outlined in Chapter Five will permit. This concentration is crudely estimated to be about four to six percent by weight.

Table 6-14 is a comprehensive listing of all cyanate bands, excluding satellites, found during this study. Included are some weak features not listed in Tables 6-1 through 6-13. Many of these features were assigned by using the results of the potential energy and anharmonic constant calculations which are presented in Chapter Seven. Table 6-14 is arranged by spectral region. It is organized to allow one to compare the effect of the lattice environment upon each transition for each isotopic species for which an absorbance has been observed.

TABLE 6-12. SUMMARY OF CYANATE BANDS IN KCL IN ORDER OF APPARENT ABSORBANCE STRENGTH[-9,10]

Transition	$^{14}N^{12}C^{16}O^-$	$^{14}N^{13}C^{16}O^-$	$^{15}N^{12}C^{16}O^-$	$^{14}N^{12}C^{18}O^-$
$00^00 \rightarrow 00^01$	2181.88	2124.10	2165.30[c]	2172.74[c]
$00^00 \rightarrow 10^00$	1210.59	1195.18[c]	1196.44[c]	1181.52[c]
02^00	1297.40	1277.43	1286.85[c]	1277.73
$00^00 \rightarrow 01^10$	631.17	614.10	627.43[c]	626.25[c]
$01^10 \rightarrow 01^11$	2170.57	2113.6	2153.94	2161.6
$01^10 \rightarrow 11^10$	1192.43	1178.67	1178.83	1164.93
03^10	1314.17	1292.53	1303.31	1293.73
$00^00 \rightarrow 10^01$	3372.5	3300.68	3341.40	3336.3[c]
02^01	3458.7	3383.08[c]	3430.52	3432.0
$00^00 \rightarrow 20^00$	2402.88	2369.23[c]	2377.47[c]	2350.66
12^00	2499.26	2473.93	2471.81[c]	2443.62[c]
04^00	2612.80	2565.16[c]	2593.60[c]	2576.10
$00^00 \rightarrow 01^11$	2801.72	2728.01[c]	2781.01[c]	2788.82
$01^10 \rightarrow 10^00$	666.88	663.90	659.35	651.45
02^00	579.65	581.32	568.92	556.
$02^20 \rightarrow 02^21$	2160.35	2102.4	2143.31	2149.5
$01^10 \rightarrow 11^11$	3342.4	3273.8	3312.7	3310.0
03^11	3462.5	3363.	3435.3	3435.5
$01^10 \rightarrow 02^21$	2791.12	2718.69	2770.71	2780.

-9 Frequencies due to isotopic species which are underlined may be distinguishable in concentrated single crystals with normally occurring cyanate dopant. The other frequencies were observed in enriched samples. All values reported here are vacuum wave numbers at 300°K.

-10 Observable in normally occurring cyanate doped crystals upon cooling to quench "hot" bands, are designated by a (c). The frequencies reported here have been corrected to 300°K.

TABLE 6-12. CONTINUED.

Transition	$^{14}N^{12}C^{16}O^-$	$^{14}N^{13}C^{16}O^-$	$^{15}N^{12}C^{16}O^-$	$^{14}N^{12}C^{18}O^-$
$02^20 \rightarrow 12^20$	1178.68		1166.32	
04^20	1326.22		1315.33	
$00^00 \rightarrow 00^02$	4341.8		4306.95	
$00^00 \rightarrow 20^01$	4544.4	4453.0	4502.0	
12^01	4640.3	4560.6	4597.0	4578.0
04^01	4751.3	4651.4	4716.2	
$02^20 \rightarrow 11^10$	682.28		675.0	
03^10	560.78		540.4	
$00^00 \rightarrow 03^10$	1823.4			
11^10	1945.3			
$01^10 \rightarrow 10^01$	2740.88			
02^01	2827.01			
$00^00 \rightarrow 30^00$	3576.1		3538.0	
22^00	3691.5		3648.7	
14^00	3798.3		3760.0	
06^00	3949.		3917.	
$10^00 \quad 11^10$	647.71			
$02^00 \quad 03^10$				
$01^10 \rightarrow 21^10$				
13^10	2639.58			
05^10				

TABLE 6-13. SUMMARY OF CYANATE BANDS IN KBR IN ORDER OF APPARENT ABSORBANCE STRENGTH[-11]

$00^00 \rightarrow 00^01$	2169.60	2112.74	2153.00[c]	2161.66[c]
$00^00 \rightarrow 10^00$	1205.47	1191.00[c]	1191.28[c]	1176.37[c]
02^00	1292.57	1271.10[c]	1282.33[c]	1272.95

[-11] See footnotes to Table 6-12. Frequencies in parenthesis were observed in the sample but were not accurately determined.

TABLE 6-13. CONTINUED.

Transition	$^{14}N^{12}C^{16}O^-$	$^{14}N^{13}C^{16}O^-$	$^{15}N^{12}C^{16}O^-$	$^{14}N^{12}C^{18}O^-$
$00^00 \rightarrow 01^10$	629.40	611.9	625.87[c]	624.72[c]
$01^10 \rightarrow 01^11$	2158.40	2102.07	2141.46	
$01^10 \rightarrow 11^10$	1187.52	1174.3	1173.84	1160.08
03^10	1308.85	1285.73	1298.72	1290
$00^00 \rightarrow 10^01$	3354.69	3283.72	3324.00	3319.2
02^01	3440.68	(3363)	3414.05	3414.7
$00^00 \rightarrow 20^00$	2393.43	2360.3	2367.45	2340.78
12^00	2487.82	2462.2[c]	2461.28[c]	2434.06
04^00	2603.61	2553.9	2584.36	2568.52
$00^00 \rightarrow 01^11$	2787.71	2714.85[c]	2767.31	2775.62
$01^10 \rightarrow 10^00$	576.05		565.29	553.2
02^00	633.48		656.23	(648)
$02^20 \rightarrow 02^21$	2148.02		2131.5	2140.0
$01^10 \rightarrow 11^11$	3325.9		3296.4	(3293)
03^11	3446.73		3420.5	3418.5
$01^10 \rightarrow 02^21$	2777.01		2757.17	
$02^20 \rightarrow 12^20$	1174.27		1161.51	
04^20	1320.63		1310.25	
$00^00 \rightarrow 00^02$	4318		4282.87	
$00^00 \rightarrow 20^01$	4523.2		4479.9	4556.7
12^01	4617.5		4573.1	
04^01	4732.0		4695.8	
$02^20 \rightarrow 11^10$	557.73			
03^10	678.89			
$00^00 \rightarrow 03^10$	1817.10			
11^10	1938.42			
$01^10 \rightarrow 10^01$	2725.44			
02^01	2811.73			

TABLE 6-13. CONTINUED.

Transition	$^{14}N^{12}C^{16}O^-$	$^{14}N^{13}C^{16}O^-$	$^{15}N^{12}C^{16}O^-$	$^{14}N^{12}C^{18}O^-$
$00^00 \rightarrow 30^00$	3563.6		3523.8	
22^00	3675.6		3631.6	
14^00	3781.4		3747.6	
06^00	3930		3904	
10^00 11^10	645.3			(634)
02^00 03^10				
21^10				
$01^10 \rightarrow 13^10$	2628.3			
05^10				

TABLE 6-14. SUMMARY OF CYANATE ION ABSORBANCE BANDS BY SPECTRAL REGION IN KCL AND KBR NOT INCLUDING SATELLITE BANDS.

1. The Bending Region(500-700 cm^{-1}):

Transition	In KCl	In KBr	Isotopic Species
$00^00 \rightarrow 01^10$	631.17	629.40	14 12 16
	627.43	625.87	15 12 16
	626.25	624.72	14 12 18
	624		15 12 18
	614.10	611.9	14 13 16
	610.53	608.95	15 13 16
	609.8	607.8	14 13 18
	606.5	604.5	15 13 18
$01^10 \rightarrow 10^00$	579.65	576.05	14 12 16
02^00	666.88	663.48	
	568.92	565.29	15 12 16
	659.35	656.23	
	556	553.2	14 12 18
	651.45	648	
	581.32		14 13 16
	663.90		

TABLE 6-14. (Continued)

Transition	In KCl	In KBr	Isotopic Species
$02^20 \rightarrow 11^10$	560.78	557.73	14 12 16
03^10	682.28	678.89	
	551	544	15 12 16
	675.0	670	
$10^00 \quad 11^10$	647.71	645.3	14 12 16
$02^00 \quad 03^10$			

2. The Symmetric Stretch Region(1150-1350 cm^{-1}):

$00^00 \rightarrow 10^00$	1210.59	1205.47	14 12 16
02^00	1297.40	1292.57	
	1196.44	1191.28	15 12 16
	1286.85	1282.33	
	1181.52	1176.37	14 12 18
	1277.73	1272.95	
	1167.5	1161	15 12 18
	1269.0	1265	
	1195.18	1191.00	14 13 16
	1277.43	1271.10	
	1171.80	1166.5	14 13 18
	1251.92	1247.59	
	1183.71	1180.03	15 13 16
	1264.92	1259.70	
$01^10 \rightarrow 11^10$	1192.43	1187.52	14 12 16
03^10	1314.17	1308.85	
	1178.83	1173.84	15 12 16
	1303.31	1298.72	
	1164.93	1160.08	14 12 18
	1293.73	1290(shoulder)	
	1178.67	1174.3	14 13 16
	1292.53	1285.70	

TABLE 6-14. (Continued)

Transition	In KCl	In KBr	Isotopic Species
$01^10 \rightarrow 11^10$	1166.03	1162.2	15 13 16
03^10	1280	1275(shoulder)	
$02^20 \rightarrow 12^20$	1178.68	1174.27	14 12 16
04^20	1326.22	1320.63	
	1166.32	1161.51	15 12 16
	1315.33	1310.25	
3. The Combination-Overtone Region I(1350-2050 cm^{-1}):			
$00^00 \rightarrow 03^10$	1823.4	1817.10	14 12 16
11^10	1945.3	1938.42	
4. The Asymmetric Stretch Region(2050-2200 cm^{-1}):			
$00^00 \rightarrow 00^01$	2097		15 13 18
	2106.86	2094.76	15 13 16
	2116.60	2104.33	14 13 18
	2124.10	2112.74	14 13 16
	2156.4	2144	15 12 18
	2165.30	2153.00	15 12 16
	2172.74	2161.66	14 12 18
	2181.88	2169.60	14 12 16
$01^10 \rightarrow 01^11$	2096.39	2084.0	15 13 16
	2113.6	2102.07	14 13 16
	2153.94	2141.46	15 12 16
	2161.6	2148	14 12 18
	2170.57	2158.40	14 12 16
$02^20 \rightarrow 02^21$	2102.4		14 13 16
	2143.31	2131.5	15 12 16
	2149.5	2140.0	14 12 18
	2160.35	2148.02	14 12 16
5. The Overtone-Combination Region II(2300-3000 cm^{-1}):			
20^00	2350.66	2340.78	14 12 18
$000 \rightarrow 12^00$	2443.62	2434.06	
04^00	2576.10	2568.52	
	2369.23	2360.3	14 13 16
	2473.93	2462.2	
	2565.16	2553.9	

TABLE 6-14 (Continued)

Transition	In KCl	In KBr	Isotopic Species
20^00	2377.47	2367.45	15 12 16
$00^00 \rightarrow 12^00$	2471.81	2461.28	
04^00	2593.60	2584.36	
	2402.88	2393.43	14 12 16
	2499.26	2487.82	
	2612.80	2603.61	
21^10			
$01^10 \rightarrow 13^10$			
05^10	2639.58	2628	14 12 16
$00^00 \rightarrow 01^11$	2728.01	2714.85	14 12 16
	2781.01	2767.31	15 12 16
	2788.82	2775.62	14 12 18
	2801.72	2787.71	14 12 16
$01^10 \rightarrow 02^21$	2718.69		14 13 16
	2770.71	2757.17	15 12 16
	2791.12	2777.01	14 12 16
$01^10 \rightarrow 10^01$	2740.88	2725.44	14 12 16
02^01	2827.01	2811.73	

6. The Overtone-Combination Region III(3000-4000 cm^{-1}):

$00^00 \rightarrow 10^01$	3300.68	3283.72	14 13 16
02^01	3383.08	3363	
	3336.3	3319.2	14 12 18
	3432.0	3414.7	
	3341.40	3324.00	15 12 16
	3430.52	3414.05	
	3351	3334	15 13 16
	3270	3254	
	3372.5	3354.69	14 12 16
	3458.7	3440.68	
$01^10 \rightarrow 11^11$	3273.8	3257	14 13 16
03^11	(masked)	(masked)	
	3310.0	3293	14 12 18
	3435.5	3418.5	

Transition	In KCl	In KBr	Isotopic Species
$01^10 \rightarrow 11^11$	3312.7	3296.4	15 12 16
03^11	3435.5	3420.5	
	3342.4	3325.9	14 12 16
	3462.5	3446.73	
30^00	3538.0	3523.8	15 12 16
$00^00 \rightarrow 22^00$	3648.7	3631.6	
14^00	3760.0	3747.6	
06^00	3917	3904	
	3576.1	3563.6	14 12 16
	3691.5	3675.6	
	3798.0	3781.4	
	3949	3930	

7. The Overtone-Combination Region IV(4000-5000 cm^{-1}):

$00^00 \rightarrow 00^02$	4306.95	4282.87	15 12 16
	4341.8	4318	14 12 16
12^01	4502.0	4479.9	15 12 16
$00^00 \rightarrow 20^01$	4597.0	4573.1	
04^01	4716.2	4695.8	
	4544.4	4523.2	14 12 16
	4640.3	4617.5	
	4751.3	4732.0	
	4578.0	4556.7	14 12 18

ISOTOPE PRODUCT RULE CALCULATIONS

Noether's Rule as presented in Chapter Four, was used to empirically explain isotopic frequency changes when deuterium was substituted for hydrogen in trihaloethanes (65, p.97-100). Owing to the abundance of isotopic data for mono-isotopically substituted cyanate, his formula (equation 4-9) was applied to predict the location of di- and tri-substituted cyanate ν_2 and ν_3 bands. Table 6-15 shows the respective ratios which are formed by permuting the isotopic substitutions in cyanate ion, and the ratios which are formed for ν_2 and ν_3 in both KBr and KCl lattices. Table 6-16 shows the results when the ratios of the mono-isotopic species are used to predict the more highly substituted ion frequencies. The agreement is good to better than ± 2 cm^{-1}. The $^{15}N^{12}C^{18}O^-$ and $^{15}N^{13}C^{18}O^-$ ν_3 fundamentals have never been reported in KBr and were not observed during this research, however, their predicted spectral locations are 2145.1 cm^{-1} and 2088.1 cm^{-1}, respectively. The application of this rule also adds weight to the previous assignments of those frequencies which were tabulated in Tables 6-5 and 6-11. The fine agreement of this empirical method to the observed frequencies probably owes its success to the simple mass dependence of the isotopic shifts and the simplicity of the linear XYZ geometry as well as the low percent isotopic mass changes.

The Redlich-Teller Frequency Product Rule was used to verify ν_2 fundamentals' assignments for the di- and tri-substituted cyanate ions. The equation used to calculate theoretical ratios was equation 4-7A with $\rho = 1.0513$. It was found that varying ρ by ± 0.01 from this value, changed the theoretical by 1.6×10^{-4} at most for the $^{14}N^{13}C^{18}O^-/^{14}N^{12}C^{16}O^-$ ratio; the mean ratio change was $\pm 0.4 \times 10^{-4}$. A ratio change of 1.6×10^{-4} corresponds

TABLE 6-15. NOETHER'S EMPIRICAL RULE EQUATIONS FOR ISOTOPIC FREQUENCIES FOR THE CYANATE ION OBSERVABLE FUNDAMENTALS.

$$[\nu_k^o(XY^*Z)/\nu_k^o(XYZ)]\ \nu_k^o(XYZ^*) = \nu_k^o(XY^*Z^*)$$

where k = 2 or 3, and ν_k^o is observed experimentally. The equations shown below were used to test Noether's Rule:

a. $[\nu(14\ 13\ 16)/\nu(14\ 12\ 16)]\ \nu\ (14\ 12\ 18) = \nu\ (14\ 13\ 18)$

ν_3 in KCl: [0.97352]
ν_3 in KBr: [0.97379]

b. $[\nu(15\ 12\ 16)/\nu(14\ 12\ 16)]\ \nu\ (14\ 13\ 16) = \nu\ (15\ 13\ 16)$

ν_3 in KCl: [0.99240]
ν_3 in KBr: [0.99235]

c. $[\nu(14\ 12\ 18)/\nu(14\ 12\ 16)]\ \nu\ (15\ 12\ 16) = \nu\ (15\ 12\ 18)$

ν_3 in KCl: [0.99581]
ν_3 in KBr: [0.99634]

d. $[\nu(15\ 13\ 16)/\nu(15\ 12\ 16)]\ \nu\ (15\ 12\ 18) = \nu\ (15\ 13\ 18)$

ν_3 in KCl: [0.97301]
ν_3 in KBr: [0.97295]

e. $[\nu(15\ 12\ 18)/\nu(14\ 12\ 18)]\ \nu\ (14\ 13\ 18) = \nu\ (15\ 13\ 18)$

ν_3 in KCl: [0.99248]
ν_3 in KBr: [0.99232]

The $\nu_k(15\ 13\ 18)$ were obtained by taking the mean of the results of equations d. and c. to obtain a prediction. The numbers below each equation above are the actual observed ratios for the ν_3.

TABLE 6-16. TEST OF NOETHER'S RULE APPLIED TO ISOTOPIC CYANATE OBSERVED FUNDAMENTAL FREQUENCIES.

1. The Bending Mode, ν_2, in KCl and KBr:

	In KCl			In KBr		
Isotopes	Calc	Obs	$\lvert\Delta\rvert$	Calc	Obs	$\lvert\Delta\rvert$
14 13 18	609.3	609.8	0.5	607.3	607.8	0.5
15 13 16	610.5	610.5	0.0	608.5	609.0	0.5
15 12 18	622.5	624	1.5	621.2		
15 13 18	605.7	606.5	0.8	603.7	604.5	0.8

TABLE 6-16. (Continued).

2. The Asymmetric Stretch, ν_3, in KCl and KBr:

	In KCl			In KBr		
Isotopes	Calc	Obs	$\lvert\Delta\rvert$	Calc	Obs	$\lvert\Delta\rvert$
14 13 18	2115.2	2116.6	1.4	2105.0	2104.3	0.7
15 13 16	2107.9	2106.9	1.0	2096.6	2094.8	1.8
15 12 18	2156.2	2156.4	0.2	2145.2		
15 13 18	2098.2	2097	1.2	2088.1		

to 0.10 cm^{-1} at 630 cm^{-1} for frequency calculated from these theoretical ratios. This tends to indicate that a change in the assumed equilibrium bond lengths by 0.01 Å will not easily be detected owing to experimental error as outlined at the end of Chapter Five. Table 6-18 lists the theoretical ratios for ν_2 of the cyanate ion.

Table 6-17 shows product rule calculations for ν_2. In all cases involving ^{13}C-substitution, the ν_2^* (observed) were greater than ν_2^* (calculated) as expected (see Chapter Four, p.38). This indicates that X_{ik} will be greater than X_{ik}^* for this type substitution. However, for 14 12 18 and 15 12 16, the converse should be true. On the whole, agreement between calculated and observed ratios was within experimental error. This indicates that the anharmonicity of the bending mode is not large, and certainly X_{22} should be no greater than 2 cm^{-1}. Table 6-18 compares the theoretical ν_2^*/ν_2 ratios to those observed in both KCl and KBr lattices. Deviation from the theoretical harmonic ratios for cyanate ion appear to be greater in KCl. This suggests that the bending mode is slightly more anharmonic in KCl than in KBr.

TABLE 6-17. PRODUCT RULE CALCULATIONS FOR THE CYANATE ION BENDING MODE FUNDAMENTALS IN KCL AND KBR.

Isotopic Species (N C O)[-12]	In KCl Host Lattice ν_2(Calc) (cm^{-1})	ν_2(Obs) (cm^{-1})	Δ[-13]	In KBr Host Lattice ν_2(Calc) (cm^{-1})	ν_2(Obs) (cm^{-1})	Δ[-13]
15 12 16	627.80	627.43	0.37	626.04	625.87	0.17
14 12 18	626.69	626.25	0.44	624.93	624.72	0.21
14 13 16	613.57	614.10	-.53	611.85	611.90	-.05
15 13 16	610.10	610.53	-.43	608.39	608.95	-.56
15 12 18	623.29	624	-.7	621.55		
14 13 18	608.97[-14]	609.8	-.8	607.26[-14]	607.8	-.5
	609.49[-14]		-.3	607.30[-14]		-.5
15 13 18	605.47[-14]	606.5	-1.0	603.77[-14]	604.5	-.7
	605.99[-14]		-.5	603.82[-14]		-.7

TABLE 6-18. PRODUCT RULE CALCULATIONS FOR THE CYANATE ION BENDING MODE RATIOS IN KCL AND KBR.

Isotopic Ratio $\nu_2(NCO^-):\nu_2(NCO^-)$	Theoretical Ratio(with ρ = 1.0513)[-16]	Ratio in KCl (Obs)	Δ[-15] (X 10^4)	Ratio in KBr (Obs)	Δ[-15] (X 10^4)
15 12 16:14 12 16	0.99466	0.99407	5.9	0.99439	2.7
14 12 18:14 12 16	0.99290	0.99220	7.0	0.99256	3.4
14 13 16:14 12 16	0.97212	0.97295	-8.3	0.9722	-1.0
15 13 16:14 12 16	0.96662	0.96730	-6.8	0.96751	-8.9
15 12 18:14 12 16	0.98752	0.9886	-11		
14 13 18:14 12 16	0.96482	0.9661	-13	0.9656	-7
15 13 18:14 12 16	0.95928	0.9609	-16	0.9604	-11

[-12] Bases on ν_2 (14 12 16) 631.17 cm^{-1} for KCl, 629.40 cm^{-1} for KBr.
[-13] Δ = calculated minus observed frequencies.
[-14] Calculated from the observed 14 13 16 frequency.
[-15] Δ = calculated-observed.
[-16] A variation of ρ by 0.01 shifts the ratio from 0.1 x 10^{-4} for ^{13}C- to 1.6 x 10^{-4} for ^{18}O-substituted cyanates. The average being $\pm$0.44 x 10^{-4}.
[-17] Calculated to test consistancy of the method.

TABLE 6-18. CONTINUED.

Isotopic Ratio $\nu_*(NCO^-):\nu_2(NCO^-)$	Theoretical Ratio[16]	Ratio in KCl	Δ -15 ($\times 10^4$)	Ratio in KBr	Δ -15 ($\times 10^4$)
Other isotopic ratios:[17]					
14 12 18:15 12 16	0.99824	0.99812	1.2	0.99816	0.8
14 13 16:15 12 16	0.97735	0.97875	-14.0	0.97767	-3.2
14 13 16:14 12 18	0.97907	0.98060	-15.3	0.97948	-3.9
15 13 16:14 13 16	0.99434	0.99419	1.5	0.9952	-9
14 13 18:14 13 16	0.99249	0.9930	-6.0	0.9933	-8.1
15 13 18:14 13 16	0.98679	0.9876	-9	0.9879	-12

The Redlich-Teller Frequency Product Rule was applied to the stretching modes which are both Σ symmetry and should obey equation 4-6. Theoretical ratios are shown in Table 6-19 in the second column. In order to calculate the observed ratio, ν_1^o, the unperturbed symmetric stretch must be calculated. This was done using the respective least squares k_{122} (as determined in Chapter Seven) for each isotopic species in the following equation:

$$\{\nu_1^o,\ 2\nu_2^o\} = (1/2)\ (\nu_+ + \nu_-) \pm[(1/2)\ (\nu_+ - \nu_-)^2 - 2k_{122}^2]^{1/2} \qquad (6\text{-}1)$$

where ν_1^o and $2\nu_2^o$ are the unperturbed frequencies, ν_+ and ν_- are the observed Fermi resonant peaks, and k_{122} is the interaction constant. The Fermi resonance complicates matters, as the question now becomes which frequency in equation 6-1 is ν_1^o. From previous work (18,p.1287) it is known that for the 14 13 16 species, ν_1^o is greater than $2\nu_2^o$, but that $\nu_1^o < 2\nu_2^o$ for normal cyanate and the other mono-isotopically substituted species. Table 6-19 shows how the product rule behaves when this uncertainty in the ν_1^o assignment is introduced into the observed ratio calculations. Best agreement of the observed ratios to the theoretical ratios is obtained if $2\nu_2^o < \nu_1^o$ for the 14 13 16 species and that $2\nu_2^o > \nu_1^o$

TABLE 6-19. PRODUCT RULE CALCULATIONS FOR THE CYANATE ION STRETCHING MODES IN KCL AND KBR.

Cyanate Species	Theoretical $\omega_1^*\omega_3^*/\omega_1\omega_3$ (to 14 12 16)	Assign-ments	Observed in KCl	Δ (X 10^4)	Observed in KBr	Δ (X 10^4)
15 12 16	0.97760	$2\nu_2^\circ > \nu_1^\circ$	0.97808	-4.8	0.97845	-8.5
14 13 16	0.97205	$2\nu_2^\circ > \nu_1^\circ$ $2\nu_2^\circ < \nu_1^\circ$	0.96270 0.97556	93.5 -35.1	0.96301 0.97490	90.4 -29.5
14 12 18	0.96491	$2\nu_2^\circ > \nu_1^\circ$	0.96479	1.2	0.96581	-9.0
15 13 16	0.95002	$2\nu_2^\circ < \nu_1^\circ$ $2\nu_2^\circ > \nu_1^\circ$	0.95830 0.94791	-83.0 21.1	0.95468 0.95302	46.8 -30.2
15 12 18	0.94280	$2\nu_2^\circ > \nu_1^\circ$	0.94331	-5.1		
14 13 18	0.93745	$2\nu_2^\circ < \nu_1^\circ$ $2\nu_2^\circ > \nu_1^\circ$	0.95446 0.93876	-170.1 -13.1	0.95915 0.93712	-280.7 -60.4

for all the others. With two exceptions (when the preceding conclusion is drawn), the observed ratios are greater than the calculated ones, suggesting that $x_{11}x_{33} > x_{11}^{*}x_{33}^{*}$. The 14 12 18 and 15 13 16 species in potassium chloride host have their observed ratios greater than their respective theotetical ratios and the converse is suggested; however, in potassium bromide the opposite is true and the meaning of this result is not clearly understood. As in the bending mode product rule calculations, anharmonic effects are greater in KCl than in KBr. Because of the Fermi resonance, and the associated difficulty of determining ν_1^{o}, the product rule is not very useful for predicting ν_3 frequencies to any acceptable degree of accuracy. The deviations listed in Table 6-19 correspond to prediction errors of from 0.3 to 16 cm^{-1} at 2000 cm^{-1}. For a quick indication of where to look for a doubly or tri-substituted cyanate ν_3 fundamental, Noether's empiricism is more practical. The power of the product rule derives from its firm theoretical basis.

This chapter has presented spectral data and assignments. We have also applied the product rule and tested Noether's empiricism.

CHAPTER 7

POTENTIAL ENERGY CALCULATIONS

In the linear unsymmetric triatomic molecule there are nineteen constants in the general internal coordinate potential energy expansion through quartic terms. There are also nineteen constants in symmetry coordinates and eighteen constants in normal coordinates. In normal coordinates, some of the force constants do not contribute to the energy in the second order approximation (the k_{ijkk}'s). The coefficients of the quadratic terms in equation 2-5 are conventionally designated harmonic force constants while the coefficients of higher order terms are anharmonic force (potential) constants.

Anharmonic force constants are difficult to determine precisely because of the large number of these constants in the general quartic field, (86). Only recently have linear triatomics been subjected to this depth of analysis. The factor which limits a complete anharmonic determination is the availability of sufficient and accurate experimental data. Nature herself has placed a formidable barrier to the analytic anharmonic determination of general potential constants. Generally, there is insufficient data determinable to calculate a unique set of constants without assuming some sort of empirical model (21,76). Resonance interactions also complicate matters. At this point, one may ask, why do we need to determine 15 to 19 potential constants, when the anharmonicity constants, x_{ij}, and the harmonic frequencies ω_i, are determinable from the isotopic experimental data using equations 2-20, 2-21 and 2-22 and the relations presented in Chapter Four.

Until recently spectroscopists did indeed use this approach. Their anharmonicity constants did reproduce spectra to an acceptable degree. However this procedure suffers from some very basic flaws. In 1953, Lippincott (50,p.2070) pointed out that most

potentials determined in this way had little use in predicting bond dissociation energies.[-18] He also pointed out that in most cases, all the spectroscopic data available must be used to get the constants, so that little is really predicted. Anharmonicity can effect calculated r^e values by as much as 0.01 Å (21). These criticisms were only symptomatic to the real deficiencies of this method, as is pointed out by Pariseau (72,p.95). She argues that the experimental ω_i, x_{ij}, etc., determined in the usual way are not the actual coefficients in equation 2-21, but contain contributions from higher terms. If the cubic terms are used in the energy expression, the quantity determinable from observation of the fundamental and the first overtone (e.g. of ν_1) is not x_{11}, but in reality is given by x_{11} (observed) = x_{11} + higher terms. This becomes evident when one compares the calculated $3\nu_1$ and $4\nu_1$ frequencies to those actually observed. Dennison has noted that from 1-5 percent of the frequency contribution to an observed transition is anharmonic (21). Maki and Decius (55,p.779) make the same observation for their b, which contains the Fermi interaction constant. The bond force constants, however, are directly related to the ω_i and x_{ij} and if the experimental quantities being used contain contributions from higher terms, the force constants calculated from them, will be in error. Another observation which reinforces Pariseau's (70,p.40) arguments is that the x_{ij} are not uniquely determined by extracting them from the experimental data using equation 2-21 (54,p.126). Also, data from two different researchers yield different x_{ij}'s. These two criticisms will be elaborated upon later in this chapter.

Another complication results from the presence of Fermi resonance. In this analysis of the resonance, the determination of unperturbed levels is difficult and commonly neither precise nor

---

[-18] Once the x_{ij}'s etc. have been determined, the potential constants may be estimated using Nielsen's equation which are shown in Appendix II.

accurate (3). The values of the ω_i and x_{ij} connected with the resonating levels will be very sensitive to this determination. In part, the inaccuracy may result from the assumption of the validity of the perturbation method and the power series expressions obtained. Dennison (21,p.175-210) has noted that when the potential energy is expanded, potential constants of one order are often quite unequal, so that if the expansion is truncated at a certain order, it is likely that higher order terms will have an appreciable effect. If this is indeed the case, then the perturbation should be extended to higher orders as was suggested by Maki (54,p.38). This extension is of course limited by the experimental accuracy of the observables, and is not easily justifiable in the present case. This effect has, however, been noted in the x_{22} and $x_{\ell_2\ell_2}$ terms of CO_2 by Pariseau (72, 73) and by Lide (48).

The treatment of the cyanate data by the method alluded to above was performed first to a limited degree by Maki and Decius (55) and more recently by Schettino and Hisatsune (84) whose treatment was more complete and detailed. Prior to the publication of the latter researchers' results it had been a goal of this research to obtain and refine the experimental spectroscopic quantities necessary to fit equation 2-21 to the data. However, in light of Schettino and Hisatsune's work and the likely deficiencies of the constants determined in this way, little would be achieved by this endeaver. For this reason it was decided to calculate the potential constants, as sufficient data appears to be available to accomplish this, and then determine the anharmonicities and harmonic frequencies.

In the following discussion, the lower case k's refer to normal coordinates and the capital K's refer to instantaneous internal coordinates. In this convention, the subscript numeral "1" refers to the C-N stretch "2" refers to the C-O (symmetric) stretch, and "3" refers to the bend; these designations hold for the

instantaneous internal coordinate K's. The "1", "2", and "3" subscript numerals for normal coordinate potential constants retain the mode designations introduced in Chapter Two. The terminology "spectroscopic constants" refers to the ω_i's and the x_{ij}'s.

For any one cyanate isotopic species there are only eleven pieces of experimentally determined data using equation 2-21. These are ω_1, ω_2 , ω_3 , x_{11},x_{12}, x_{13}, x_{22}, x_{23}, x_{33}, $x_{\ell_2\ell_2}$ (also known as known as g_{22}) and k_{122}. As we pointed out above, since these anharmonicity constants contain combinations of the k_{ijk}'s and k_{ijk} 's, determination of all of the normal coordinate potential constants from them is impossible. However, if we first determine the internal coordinate constants (and by transformation, the normal coordinate k's) we can readily calculate these anharmonicities and harmonic constants using Nielsen's equations. Through the use of isotopic data, we can more accurately fix the K's and obtain the best set of potential constants using a least squares technique.

When the potential energy is expressed in internal coordinates, as with other coordinates, the number of potential constants is larger than the number of independent spectroscopic parameters (21,p.175). This means that a certain number of the force constants in internal coordinate space are indeterminable from the latter and in some way the number of variables must be reduced. Two methods have been utilized to attempt a remedy to this situation (72,p.16). Either some of the potential constants are assumed vanishingly small, or some potential model is utilized which provides constraining relations among the potential constants. Pariseau has given a comprehensive discussion of some earlier models (72,p.16-25).

Two main groups of researchers have been working with triatomic molecule anharmonic potential functions. Pliva, et al. in Czechoslovakia (69,70,71,76, and 77) have developed potential

functions which represent some triatomic molecules and have a smaller number of parameters to adjust; these parameters are somewhat restricted by the available experimental data. These functions are based upon a model using Lippincott function (49, 50) to represent the bond stretches and a sine function for the bends. Their calculations have worked well for HCN, DCN, H_2O and D_2O (76). Pliva's method can be characterized as one which fits the harmonic frequencies to the assumed adjusted potential function (77). Overend, et al. (52, 72, 83, 86, and 90) have developed a somewhat more general approach (73).

Until now these comprehensive energy treatments of triatomics were applied only to gas phase spectra. This had been the case because sufficient data for ions and other molecules was not available. An additional advantage afforded by gas phase spectra results from the determination of rotational constants. These constants are very dependent upon the cubic normal coordinate potential constants, and have been used to determine them in most potential energy calculations. In the case of cyanate ion in alkali halide lattices, rotational constants are not determined and in our calculations, Morse parameters were used to constrain the cubic parameters. This application to cyanate ion represents an important step into solids for this method. The remainder of this chapter gives a brief description of Smith-Overend model (86), which was applied to the cyanate data, the calculated results, and a discussion of the results.

The Smith-Overend model has evolved since 1963 (72) under the direction of Dr. John Overend at the University of Minnesota. The model is largely described in papers by Machida and Overend (52, 53), Reichman and Overend (83), and Smith and Overend (86). Pariseau, Suzuki and Overend have applied it to CO_2 (73) and HCN (90). Smith and Overend have used the program in its current modification to successfully redetermine the potential constants

of CO_2, CS_2, OCS, N_2O and HCN (86). The current model reduces the number of parameters in the force field of unsymmetric linear molecules from nineteen to eleven. The computer program which they have developed for the Control Data Corporation 6600 system is targeted at arriving at the best $V(R_i)$, consistent with the data and the model parameters. A schematic flow chart is shown in Appendix IV B. The general algorithm for the least squares adjustment of the anharmonic force constants is found in detail in reference (73).

The following assumptions are made using their method: (i) the effective equilibrium length of the i^{th} bond is a function of the other coordinates in the molecule; (ii) the effective quadratic and cubic force constants of the i^{th} bond are functions of the other coordinates and that changing the other coordinates not only displaces the bond potential function of the i^{th} bond, but also distorts the shape of the $V(R_i)$; (iii) displacement of r_i^e and ΔK_{ii} and ΔK_{iii} are due to electronic changes in the i^{th} bond and are amenable to Badger's empiricism Δr_i^e and ΔK_{ii}. From the first two model assumptions, new coefficients are found between which certain constraints can operate:

$$\Delta R_i^e = \sum_{j\neq i} a_j^i R_j + \sum_j \sum_{k\neq i} a_{jk}^i R_j R_k + \sum_j \sum_k \sum_{l\neq i} a_{jkl}^i R_j R_k R_l + \cdots \quad (7\text{-}1)$$

$$(\Delta K_{ii}/K_{ii}) = \sum_{j\neq i} b_j^{ii} R_j + \sum_j \sum_{k\neq i} b_{jk}^{ii} R_j R_k + \cdots \quad (7\text{-}2)$$

$$(\Delta K_{iii}/K_{iii}) = \sum_{j\neq i} c_j^{iii} R_j + \cdots \quad (7\text{-}3)$$

Using these parameters, Smith and Overend have written a computer program which allows the direct introduction of the model constraints into the force field and the least squares adjustment

of the model parameters directly to the observed data without requiring the general quartic force constants as intermediate variables(86). An example of model constraints can be found for the stretches when the "b" and "c" parameters can be expressed as a function of the "a" coefficients and the principal force constants using Badger's Rule(4):

$$a_2^1 = \left(\frac{K_{22}}{K_{11}}\right) a_1^2 \quad , \text{ and} \qquad b_{22}^{11} = \left[\frac{6(a_2^1)^2}{(r_1^e - d_{ij})} - \frac{3(a_{22}^1)}{(r_i - d_{ij})}\right], \quad (7\text{-}4)$$

where r_i^e is the equilibrium length of bond one and d_{ij} is the Badger's Rule parameter(4). For the stretch-stretch interactions, it was found that the following inverse-power relation represents the situation quite well(52):

$$r_1^o = [\, \alpha_1 / (r_2 + r_2^e)^{\gamma_1} \,] + r_1^D \quad (7\text{-}5)$$

where r_1^o is the instantaneous equilibrium length of the first bond and the second is stretched a distance r_2 from r_2^e, r_1^o is the equilibrium length of the first bond in the corresponding diatomic molecule and is the limiting value of r_1^o at $r_2 = \infty$, α_1 is fixed by the requirement that $r_1^o = r_1^e$ at $r_2 = 0$, γ_1 is the only adjustable parameter in the relationship, and $\gamma_1 = (K_{12}/2K_{11})(r_2^e/\delta)$ where $\delta = (r_2^e - r_2^D)$. The stretch-bend interactions are generally expressed in the form:

$$\bar{K}_{33} = K_{33} \exp[\, A R_1 + B R_2 \,] \quad (7\text{-}6)$$

where $\bar{K}_{33}$ is the instantaneous value in terms of coordinates R_1 and R_2, and A and B are model parameters. This expression is easily expressed in terms of "a", "b", and "c", using a Taylor series expansion, and equating the proper coefficients.

Instantaneous internal coordinates are utilized for several reasons. The Eckart-Savetz conditions (expressed by equations 2-1 and 2-2) separate translation and vibration completely, but for rotation only specify that there be no angular momentum due to vibrational motions through the first order terms in the kinetic energy. This situation could conceivably break down when the amplitudes of vibration are appreciable. Internal coordinates circumvent this problem somewhat because they are defined by the relative positions of the atoms with respect to each other in the potential energy equation. They are more easily visualized in terms of chemical valence bond motions. Now kinetic and potential energies must be in the same coordinate space in order to get the normal coordinates by some transformations. If the internal coordinates are to be exactly along the bond between atoms at each instant, the relation between R and Q is not linear if the amplitudes of vibration are not infinitesmal (73,p. 2336). Overend, et al. have developed the necessary analytic expressions to overcome these difficulties.

The Smith-Overend computer program proceeds in several stages. This account refers to how cyanate ion in KCl, KBr and KI was treated. The block diagram in Appendix IV outlines the procedure. Initially the equilibrium bond lengths (r^e_{NC} = 1.17 Å, r_{CO} = 1.23Å) were used in conjunction with transferred Morse parameters, a_i, to derive relations between the principal stretching internal force constants in order to generate an initial set of these constants. The stretch-stretch interaction inverse power relation (previously stated in equation 7-5) and the stretch-bend interaction model (stated in equation 7-6) were used to generate relations between the a, b, and c, coefficients and the internal force constants. At this point, the expressions computed above were used to express the stretch-stretch and stretch-bend interaction force constants in terms of a, b, and c parameters

which are analytically related to the principal internal force constants, K_{ii}, K_{iii} and K_{iiii}. This treatment computes the 19 internal force constants and generates the initial quartic field in internal coordinates. A nonlinear transformation is now performed to normal coordinate space and Nielsen's equations are used to generate the spectroscopic parameters (X_{ij}) and predicted energy level eigenvalues. The computer has been previously instructed as to which and what kind of resonance interactions to calculate so that the appropriate Nielsen expression is used. At this point the observed energy values, shown in Table 7-1, are compared to the calculated ones. The program now calculates required corrections to the internal force constants and model parameters by a nonlinear least squares technique. If a correction to a force constant is greater than 0.005, then the entire procedure is repeated. Otherwise the program dumps the following useful out-put:

(1) The final set of internal force constants as shown in Table 7-9 with their principal least squares dispersion.

(2) All of the final model parameters used to determine the final set of internal force constants. These are presented in Appendix IV.

(3) For each cyanate isotope species, the following quantities are computed.

(a) The harmonic frequencies and anharmonicity constants shown in Tables 7-2, 7-3 and 7-4 for cyanate ion in KCl, KBr, and KI, respectively. The KI calculations were accomplished using the data of Schettino and Hisatsune (84,p.20).

(b) The normal coordinate potential constants for cyanate ion in KCl, KBr, and KI are shown in Tables 7-6, 7-7 7-8, respectively.

(c) The calculated and observed energy levels are presented in Table 7-6.

(4) A correlation matrix which shows how closely the calculated internal potential interaction constants depend upon one

another. The three correlation matrices are presented in Appendix IV.

In general, there exist a few limitations to the least squares technique. The last bit of output mentioned above can be quite instrumental in illustrating a major criticism. If the force constants are strongly correlated, in combination they may be quite important in the energy, but their actual numerical values are strongly dependent upon the values of other constants as would be expected. Hence, the magnitude of a particular force constant does not necessarily give a criterion of the effect of that constant on the energy. The correlation matrix shows which constants are strongly interdependent. Another shortcoming can be seen in some quartic interaction constants. These make small contributions to the energy and are extremely sensitive to experimental accuracy. For instance, k_{2222} is small but has an appreciable effect on the anharmonicity constants g_{22} and X_{22}. Thus assuming it to be zero (see Amat and Pimbert, reference 3) may be questioned. This particular calculation of k_{2222} has a dispersion averaging between eight and twelve percent, (see K_{3333}) depending upon the alkali halide. This dispersion gives one an estimate of the constants accuracy but may easily be artificial due to the smallness of the quantity. In the initial phase of the computer work, the initial set of force constants must be fairly close to the final ones. Due to this non-linear least squares technique, we used quadratic force constants and harmonic frequencies calculated by Schettino and Hisatsune (84) in order to insure convergence for the final set of results from the spectral data arrived at in this work. The results of the cyanate ion calculations have been consistent with expectations, and no real anomalies have been produced. Quite to the contrary, several new levels have been discovered as depicted by the values in parenthesis in Table 7-6. Also some typographical errors in this text were corrected through the use of calculated energy levels.

TABLE 7-1. ENERGY LEVELS USED IN THE CALCULATIONS.[-19]

Level[-20]	$^{14}N^{12}C^{16}O^-$			$^{15}N^{12}C^{16}O^-$			$^{14}N^{13}C^{16}O^-$			$^{14}N^{12}C^{18}O^-$			$^{15}N^{13}C^{16}O^-$		
$01^{1}0$	1	1	1	1	1	1	1	1	1	1	1	1	1	1	1
$10^{0}0$, $02^{0}0$	2	2	2	2	2	2	2	2	2	2	2	2	2	2	2
$11^{1}0$, $03^{1}0$	2	2	2	2	2	2	2	2	0	2	1	0	2	1	1
$00^{0}1$	1	1	1	1	1	1	1	1	1	1	1	1	1	1	1
$20^{0}0$, $12^{0}0$ $04^{0}0$	3	3	3	3	3	1	3	3	1	3	3	0	0	0	1
$01^{1}1$	1	1	1	1	1	1	1	1	1	1	1	1	1	1	1
$10^{0}1$, $02^{0}1$	2	2	2	2	2	2	2	2	2	2	2	2	2	2	2
$02^{2}1$	1	1	1	1	1	0	1	0	0	1	0	0	0	0	0
$11^{1}1$, $03^{1}1$	2	2	2	2	2	2	1	0	0	2	2	0	0	0	0
$02^{2}0$	1	1	1	1	0	0	0	0	0	0	0	0	0	0	0
$12^{2}0$, $04^{2}0$	2	2	2	2	0	0	0	0	0	0	0	0	0	0	0
$00^{0}2$	0	0	0	1	1	0	0	0	0	0	0	0	0	0	0

[-19] The digits indicate how many observed bands were used in the calculations for each isotopic species in each lattice. Entries in each column are given in the order KCl, KBr, KI. Additionally all four observed fundamentals for $^{14}N^{13}C^{18}O^-$ in both KBr and KCl were used, and the four fundamentals for $^{15}N^{12}C^{18}O^-$ in KCl were included. All digits in this chart refer to experimental quantities which were given a weight of 1.0 in the calculations. In the KBr and KI calculations three frequencies from the 300, 220, 140, 060 $^{14}N^{12}C^{16}O^-$ tetrad were used and in KBr one frequency from the 201, 121, 041 triad was also used. The known experimental error for the other isotopic cyanate frequencies for these polyads precluded their use in the calculation.

[-20] The observed frequencies for each level were expressed in cm^{-1} above the $00^{0}0$ level using the Ritz principle.

The principle energy levels used in the calculations are shown schematically in Table 7-1. They corresponded to the data tables presented in Chapter Six and to Schettino's data for cyanate ion in KI (84,p.20). Additionally, all available fundamental frequencies for every cyanate species were included. Eighty levels for seven isotopic cyanate species were included in the KCl calculation, 70 levels for six cyanate species in KBr, and 59 levels for five cyanate species in the KI case. The energy levels not observed as transitions from the $00^0 0$ level were derived as explained in in the footnotes to Table 7-6. The levels listed in Table 7-1 and observed directly were assigned weights between 0.75 and 1.00 depending upon the experimental error.

The spectroscopic parameters are shown in Tables 7-2, 7-3 and 7-4 for cyanate ion in KCl, KBr and KI, respectively. These are a result of the model calculations. The zero order ω_i° were computed using equation 2-22.

The harmonic frequencies, ω_i, agree very well with theoretical expectations. In any given halide environment the substitution of a 13-carbon isotope effect the ω_2 markedly and decreases the ω_3. The symmetric-like ω_1 is hardly changed. The Redlich-Teller product rule is accurately obeyed as is shown in Table 7-5 (i). The product rule is remarkably stable from lattice to lattice indicating that no frequency mode is differently effected with respect to any other mode with lattice change. The average ratio deviations from theoretical predictions were found to be $\pm 0.43 \times 10^{-5}$ for any given value. There was no general trend to the deviations which oscillated about the predicted value. This result may be contrasted with the ratios calculated from harmonic frequencies calculated by Schettino and Hisatsune which are presented in Table 7-5 (ii). These frequeny ratios were found to deviate from 2.1×10^{-5} in the KI case to 11.6 $\times 10^{-5}$ in the KBr case. The ratios were uniformly larger than the theoretical ratio, thus indicating that more anharmonicity corrections were needed. Harmonic frequencies for $^{14}N^{12}C^{16}O^-$ and $^{14}N^{13}C^{16}O^-$ in

TABLE 7-2. SPECTROSCOPIC CONSTANTS FOR CYANATE ION IN POTASSIUM CHLORIDE.

Parameter	$^{14}N^{12}C^{16}O^-$	$^{15}N^{12}C^{16}O^-$	$^{14}N^{13}C^{16}O^-$	$^{14}N^{12}C^{18}O^-$	$^{15}N^{13}C^{16}O^-$	$^{14}N^{13}C^{18}O^-$	$^{15}N^{12}C^{18}O^-$
ω_1°	1247.09	1229.02	1246.37	1207.71	1228.66	1206.62	1189.92
ω_2°	629.08	625.78	611.69	624.77	608.32	607.26	621.44
ω_3°	2192.90	2175.34	2134.84	2185.01	2116.54	2127.18	2166.88
x_{11}	-3.39	-3.19	-3.59	-2.95	-3.38	-3.24	-2.75
x_{22}	0.564	0.586	0.520	0.524	0.544	0.479	0.548
x_{33}	-11.06	-10.87	-10.45	-11.06	-10.24	-10.46	-10.85
x_{12}	-4.44	-4.35	-4.31	-4.27	-4.22	-4.15	-4.19
x_{13}	-19.17	-19.10	-17.96	-19.23	-17.94	-17.64	-19.24
x_{23}	-11.13	-11.18	-10.38	-10.88	-10.44	-10.13	-10.93
g_{22}	-0.448	-0.474	-0.411	-0.405	-0.438	-0.367	-0.433
k_{122}	-58.920	-58.904	-56.913	-56.744	-56.973	-54.678	-56.777
ω_1	1264.50	1246.11	1263.25	1224.60	1245.23	1222.83	1206.48
ω_2	637.96	634.55	620.18	633.43	616.67	615.52	630.00
ω_3	2224.67	2206.94	2164.65	2216.57	2146.19	2156.59	2198.28

TABLE 7-3. SPECTROSCOPIC CONSTANTS FOR CYANATE ION IN POTASSIUM BROMIDE.

Parameter	$^{14}N^{12}C^{16}O^-$	$^{15}N^{12}C^{16}O^-$	$^{14}N^{13}C^{16}O^-$	$^{14}N^{12}C^{18}O^-$	$^{15}N^{13}C^{16}O^-$	$^{14}N^{13}C^{18}O^-$
ω_1°	1239.97	1221.81	1239.30	1201.01	1221.54	1199.93
ω_2°	626.57	623.57	609.52	622.54	606.13	605.09
ω_3°	2180.93	2163.66	2123.05	2172.91	2105.11	2115.21
x_{11}	-3.36	-3.18	-3.54	-2.95	-3.35	-3.21
x_{22}	0.822	0.843	0.765	0.777	0.786	0.719
x_{33}	-11.36	-11.15	-10.73	-11.37	-10.51	-10.76
x_{12}	-4.45	-4.36	-4.33	-4.29	-4.24	-4.16
x_{13}	-19.11	-19.03	-17.98	-19.07	-17.94	-17.59
x_{23}	-10.90	-10.96	-10.17	-10.65	-10.23	-9.91
g_{22}	-0.515	-0.542	-0.474	-0.469	-0.502	-0.427
k_{122}	-58.007	-58.029	-56.018	-55.818	-56.118	-53.769
ω_1	1257.34	1238.92	1256.16	1217.79	1238.10	1216.10
ω_2	635.12	631.72	617.41	630.61	613.92	612.77
ω_3	2212.75	2195.34	2152.94	2204.47	2134.82	2144.68

TABLE 7-4. SPECTROSCOPIC CONSTANTS FOR CYANATE ION IN POTASSIUM IODIDE.

Parameter	$^{14}N^{12}C^{16}O^-$	$^{15}N^{12}C^{16}O^-$	$^{14}N^{13}C^{16}O^-$	$^{14}N^{12}C^{18}O^-$	$^{15}N^{13}C^{16}O^-$
ω_1^o	1234.21	1214.95	1232.73	1194.86	1214.74
ω_2^o	626.12	622.84	608.84	621.82	605.46
ω_3^o	2168.74	2151.30	2108.96	2159.29	2092.78
x_{11}	-3.30	-3.13	-3.43	-2.93	-3.26
x_{22}	0.593	0.612	0.550	0.555	0.569
x_{33}	-11.67	-11.45	-11.03	-11.70	-10.80
x_{12}	-4.18	-4.09	-4.06	-4.02	-3.97
x_{13}	-19.07	-18.94	-18.05	-18.87	-17.97
x_{23}	-11.79	-11.81	-11.02	-11.57	-11.04
g_{22}	-0.458	-0.481	-0.422	-0.417	-0.446
k_{122}	-57.406	-57.315	-55.51	-55.33	-55.48
ω_1	1250.27	1231.64	1249.25	1211.25	1230.95
ω_2	635.01	631.62	617.31	630.50	613.81
ω_3	2200.78	2184.03	2141.04	2191.97	2123.60

KBr calculated by Maki and Decius (54, p.779) for KBr were in slightly better agreement with the values calculated in this work than those calculated by Schettino and Hisatsune(84). It is indeed tempting to say that the force constants arrived at in this treatment are better than those previously obtained (from this product rule argument) were it not for the uncertainty in r_i^e.

The anharmonicity constants in Tables 7-2, 7-3 and 7-4 also vary from isotopic species to isotopic species as is expected from their mass dependence. They fit equation 4-8 very closely. Their values and signs are similar to those obtained for CO_2 and N_2O, as is demonstrated in Table 7-12. A discussion of these constants compared to those found by Schettino and Hisatsune will be deferred to Chapter Eight. The x_{22} and g_{22} are small as expected, however, it should be noted that these values are extremely sensitive to experimental accuracy and may be a feature of the bending model function. Table 7-6 shows that this set of constants reproduce the cyanate spectrum very well and in most cases to within absolute accuracy estimates. The fit is especially pleasing when one examines the higher Fermi multiplets, as compared to earlier spectral fits obtained from spectroscopic constants.

The estimation of x_{33} has been a subject of concern.(54,84) The initial calculations with the Smith-Overend program indicated where $2\nu_3$ should occur; this overtone would enable us to calculate ω_3 and x_{33} more accurately. With the help of D. Foss Smith, Jr.,[-22] this very weak band was found in concentrated ^{15}N-enriched cyanate samples in both KBr and KCl, and subsequently was observed in normal cyanate doped KCl and KBr crystals. This band was

---

[-22] Current address: Molecular Spectroscopy Laboratory, University of Minnesota, Minneapolis, Minnesota 55240.

TABLE 7-5. CYANATE ION PORDUCT RULE CALCULATIONS. This table compares the least-squares harmonic frequencies from the Smith-Overend model to the best-fit harmonic frequencies[-21] obtained directly from observed spectra in KCl, KBr, and KI in product rule ratios.

Cyanate Isotopes	Theoretical Ratio	(i) Least-Squares Frequency Ratios In KCl	In KBr	In KI	(ii) Best-Fit Frequency Ratios In KCl	In KBr	In KI
1. The Stretching Ratios, $\omega_1^*\omega_3^*/\omega_1\omega_3$ ($^{14}N^{12}C^{16}O^-$):							
15 12 16	0.977595	0.977598	0.977597	0.977602	0.977619	0.977667	0.977601
14 13 16	0.972052	0.972054	0.972057	0.972061	0.972035	0.972141	0.972070
14 12 18	0.964912	0.964915	0.964920	0.964913	0.964921	0.964956	0.964888
15 13 16	0.950017	0.950017	0.950018	0.950020	0.949978	0.950050	0.950068
15 12 18	0.942796	0.942794					
14 13 18	0.937447	0.937448	0.937447				
2. The Bending Ratios, ω_2^*/ω_2 ($^{14}N^{12}C^{16}O^-$):							
15 12 16	0.99466	0.99465	0.99465	0.99466	0.99468	0.99498	0.99465
14 13 16	0.97212	0.97213	0.97212	0.97213	0.97215	0.97221	0.97215
14 12 18	0.99290	0.99290	0.99290	0.99290	0.99296	0.99309	0.99292
15 13 16	0.96662	0.96663	0.96662	0.96661	0.96667	0.96671	0.96664
15 12 18	0.98752	0.98752					
14 13 18	0.96482	0.96483	0.96481				

[-21] The ω_i for these calculations came from Schettino and Hisatsune (84,p.15,17, and 19).

TABLE 7-6. ENERGY LEVEL CALCULATIONS FOR CYANATE ION IN KCL,KBR AND KI.[23]

Energy Level[24]	$^{14}N^{12}C^{16}O^-$	$^{15}N^{12}C^{16}O^-$	$^{14}N^{13}C^{16}O^-$	$^{14}N^{12}C^{18}O^-$	$^{15}N^{13}C^{16}O^-$
1. In KCl:					
01^10	-0.25	-0.64	-0.12	-0.77	-0.00
10^00	-0.71	-0.90	-0.36	-1.27	-0.14
02^00	0.13	0.11	0.37	0.19	0.47
11^10[25]	-0.67	-0.79	-0.61	-1.50	-0.15
03^10	0.15	-0.44	0.46	0.09	-0.67
00^01	0.03	0.82	-0.29	-1.22	0.56
20^00	0.36	0.74	1.78	-0.77	2345.2
12^00	0.70	0.70	0.44	-0.06	2446.0
04^00	-0.66	0.43	-0.03	-0.65	2542.9
21^10[26]	3000.2	2970.8	2951.9	2945.4	2925.1
13^10	3129.9	3100.5	3083.0	3073.1	3053.6
05^10	1.2	3248.9	3206.5	3227.9	3180.8
01^11	-0.42	-0.36	0.02	-1.28	0.53
10^01	-0.29	-0.26	0.36	-0.62	-0.67
02^01	0.65	0.60	0.74	1.29	-0.41
02^21[26]	-0.37	-0.34	0.99	0.02	3306.7
11^11[26]	-0.84	0.03	(1.29)	0.42	3853.1
03^11	-1.15	-0.52	4000.91	-0.16	3967.1
30^00	2.3[23]	1.0	3519.9	3503.5	3487.0
22^00	1.0	0.6	3652.3	3603.8	3613.2
14^00	0.7	-0.7	3750.0	3725.3	3710.5
06^00	1.0	-0.2	3866.8	3890.6	3835.7
20^01	-0.9	1.7	(0.5)	4485.4	4412.3
12^01	0.3	2.0	(0.6)	(0.9)	4514.5
04^01	-1.1	0.6	-0.8	4708.3	4609.8

[23] The deviations are observed minus calculated values shown for each isotopic cyanate species. Where no frequency was observed, a predicted value occurs. The values in parentheses show deviations for energy levels observed but not used in the potential calculation because of experimental error. The KI calculations can be compared to the data in reference 84, p.18. The KCl and KBr spectra can be calculated from the data in Chapter Six. The convention followed here goes from lower to higher frequencies within resonant polyads. Units are cm^{-1}.

TABLE 7-6. (Continued)

Energy Level	$^{14}N^{12}C^{16}O^-$	$^{15}N^{12}C^{16}O^-$	$^{14}N^{13}C^{16}O^-$	$^{14}N^{12}C^{18}O^-$	$^{15}N^{13}C^{16}O^-$
02^20 [-27]	-0.13	-0.67	1228.2	1254.3	1221.3
12^20 [-28]	0.65	1.30	2392.5	2406.0	2373.4
04^20	-0.21	-1.07	2532.0	2558.9	2513.4
00^02	0.2	0.27	4227.9	4325.8	4192.1
00^03	6479.2	6428.2	6310.5	6455.5	6257.4
2. In KBr:					
01^10	0.01	-0.18	-0.08	-0.28	0.41
10^00	-0.70	-0.64	-0.22	-0.96	0.78
02^00	0.69	0.71	1.52	-0.27	1.08
11^10 [-25]	-0.48	-0.56	-0.23	-1.08	0.51
03^10	0.33	0.22	0.87	0.50	1883.2
00^01	0.01	-0.42	-0.43	-0.12	0.16
20^00	-0.09	0.37	0.24	-0.64	2337.2
12^00	0.22	1.05	-0.43	0.48	2435.0
04^00	-0.36	-0.63	-0.42	0.11	2532.5
21^10 [-26]	2990.2	2960.1	2943.4	2934.5	2916.0
13^10	3118.3	3088.8	3071.5	3062.0	3042.0
05^10	(-2.0)	3238.5	3194.3	3218.4	3169.1
01^11	-0.36	-0.35	0.72	-0.28	0.04
10^01	-0.92	-0.60	-0.44	-0.12	-0.65
02^01	0.04	0.89	-1.23	-0.07	-0.02
02^21 [-26]	-0.71	-0.31	3316.5	3390.9	3291.8
11^11 [-26]	-0.80	0.35	3869.4	0.63	3835.8
03^11	0.17	1.35	3981.5	-0.42	3948.3

[-24] The energy levels conform to the energy level diagram for cyanate ion given by Decius, et al.(19, p.2183). Values used in the potential calculations were based on the 00^00 level.

[-25] Observed directly in $^{14}N^{12}C^{16}O^-$ for the three halides. All other values were computed from the $01^10 \rightarrow \{11^10, 03^10\}$ transition.

[-26] Computed from the respective 01^10 transition.

TABLE 7-6. (Continued)

Energy Level	$^{14}N^{12}C^{16}O^-$	$^{15}N^{12}C^{16}O^-$	$^{14}N^{13}C^{16}O^-$	$^{14}N^{12}C^{18}O^-$	$^{15}N^{13}C^{16}O^-$
30^00	(1.7)	(-0.5)	3510.2	3490.0	3476.5
22^00	0.71	(-0.5)	3638.3	3588.4	3598.4
14^00	-1.2	(1.2)	3734.0	3712.1	3694.8
06^00	(2.7)	(1.5)	3852.3	3879.7	3821.9
20^01	(0.8)	(0.5)	4433.5	4463.5	4393.1
12^01	(0.5)	(0.5)	4537.3	(1.6)	4492.0
04^01	(0.6)	(-0.6)	4627.9	4688.2	4588.0
02^20[-27]	-0.15	1252.7	1224.6	1250.6	1217.7
12^20[-28]	0.11	2412.9	2385.7	2398.1	2366.3
04^20	-1.23	2564.1	2523.1	2551.4	2504.7
00^02	(2.2)	0.21	4202.9	4300.3	4167.9
00^03	6440.0	6390.4	6272.0	6416.4	6220.7
3. In KI:					
01^10	-0.36	-0.33	-0.51	-0.68	-0.28
10^00	-0.69	-0.53	-0.35	-0.82	-0.77
02^00	0.84	0.81	0.03	0.19	0.95
11^10[-25]	-0.94	-0.59	1781.1	1780.0	1765.2
03^10	0.52	-0.41	1892.2	1907.9	0.47
00^01	-0.36	-1.15	0.23	0.61	-0.60
20^00	-0.41	2357.7	2352.3	2331.9	2329.2
12^00	1.24	-1.83	2451.9	2424.1	0.43
04^00	0.71	2575.6	2544.8	2560.1	2522.9
21^10[-26]	2980.0	2949.7	2933.9	2924.2	2906.5
13^10	3106.2	3076.7	3059.8	3050.9	3029.9
05^10	3249.4	3226.3	3182.7	3207.4	3157.1
01^11	-0.24	2753.1	-0.18	0.06	-0.04

[-27] The 02^20 level is computed from the $02^20 \rightarrow \{11^10, 03^10\}$ and the $01^10 \rightarrow \{11^10, 03^10\}$, and the $01^10 \rightarrow 02^21$ and $02^20 \rightarrow 02^21$ transitions. The average value was used in the calculations and amounts to a mean deviation of ± 0.3 cm-1.

[-28] These levels were calculated from the $02^20 \rightarrow \{12^20, 04^20\}$ transition.

TABLE 7-6. (Continued)

Energy Level	$^{14}N^{12}C^{16}O^-$	$^{15}N^{12}C^{16}O^-$	$^{14}N^{13}C^{16}O^-$	$^{14}N^{12}C^{18}O^-$	$^{15}N^{13}C^{16}O^-$
10^01	-0.09	-0.45	-0.51	-0.58	-0.24
02^01	1.42	0 .95	0.21	1.03	0.47
02^21^{-26}	0.33	3366.5	3299.2	3372.7	3157.1
11^11^{-26}	-0.09	-0.05	3849.1	3896.0	3816.4
03^11	1.69	0.19	3960.2	4022.0	3927.6
30^00	1.83	3511.0	3498.5	3476.8	3464.7
22^00	0.83	3615.1	3623.0	3573.1	3582.4
14^00	-0.29	3730.5	3717.8	3698.0	3678.3
06^00	3917.5	3889.6	3837.7	3865.5	3806.8
20^01	-0.23	4456.1	4410.5	4439.2	4370.9
12^01	0.31	4547.7	4512.1	4530.1	4467.2
04^01	-2.76	4670.5	4603.1	4663.2	4563.8
02^20^{-27}	-0.36	1250.3	1222.3	1248.2	1215.4
12^20^{-28}	0.67	2405.6	2378.9	2390.9	2359.4
04^20	-0.25	2555.7	2515.1	2543.6	2496.5
00^02	4290.1	4257.8	4176.9	4273.0	4143.4
00^03	6401.8	6353.9	6234.0	6376.2	6184.2

instrumental in fixing the normal coordinate, k_{3333}, k_{333}, k_{331} and of course the harmonic, ω_3 and f_{NC} force constant.

Table 7-7 shows how the anharmonicity constants vary from lattice to lattice for $^{14}N^{12}C^{16}O^-$ cyanate. Owing to the extremely small variation and absence of significant trends one may draw the conclusion that anharmonicity constants are largely independent of the alkali halide environment. In addition the X_{22} values for cyanate isotopes in KBr appear to be large. The average deviations listed in column five are typical for all the species treated. These deviations are certainly within experimental error.

To illustrate the non-uniqueness of a set of anharmonicity constants when the criteria of their correctness is solely the reproduction of spectral observations, we need only examine Maki's results for $^{14}N^{12}C^{16}O^-$ in KBr. These are shown in column 6, Table 7-7. They did reproduce the cyanate frequencies very closely. Table 7-6 shows the remarkably close agreement with the observed spectra that the constants listed in Tables 7-2, 7-3 and 7-4 produce. The anharmonicity published by Schettino and Hisatsune do equally well (84). It is interesting that the anharmonicity constants arrived at in our work originate from normal coordinates conditioned by the data (and model potentials) and were not derived using equation 2-21.

The Fermi resonance term, k_{122}, also follows its mass dependence influenced behavior from isotope to isotope very well. It also follows the harmonic frequency trends from KCl to KI as illustrated in Table 7-7 for the 14 12 16 isotope. This is in accord with the increasing separations of the Fermi peaks in going from KI to KCl. Previously, Maki had expressed concern that his k_{122} for the ^{13}C cyanate ion decreased by 15% when the decrease was expected to be about 3% (analogous to the CO_2 case) (54,p.134). Our k_{122} decreases about 3.4% from $^{14}C^{12}N^{16}O^-$ to $^{14}N^{13}C^{16}O^-$. The root of Maki's dilemma was found to be the phenomenon that $2\nu_2^{\circ}$ is less than ν_1° in the ^{13}C case (16).

TABLE 7-7. VARIATION OF ANHARMONICITY AND FORCE CONSTANTS[-29] WITH ALKALI HALIDE ENVIRONMENTS FOR $^{14}N^{12}C^{16}O^-$ CYANATE.

Constant	In KCl	In KBr	In KI	Average	In KBr[-30]
x_{11}	-3.39	-3.36	-3.30	-3.35 ± 0.03	-4.92
x_{22}	0.56	0.82	0.59	0.66 ± 0.08	-2.58
x_{33}	-11.06	-11.36	-11.67	-11.36 ± 0.20	-13.0
x_{12}	-4.44	-4.45	-4.18	-4.36 ± 0.12	9.40
x_{13}	-19.17	-19.11	-19.07	-19.12 ± 0.04	-18.0
x_{23}	-11.13	-10.90	-11.79	-11.27 ± 0.34	-11.05
g_{22}	-0.45	-0.52	-0.46	-0.47 ± 0.03	2.33
k_{122}	-58.92	-58.01	-57.41	-58.11 ± 0.54	
ω_1	1264.50	1257.34	1250.27		1258.55
ω_2	637.96	635.12	635.01		635.62
ω_3	2224.68	2212.75	2200.78		2215.7
f_{NC}	15.487	15.233	14.826		15.879
f_{CO}	11.452	11.383	11.416		11.003
f_{NC-CO}	1.254	1.209	1.127		1.422
f_α	0.7372	0.7306	0.7304		0.7319

[-29] These values were obtained from Table 7-12. The factor of two enters because the expansion of $V(R_i)$ includes a (1/2) in the quadratic force constants.

[-30] Maki and Decius results are presented for comparison (56, p.779-780).

A comparison of spectroscopic constants for N_2O, NCO^-, and CO_2 is shown in Table 7-8. It is remarkable that they are all quite similar, especially X_{12}, X_{23} and X_{33}. Cyanate ion's anharmonicity constants appear to be more closely related to those calculated for CO_2 than for N_2O. The behavior of cyanate ion's X_{11} with mass change and its numerical closeness to CO_2's X_{11}, suggests that ω_1 is indeed more of a symmetric stretch than merely a C-O vibration. The series is isoelectronic and, if one compares the respective anharmonicity constants looking for trends with the shift of the molecular center of mass, there is no simple principle evident. This lack of correlation of anharmonicity constants also suggests that it is the electronic charge distribution which governs anharmonicity, not just mass relationship. This probably is the result of the Morse parametric constraints imposed by the model on the cubic constants used to arrive at the cyanate anharmonicity constants. The similarity of all the anharmonicity constants also illustrates how decoupled the cyanate ion is from the lattice and how closely NCO^- resembles the gas model.

The normal coordinate cubic and quartic potential constants which fit equations 2-14 and 2-15 are shown in Tables 7-9, 7-10 and 7-11 for cyanate ion in KCl, KBr and KI respectively. It is pleasing to note that the k_{122} is larger than k_{233}. This suggests that any resonance between the ν_1, $2\nu_2$ diad and the ν_3 vibration will be small though not entirely negligible. The k_{223} found to be the order of 45 indicates a correction to the observed frequency of ν_3 of about 0.5 cm^{-1} higher than the observed perturbed value. The computer program utilizes a perturbation technique to incorporate these indicated corrections to the higher frequencies as a result of this type coupling. This satisfies the Fermi resonance interactions symbolized in equation 3-10, and constitutes a further strength of this technique and the

results thus derived. Considerations of this type are thought to explain why the higher Fermi multiplets are better predicted by the spectroscopic constants presented in this chapter as opposed to those reported by Schettino and Hisatsune which were derived through the use of equation 2-21.

TABLE 7-8. COMPARISON OF SPECTROSCOPIC CONSTANTS CALCULATED FROM THE SMITH-OVEREND MODEL FOR ISOELECTRONIC LINEAR TRIATOMIC MOLECULES.[-31]

Constant	$^{12}C^{16}O_2$	$^{15}N^{12}C^{16}O^-$	$^{14}N^{12}C^{16}O^-$	$^{14}N^{13}C^{16}O^-$	$^{14}N^{14}N^{16}O$[-32]
ω_1	1353.40	1238.92	1257.34	1256.16	1300.41
ω_2	673.62	631.72	635.12	617.41	596.48
ω_3	2396.28	2195.34	2212.75	2152.94	2281.52
X_{11}	-3.08	-3.17	-3.35	-3.52	-4.84
X_{12}	-4.69	-4.27	-4.36	-4.23	-4.46
X_{13}	-19.84	-19.02	-19.12	-18.00	-27.39
X_{22}	1.12	0.68	0.66	0.61	1.08
X_{23}	-12.42	-11.32	-11.27	-10.52	-13.89
X_{33}	-12.07	-11.16	-11.36	-10.74	-15.06
g_{22}	-0.89	-0.50	-0.47	-0.43	-0.53

The internal coordinate potential constants through the quartic terms are presented in Table 7-12 for cyanate ion in KCl, KBr and KI. These constants fit the potential function given in equation 7-7:

[-31] Cyanate harmonic frequencies are those calculated for a KBr lattice environment. The anharmonicity constants are average values for the three lattices, and are found to vary less than 0.3 cm^{-1} from lattice to lattice.

[-32] Reference 86.

TABLE 7-9. NORMAL COORDINATE CUBIC AND QUARTIC FORCE CONSTANTS FOR CYANATE ION IN POTASSIUM CHLORIDE.

Constant	$^{14}N^{12}C^{16}O^-$	$^{15}N^{12}C^{16}O^-$	$^{14}N^{13}C^{16}O^-$	$^{14}N^{12}C^{18}O^-$	$^{15}N^{13}C^{16}O^-$	$^{14}N^{13}C^{18}O^-$	$^{15}N^{12}C^{18}O^-$
k_{111}	49.8414	48.1394	50.0912	48.1147	48.3431	48.3765	46.4546
k_{333}	47.2313	41.7998	47.6491	51.6706	42.0451	52.1579	46.4247
k_{122}	-58.9197	-58.9040	-56.9126	-56.7440	-56.9728	-54.6779	-56.7771
k_{113}	-47.3950	-44.5172	-47.6459	-47.5939	-44.7108	-47.8233	-44.9634
k_{223}	-47.7084	-43.3477	-46.7813	-52.3540	-42.3275	-51.5030	-48.0288
k_{133}	203.4789	204.3756	195.8225	195.3451	197.0950	187.4527	196.3713
k_{1111}	2.4121	2.2754	2.4426	2.3281	2.2998	2.3604	2.1962
k_{2222}	1.9999	1.9296	1.8973	2.0516	1.8264	1.9502	1.9749
k_{3333}	5.5705	5.4244	5.3055	5.5975	5.1514	5.3400	5.4396
k_{1223}	-0.7656	-0.3764	-0.7054	-1.3861	-0.3229	-1.3240	-1.0136
k_{2233}	-25.9749	-25.4385	-24.6053	-26.0157	-24.0592	-24.6621	-25.4357
k_{1133}	15.9267	16.0234	15.2450	14.8986	15.3914	14.1973	15.0216
k_{1122}	-9.7236	-9.6224	-9.4252	-9.2083	-9.3353	-8.9038	-9.1223
k_{1333}	2.6784	2.1633	2.7858	3.0491	2.2623	3.1503	2.5727
k_{1113}	-5.1672	-4.8277	-5.1863	-5.0951	-4.8431	-5.1087	-4.7883

TABLE 7-10. NORMAL COORDINATE POTENTIAL CONSTANTS FOR ISOTOPIC CYANATES IN POTASSIUM BROMIDE.

Constant	$^{14}N^{12}C^{16}O^-$	$^{15}N^{12}C^{16}O^-$	$^{14}N^{13}C^{16}O^-$	$^{14}N^{12}C^{18}O^-$	$^{15}N^{13}C^{16}O^-$	$^{14}N^{13}C^{18}O^-$
k_{111}	49.1978	47.5445	49.4247	47.4791	47.7276	47.7194
k_{333}	47.7536	42.2724	48.1708	52.3091	42.4614	52.7544
k_{122}	-58.0065	-58.0291	-56.0183	-55.8175	-56.1175	-53.7691
k_{113}	-44.4624	-41.5255	-44.7938	-44.9042	-41.7844	-45.2265
k_{223}	-50.4531	-46.1034	-49.3837	-55.0543	-44.9412	-54.0610
k_{133}	206.4171	207.1440	198.7842	198.2757	199.8804	190.4011
k_{1111}	2.3566	2.2255	2.3846	2.2735	2.2476	2.3036
k_{2222}	2.2206	2.1440	2.1064	2.2748	2.0292	2.1618
k_{3333}	5.8055	5.6488	5.5304	5.8386	5.3656	5.5712
k_{1223}	-1.8492	-1.4436	-1.7433	-2.4399	-1.3454	-2.3316
k_{2233}	-26.1266	-25.5607	-24.7598	-26.1960	-24.1838	-24.8453
k_{1133}	16.1968	16.2780	15.5172	15.1602	15.6477	14.4601
k_{1122}	-9.6008	-9.5106	-9.3003	-9.0837	-9.2220	-8.7771
k_{1333}	3.0275	2.5074	3.1151	3.3956	2.5864	3.4779
k_{3111}	-4.8635	-4.5202	-4.8911	-4.8208	-4.5424	-4.8441

TABLE 7-11. NORMAL COORDINATE POTENTIAL CONSTANTS FOR ISOTOPIC CYANATES IN POTASSIUM IODIDE.

Constant	$^{14}N^{12}C^{16}O^-$	$^{15}N^{12}C^{16}O^-$	$^{14}N^{13}C^{16}O^-$	$^{14}N^{12}C^{18}O^-$	$^{15}N^{13}C^{16}O^-$
k_{111}	48.0279	46.4496	48.2177	46.3401	46.5988
k_{333}	46.0433	40.5198	46.3803	50.8645	40.6676
k_{122}	-57.4062	-57.3148	-55.5055	-55.3333	-55.4825
k_{113}	-39.8370	-36.7853	-40.2793	-40.7240	-37.1260
k_{223}	-43.1096	-38.8786	-42.2895	-47.7697	-37.9659
k_{133}	211.7354	212.0851	204.1993	203.6199	204.8993
k_{1111}	2.2427	2.1210	2.2663	2.1634	2.1391
k_{2222}	1.8752	1.8106	1.7788	1.9219	1.7137
k_{3333}	6.0569	5.8953	5.7668	6.0925	5.5973
k_{1223}	-1.6252	-1.2282	-1.5301	-2.2137	-1.1406
k_{2233}	-26.3939	-25.8470	-25.0045	-26.4348	-24.4481
k_{1133}	16.7278	16.7655	16.0604	15.6845	16.1454
k_{1122}	-9.3745	-9.2746	-9.0850	-8.8828	-8.9960
k_{1333}	3.2256	2.6956	3.2966	3.6134	2.7562
k_{1113}	-4.3628	-4.0096	-4.4035	-4.3762	-4.0414

TABLE 7-12. INTERNAL COORDINATE FORCE CONSTANTS OF CYANATE ION IN KCL, KBR, AND KI. Statistical dispersions are shown in parentheses.

Constant	In KCl	In KBr	In KI
K_{11}	7.7434 (0.0337)	7.6166 (0.0029)	7.4137 (0.0528)
K_{12}	1.2542 (0.0248)	1.2085 (0.0218)	1.1274 (0.0329)
K_{22}	5.7260 (0.0243)	5.6923 (0.0219)	5.7076 (0.0372)
K_{33}	0.3686 (0.0005)	0.3653 (0.0004)	0.3652 (0.0005)
K_{111}	-16.7895	-16.9639	-16.0747
K_{112}	-2.1032	-1.9656	-1.7196
K_{122}	-3.0595	-2.8932	-2.5843
K_{133}	-0.5049 (0.0372)	-0.4426 (0.0280)	-0.5334 (0.0385)
K_{222}	-13.2419	-13.0633	-13.1993
K_{233}	-0.7296(0.0262)	-0.7766 (0.0212)	-0.7172 (0.0271)
K_{1111}	21.2352	22.0398	20.3312
K_{1112}	2.7556	2.5089	2.0884
K_{1122}	1.6856	1.7741	1.3395
K_{1133}	0.3458	0.2681	0.3895
K_{1222}	5.2541	4.9198	4.2270
K_{1233}	1.9987	1.8819	2.0949
K_{2222}	17.8634	17.4876	17.8059
K_{2233}	0.7221	0.8255	0.7042
K_{3333}	0.0389 (0.0047)	0.0535 (0.0039)	0.0409 (0.0046)

$$V = K_{11}R_1^2 + K_{12}R_1R_2 + K_{22}R_2^2 + K_{33}R_3^2 + K_{111}R_1^3 + K_{112}R_1^2R_2 +$$
$$+ K_{122}R_1R_2^2 + K_{133}R_1R_3^2 + K_{233}R_2R_3^2 + K_{1111}R_1^4 + K_{1112}R_1^3R_2$$
$$+ K_{1122}R_1^2R_2^2 + K_{1133}R_1^2R_3^2 + K_{1222}R_1R_2^3 + K_{1233}R_1R_2R_3^2$$
$$+ K_{2222}R_2^4 + K_{2233}R_2^2R_3^2 + K_{3333}R_3^4 + K_{222}R_2^3 , \qquad (7\text{-}7)$$

where R_1 is the N-C stretch, R_2 is the C-O stretch R_3 is the bending coordinate. The potential function is a Taylor series expansion, hence $2K_{ii} = f_{ii}$ where f_{ii} are the conventionally discussed quadratic force constants. As shown in Table 7-7, these agree reasonable well with the previously published values. The asymmetric stretch force constants, K_{22} for the cyanate ion in KI appears to be larger than expected. The K_{22}'s which were calculated for cyanate ion in KCl and KBr were higher before $2\nu_3$ was discovered. Thus it is believed that this slightly increased K_{22} for cyanate in KI is a result of not having a reliable $2\nu_3$ value.

Smith and Overend, using their model to calculate free gas and matrix isolated gas spectra, have noted that the observed frequency shifts could be accounted for with the quadratic potential constants.[-33] As sufficient data for matrix isolated gases was not available to permit the calculation of cubic and quartic force constants, the free gas anharmonic potential constants were used with the matrix isolated quadratic constants to calculate the observed spectra. The close agreement obtained suggested that anharmonic effects and general bond character are not appreciably different from free gas to matrix isolated gas and indeed in going from one matrix to another.[-33] The cyanate ion data provided an interesting test of these observations. When the model was applied to the cyanate ion data in

[-33] Private communication, D. Foss Smith Jr., 7 December 1970.

TABLE 7-13. COMPARISON OF INTERNAL COORDINATE FORCE CONSTANTS FOR SOME LINEAR TRIATOMIC MOLECULES.[-34]

Constant	OCO	NCO[-35]	NNO	OCS	HCN[-36]
K_{11}	8.008	7.617	9.107	7.815	9.318
K_{12}	1.249	1.209	1.034	0.730	
K_{22}		5.692	6.008	3.826	
K_{33}	0.392	0.365	0.333	0.326	
K_{111}	-19.055	-16.884	-23.320	-17.378	-20.917
K_{112}		-1.963	-1.656	-1.513	
K_{122}	-2.040	-2.897	-1.358	-0.910	
K_{133}	-0.604	-0.444	-0.630	-0.414	
K_{222}		-13.201	-16.623	-7.146	
K_{233}		-0.775	-0.885	-0.494	
K_{1111}	26.670	21.833	32.801	21.099	27.051
K_{1112}	2.739	2.509	1.954	2.450	
K_{1122}	2.944	1.738	1.605	0.413	
K_{1133}	0.466	0.270	0.596	0.264	
K_{1222}		4.926	1.479	0.825	
K_{1233}	1.864	1.886	3.350	1.258	
K_{2222}		17.861	24.456	9.880	
K_{2233}		0.823	1.177	0.375	
K_{3333}	0.035	0.053	0.081	0.052	

[-34] Calculated from the Smith-Overend model potential(86).

[-35] Force constants for cyanate ion in KBr are shown.

[-36] Only those values pertaining to the CN bond are listed.

the three different lattices, the anharmonic potential constants did not in fact vary significantly. This supports arguments that the chemical bonding in each of the matrices is very similar and that the model does represent the situation nicely.

Table 7-13 presents a comparison of internal coordinate potential constants between linear triatomics. The quadratic constants correlate very well to the bond type considered. The constants for CO_2, N_2O and OCS presented in this table agreed within 0.03 through cubic constants, within 0.10 for quartic constants, with general quartic field calculations (86). This attests to the strength of the Smith-Overend model and lends reliability to the cyanate results.

The quadratic force constants for cyanate can be compared to bond order correlations given by Wilson, Decius and Cross (95,p. 175). In this analysis, the C-O bond order is slightly less than two and the N-C bond order is slightly less than three.

CHAPTER 8

CONCLUDING DISCUSSION

In 1966 Schettino and Hisatsune undertook the reinvestigation of cyanate and its isotopic species in KCl, KBr and KI (84). Independently they have reached many of the same conclusions arrived at in earlier sections of this paper. They studied cyanate spectra from 400-5000 cm^{-1} for $^{14}N^{12}C^{16}O^-$, $^{15}N^{12}C^{16}O^-$, $^{14}N^{13}C^{16}O^-$, $^{14}N^{12}C^{18}O^-$ and $^{15}N^{13}C^{16}O^-$. From spectra, they have calculated a set of anharmonicity constants, harmonic frequencies, and force constants. Their sophisticated use of the pellet technique also enabled them to obtain absolute intensity data and molar extinction coefficients. Their results agree very well with those presented in Chapters Six and Seven. This chapter will discuss and compare our work to theirs and will conclude with a summary of conclusions drawn from our studies.

Several aspects of the experimental work of Schettino and Hisatsune merit mention. They apparently improved upon the cyanate sampling pellet techniques presented in Chapter Five. Schettino and Hisatsune prepared their isotopic cyanates in the appropriate alkali halide by the reactions shown below at 300°C to 500°C:

$$^{15}NH_4X + K_2CO_3 \xrightarrow[\Delta]{KX} K^{15}NCO + 2H_2O \qquad (8\text{-}1)$$

$$NH_4X + K_2{}^{13}CO_3 \xrightarrow[\Delta]{KX} KN^{13}CO + 2H_2O \qquad (8\text{-}2)$$

$$NH_4X + K_2C^{18}O_3 \xrightarrow[\Delta]{KX} KNC^{18}O + 2H_2O \qquad (8\text{-}3)$$

where X = Cl, Br or I. Except in the $NC^{18}O^-$ synthesis, an excess of NH_4X was utilized to drive the reaction and to stabilize the product cyanate until the final pellet preparation, at which time the NH_4X was sublimed off. These researchers found that the cyanate would go into solid solution in the alkali halide by heating a

cyanate doped pellet at 500-550°C for six hours. Their observation (84,p.14) that in oxygen 18 enriched cyanate, the oxygen rapidly exchanges with atmospheric oxygen and atmospheric water, supports our observation and experiences (explained in Chapter Five) with this cyanate species. Schettino and Hisatsune's 18-oxygen enriched cyanate pellets contained large excesses of carbonate ^{18}O. This explains why their $NC^{18}O^-$ spectral observations were not as extensive as ours.

While it is difficult to ascertain whether or not Schettino and Hisatsune were able to obtain more concentrated cyanate solid solutions than were obtained by our pellet endeavers, they were able to reduce carbonate interference using ammonium halides. This enabled them to obtain spectra comparable to our single crystal spectra. However, in the isotopic studies, our crystals revealed 40 more isotopic peaks for the same species studied; and, in addition we observed many bands for $^{15}N^{12}C^{18}O^-$ and $^{14}N^{13}C^{18}O^-$ which they were evidently unable to determine due to the carbonate complications.

An interesting finding during their experimentation was that satellite peak relative intensities could be a crude indicator of solid solution homogeneity. They found the more homogeneously (through freeze-drying) cyanate was mixed with the potassium halide, the lower the relative intensity of the satellite (to the main peak) became. This also points up an advantage of the pellet technique. Concentrations may more easily be studied in this method, than in single crystals; although now that extinction coefficients are available it should be possible to estimate concentration in our crystals. Their studies reinforce earlier conclusions deduced by Decius, et al. (19) as to the origin of the satellite peaks as ion cluster effects.

-37 Schettino and Hisatsune claim accuracy within ±0.2 cm^{-1} for most of their observations.

Overall, the spectral data for NCO^-, $^{15}NCO^-$, $N^{13}CO^-$, $NC^{18}O^-$ and $^{15}N^{13}CO^-$ in KCl and KBr determined by Schettino and Hisatsune agree very well with our data. The agreement is within experimental error from 500 cm^{-1} to 2000cm^{-1} for all fundamental frequencies except the upper member of the Fermi diad for the $^{13}C^-$ cyanate in KBr.[37] About 20% of our peaks for the isotopic species between 2000 and 4000 cm^{-1} appear to be from 0.7 cm^{-1} to 2.5 cm^{-1} higher than theirs. The origin of this observation is not readily explained, and probably indicates further investigation. Generally, the differences between the two sets of data increase as the weaker and more diffuse bands are compared. It is well known that weak spectral features in a poly-crystalline matrix tend to be weaker and more diffuse due to thermal effects scattering phenomena. This could well account for the apparent difference in the spectral frequencies. This effect on band widths is alluded to by Schettino and Hisatsune (84,p.23). Also, the greatest deviations from our data occurred for $NC^{18}O^-$ in KCl for bands above 2000 cm^{-1}. They obtained fifteen frequencies, while we obtained twenty, thus indicating that either other impurity complications were great, or that our single crystal ^{18}O-cyanate was studied at higher concentration. In KBr, they were able to determine only eight, while we determined eighteen of the $NC^{18}O^-$ peaks, and again the agreement above 2000 cm^{-1} was one to two wave numbers off. Since, in both studies, the IUPAC tables (38) were utilized to determine frequencies, it is felt that perhaps further experimental investigations are warrented in this area.

Schettino and Hisatsune arrived at anharmonicity constants, harmonic frequencies, and quadratic force constants in their work which agree well with those calculated in this study. Table 8-1 shows a comparison of their results to ours for $^{15}N^{12}C^{16}O^-$, a typical example. They assumed a value for X_{33} of 14.0 (for $^{14}N^{12}C^{16}O^-$ in all three lattices) as they were not able to observe any overtone

TABLE 8-1. COMPARISON OF SPECTROSCOPIC CONSTANTS FOR $^{15}N^{12}C^{16}O^-$ AND CYANATE ION FORCE CONSTANTS IN KCL[-38], KBR[-39], AND KI[-40](a) Calculated using the Smith-Overend potential; and (b) Calculated from experimental data using equation 2-21.

Constant	(a) In KCl	(b) In KCl	(a) In KBr	(b) In KBr	(a) In KI	(b) In KI
x_{11}	-3.19	-2.85	-3.18	-3.10	-3.13	-3.57
x_{22}	0.586	0.415	0.843	0.513	0.612	0.534
x_{33}	-10.9	-13.8	-11.15	-13.7	-11.5	-13.9
x_{12}	-4.35	-3.56	-4.36	-3.45	-4.09	-3.74
x_{13}	-19.1	-18.4	-19.03	-18.4	-18.9	-18.1
x_{23}	-11.2	-11.2	-10.96	-11.2	-11.8	-11.0
g_{22}	-0.474	-1.91	-0.542	-1.81	-0.481	-1.63
k_{122}	58.90	58.16	58.03	57.72	57.32	57.34
ω_1	1246.11	1241.5	1238.92	1235.8	1231.64	1230.5
ω_2	634.55	635.7	631.72	633.7	631.62	632.1
ω_3	2206.94	2211.6	2195.34	2200.5	2184.03	2186.6
f_{NC}	15.487	15.423	15.233	15.281	14.826	15.142
f_{CO}	11.452	11.464	11.385	11.342	11.416	11.211
f_{NC-CO}	1.254	1.153	1.209	1.156	1.127	1.178
f_α	0.7372	0.7401	0.7306	0.7352	0.7304	0.7317

-38 Data used in (a) comes from Table 6-2. Data used in (b) comes from reference 84, p.15.

-39 Data used in (a) calculations comes from Table 6-8. Data used in (b) comes from reference 84, p.17.

-40 All data used in determining (a) and (b) comes from reference 84, p.19-20.

of ν_3 in their studies. Depending upon how X_{22} and k_{122} were determined, they obtained two sets of anharmonicity constants which reproduced the spectra equally well. The values reported in their paper were derived from best-fit X_{22} and k_{122} values, while the other constants were determined using specific transitions and equation 2-21. Table 8-1 illustrates not only the differences between model potential energy calculations versus equation 2-20 type calculations (shown very well by the KI columns[-41]) but also the effect of data differences on the calculations (illustrated in the KCl column by comparison to the closeness of the agreement in the KI case versus the closeness of agreement of the KCl case).

Schettino and Hisatsune note that their k_{122} does not contain corrections for higher vibrational quantum numbers (see equation 3-9). The closeness of all the k_{122} values demonstrates that these higher order corrections (e.g. k_{12222}) are small. All of the anharmonicity constants in Table 8-1 agree fairly well, when one takes into account the assumed X_{33} value, except for the g_{22} values. Schettino and Hisatsune note that their g_{22} varied by as much as two wave numbers depending upon which levels were considered to obtain them. The calculated g_{22} using the Smith-Overend method was fairly constant for all cyanate species. Hence, the difference between the two arises from the defination of the constant. The g_{22} constant is connected to cyanate ion's librational behavior. It is numerically small and even at best not very well determined owing to the experimental error. Further investigation in this area should prove interesting.

The harmonic frequencies in the KI case agree closely, their difference mainly being due to the method of calculation. The frequencies calculated using the Smith-Overend technique obey the Redlich-Teller rule more accurately than the experimental ones.

[-41] Calculations in the KI case were both done using the same data of Schettino and Hisatsune.

The difference in the ω_3 case arrise from the X_{33} assumption, the calculation method, and experimental results differences ($\Delta\nu_3$ = 0.7 cm^{-1})[-42]. The ω_3's calculated by Schettino and Hisatsune were obtained without observing $2\nu_3$, and without correcting for the weak Fermi interaction between ν_3 and other levels. The ω_2's agree quite closely. The ω_1 differences in KCl arrise from the anharmonicity correction differences, the method of calculation, and the resonance correction differences.

The force constants are in good agreement. It is interesting to note that the bending constant, f_α, and the f_{CO} stretching force constant are in close agreement. The f_{NC}'s in KCl agree surprisingly well while those calculated from harmonic frequencies in KI deviate by 0.3 $^{md}/\text{Å}$. The root of the problem in this instance is the lack of an experimental $2\nu_3$ value. In the KI case, the associated X_{33} correction was computed from normal coordinate potential constants for the KCl and KBr cases with the appropriate mass corrections to obtain a best fit to the observed spectra in KI. Even so, it is felt that an observed $2\nu_3$ is necessary to improve the associated f_{NC} force constants in the KI matrix. These force constants were calculated from all the isotopic data, not just for the ^{15}N case, by adjusting the normal coordinate constants for each species. Owing to the close agreement in the KCl case, it is not thought that the method of calculation should be called into question. The fault is either in the X_{33} (which has not been observed for KI) or a possible error in computation.

The results presented in this paper taken with Schettino and Hisatsune's work represent a most comprehensive study of cyanate ion in alkali halide lattices. Excepting the data for the calculations for the cyanate ion in KI discussed in Chapter Seven and Eight, all of the work contained in this paper was done independently of the aforementioned researchers. It is significant that we indicated our

[-42] $\Delta\nu_3$ = (this work) minus (reference 82) for the KCl case only.

cyanate isotopic studies by publication in 1967. Our experimental approach differed in that we used direct oxidation reactions to prepare our isotopic cyanates and studied their spectra in single crystals. We observed about 70 additional peaks, and observed overtones of ν_3. Through the use of the Smith-Overend computer program, a resonable and complete set of anharmonic internal and normal coordinate force constants have been calculated.

An analysis of these force constants has shown that the lattice frequency shift can be accounted for by the quadratic force constants. It is also found that the lattice perturbation on the internal potential function (in equation 7-7) decreases from KCl to KI matrices for the linear vibrational modes.

The anharmonicity constants determined in our calculations are felt to be the most reliable set yet obtained for the various cyanate isotopic species. This is demonstrated by the fine agreement between calculated and observed frequencies for the higher Fermi multiplets observed above 3500 cm^{-1}. They do fit the data as well as any set yet obtained but more importantly, they arrise from the normal coordinate potential function, not from free gas approximation stated in equation 2-21. Further it has been amply demonstrated that many sets of anharmonicity constants reproduce the cyanate spectrum and while that criterion is a necessary one, it is not sufficient to prove any set unique. This is an area which easily lends itself to further study. It should be added here, that the harmonic frequencies determined in this study more accurately fit the Redlich-Teller product rule than any previously reported.

This thesis has presented a most comprehensive study of cyanate ion. Earlier chapters have described previous investigations into the chemical and physical properties of this molecule. Sufficient theory was presented in the first four chapters to enable one to appreciate the findings developed in Chapter Six and

Seven. The experimental section has discussed several means by which cyanate ion may be prepared. The closed system heterogeneous oxidation of cyanide to cyanate has been thoroughly investigated. Several sampling techniques were thoroughly discussed and their application facilitated our extensive elucidation of the cyanate vibrational spectrum. Over 250 cyanate vibration bands were studied, including over 180 bands due to isotopic species. The use of isotopic cyanates has enabled us to correct and confirm many previous cyanate assignments as well as to add over 60 frequencies to the cyanate catalog. It is significant that the use of the single crystal sampling technique has enabled us to find the previously unobserved $2\nu_3$ overtone. Using the data presented in Chapter Six and the computer techniques presented in Chapter Seven, we have been able to calculate a reasonable internal potential energy equation for the cyanate ion. In the process, we have also obtained a complete set of normal coordinate potential constants and a better set of spectroscopic constants than was previously available. Minor developments of this study are contained in earlier chapters and included: the successful application of Noether's Rule to di-and tri-substituted cyanates; the use of relative intensity data and the Redlich-Teller product rule to fix the unperturbed energies of Fermi resonant modes; lattice effects on vibrational energies; and the appearance of the cyanate ion spectra from 500 cm^{-1} to 5000 cm^{-1} for 15 12 16, 14 13 16, and 14 12 18 cyanates dissolved in both KCl and KBr.

BIBLIOGRAPHY

1. Acompora, F. M., A. S. Tompa and N. O. Smith. Homogenation of solid solutions - a proposed new technique. Journal of Chemical Physics 24:1104. 1956.

2. Adel, A. and D. M. Dennison. Infrared spectrum of carbon dioxide, part I. Physical Reviews 43:716-723. 1933.

3. Amat, G. and M. Pimbert. On Fermi resonance in carbon dioxide. Journal of Molecular Spectroscopy 16:278-290. 1965.

4. Badger, R. M. The relation between the internuclear distance and force constants of molecules and its application to polyatomic molecules. Journal of Chemical Physics 3:710-714. 1935.

5. Berney, C. V. and D. F. Eggers. Infrared spectrum of carbon dioxide, enriched in oxygen 18. Journal of Chemical Physics 40:990-1000. 1964.

6. Blaine, L. R., E. K. Plyler and W. S. Benedict. Calibration of small grating spectrometers from 166 to 600 cm^{-1}. Journal of Research, Series A: Physics and Chemistry, p.223-225. 1966.

7. Bryant, J. I. and G. C. Turrell. Infrared spectra of the azide ion in alkali-halide lattices. Journal of Chemical Physics 37: 1069-1077. 1962.

8. Carrington, A., A. R. Fabris and N. J. D. Lucas. Electron resonance spectra of NCO in the gas phase. Journal of Chemical Physics 49:5545-5547. 1968.

9. Cihla, Z. and J. Pliva. Anharmonic potential function of polyatomic molecules, part V: Transformation of general valence force coordinates. Collection of Czechoslovakian Chemical Communications 28:1232-1236. 1963.

10. Cleveland, F. F. Raman spectrum of an aqueous solution of potassium cyanate. Journal of the American Chemical Society 63:622-623. 1941.

11. Cook, R. P. and P. L. Robinson. Certain physical properties of cyanogen and its halides. Journal of the Chemical Society 1935: 1001-1005.

12. Courtoy, C. P. Spectres de vibration-rotation de molecules simples diatomiques ou polyatomiques avec long parcours d'absorption XII: le Spectre de $^{12}C^{16}O_2$. Canadian Journal of Physics 35:608-648. 1957.

13. Crawford, B. L., Jr. Vibrational intensities, II. The use of isotopes. Journal of Chemical Physics 20:977-981. 1952.

14. Darling, B. T. and D. M. Dennison. The water vapor molecule. Physical Reviews 57:128-139. 1940.

15. Decius, J. C. A tabulation of general forms of inverse kinetic energy matrix elements in acyclic molecules. Journal of Chemical Physics 16:1025-1034. 1948.

16. Decius, J. C. Coupling of the out-of-plane bending mode in nitrates and carbonates of the aragonite structure. Journal of Chemical Physics 23:1290-1294. 1955.

17. Decius, J. C., E. H. Coker and G. L. Brenna. The vibrational spectra of sulfate ions in alkali halide crystals. Spectrochimica Acta 19:1281-1289. 1963.

18. Decius, J. C. and D. J. Gordon. The Fermi doublet ν_1, $2\nu_2$ in the cyanate ion. Journal of Chemical Physics 47:1286-1288. 1967.

19. Decius, J. C., et al. Cyanate ion in alkali halides: New vibrational levels and interpretation of localized lattice modes. Journal of Chemical Physics 43:2180-2186. 1965.

20. Decius, J. C., O. G. Malan, and H. W. Thompson. The effect of intermolecular forces upon the vibrations of molecules in the crystalline state. Proceedings of the Royal Society 275A: 295-309. 1963.

21. Dennison, D. M. The infrared spectra of polyatomic molecules, part II. Reviews of Modern Physics 12:175-214. 1940.

22. Dixon, R. N. Anomalous band intensity in Fermi resonance, Journal of Chemical Physics 31:258-260. 1959.

23. Dixon, R. N. The absorption spectra of the free radical NCO. Philosophical Transactions of the Royal Society, Series A: 252:165-192. 1960.

24. Dupree, D. C. and K. L. Lindsey. Preparation of metal cyanates. U. S. Patent 2,801,154. June 30, 1957.

25. Ferigle, S. M. and A. G. Meister. Kinetic energy matrix elements for linear molecules. Journal of Chemical Physics 19:982. 1951.

26. Fermi, E. Über den Ramaneffect des kohlendioxyds. Zeitschrift für Physik 71:250-259. 1931.

27. Gates, D. M., et al. Line parameters and compound spectra for water vapor bands at 2.7 μ. National Bureau of Standards Monograph 71. August 1964.

28. Gordon, H. R. and T. K. McCubbin, Jr. The 2.8 micron bands of CO_2. Journal of Molecular Spectroscopy 19:137-154. 1966.

29. Goubeau, J. Raman-effect und das konstitutions-problem des cyanatrestes. Zur kenntnis der pseudohalogene. Berichte der Deuschen Chemischen Gesellschaft 68:912-919. 1935.

30. Haley, E. E. and J. P. Lambooy. Preparation of KNCO from KCN. Journal of the American Chemical Society 76:2926-2927. 1954.

31. Hartzdorf, C. Determination of cyanide, cyanate, and carbonate in the presence of each other. Fresenius Zeitschrift für Analytikal Chemie 237:161-166. 1968.

32. Hendricks, S. E. and L. Pauling. The crystal structure of sodium and potassium trinitrides and potassium cyanate and the nature of the trinitride group. Journal of the American Chemical Society 47:2904-2920. 1925.

33. Hertzberg, G. Molecular spectra and molecular structure II. Infrared and Raman spectra of polyatomic molecules. D. Van Nostrand Company Inc. Princeton, New Jersey. 1945. 632p.

34. Hexter, R. M. and D. A. Dows. Low-frequency librations and the vibrational spectra of molecular crystals. Journal of Chemical Physics 25:504-509. 1956.

35. Hisatsune I. C. and N. H. Suarez. Infrared spectra of metaborate monomer and trimer ions. Inorganic Chemistry 3:168-174. 1964.

36. Hofman, K. A. Oxidation von gebundenem stickstoff zu salpeter bei neideren temperaturen und reduction von salpeter zum cyanid. Berichte der Deutschen Chemischen Gesellschaft 59:204-212. 1926.

37. Holmes, R. E. Electrical and optical properties of potassium chloride single crystals containing lead ion. Doctorial Dissertation, Oregon State University, September 3, 1965. p. 16-38.

38. International Union of Pure and Applied Chemistry (I.U.P.A.C.) Commission on Molecular Structure and Spectroscopy. Tables of Wave numbers for calibration of infrared spectrometers. Butterworths Scientific Publications, Ltd., London. 1961.(Reprinted from Pure and Applied Chemistry 1:537-700. 1961).

39. Jones, L. H. Infrared spectrum and structure of thiocyanate ion. Journal of Chemical Physics 25:1069-1072. 1956.

40. Jones, L. H. Polarized infrared spectrum of potassium thiocyanate. Journal of Chemical Physics 28:1234-1236. 1958.

41. Kimura, K. and M. Kimura. Approximate method in calculating mean square amplitude of bonded interatomic distances. Journal of Chemical Physics 25:362. 1956.

42. Krueger, P. J. Performance of the Beckman IR-7 infrared spectrometer 1: Frequency reproducibility and accuracy(630-4000 cm^{-1}). Applied Optics 1:443-453. 1962.

43. Krueger, P. J. Performance of the Beckman IR-7 infrared spectrometer 2: Frequency reproducibility and accuracy(200-800 cm^{-1}). Applied Optics 1:621-625. 1962.

44. Krueger, P. J. and G. H. Schulze. Beckman IR-7 infrared spectrometer modifications. The Review of Scientific Instruments 34:88-92. 1963.

45. Kyropoulos, S. Dielektrizitals konstanten regularer kristalle. Zietschrift für Anorganische und Allgemeine Chemie 156:308-313. 1926.

46. Ladd, J. A., W. J. Orville-Thomas and B. C. Cox. Molecular parameters and bond structure III: Carbon-oxygen bonds. Spectrochimica Acta 20:1771-1780. 1964.

47. Lawsen, W. D. and S. Nielsen. Preparation of single crystals. Butterworths, London. 1958. 225p.

48. Lide, D. R., Jr. Determination of anharmonic potential constants in linear XYZ molecules. Journal of Molecular Spectroscopy 33:448-459. 1970.

49. Lippincott, E. R. A new relation between potential energy and internuclear distance. Journal of Chemical Physics 21: 2070-2071. 1953.

50. Lippincott, E. R. and R. Schroeder. General relations between potential energy and internuclear distance for diatomic and polyatomic molecules. Journal of Chemical Physics 23:1131-1141. 1955.

51. Machida, K. and J. Overend. The dissociation of polyatomic molecules and the relation of ensuing geometrical changes to the force constants. Journal of Chemical Physics 50:4437-4444. 1969.

52. Machida, K. and J. Overend. Anharmonic stretch-stretch interaction force constants of triatomic molecules. Journal of Chemical Physics 50:4429-4436. 1969.

53. Machida, K. and J. Overend. General model of anharmonic interaction force constants in polyatomic molecules. Journal of Chemical Physics 51:2537-2542. 1969.

54. Maki, A. G. The infrared spectrum of cyanate ion in different environments. Doctorial Dissertation, Oregon State University. June 1960. 151p.

55. Maki, A. G. and J. C. Decius. Infrared spectrum of cyanate ion as solid solution in a potassium iodide lattice. Journal of Chemical Physics 28:1003-1004. 1958.

56. Maki, A. G. and J. C. Decius. Vibrational spectrum of cyanate ion in various alkali halide lattices. Journal of Chemical Physics 31:772-782. 1959.

57. Mantz, A. W., et al. Vibration-rotation bands of $^{15}N_2{}^{18}O^-$ effects of Fermi resonance and ℓ-type doubling. Journal of Molecular Spectroscopy 30:513-530. 1969.

58. McCarthy, D. E. The reflection and transmission of infrared materials 1: Spectra from 2-50 microns. Applied Optics 2: 591-603. 1963.

59. Menzies, A. C. and J. Skinner. The growing of crystals. Discussions of the Faraday Society 5:306-312. 1949.

60. Miller, F. A. and C. H. Williams. Infrared spectra and characteristic frequencies of inorganic ions. Analytical Chemistry 24:1253-1294. 1952.

61. Milligan D. E. and M. E. Jacox. Matrix isolation study of the infrared and ultraviolet spectra of the free radical NCO. Journal of Chemical Physics 47:5157-5168. 1967.

62. Moelwyn-Hughes, E. A. Physical chemistry. Pergamon Press, New York, 1961. 1307p.

63. Nielsen, A. H. The vibration-rotation energies of the linear XYZ type molecule. Journal of Chemical Physics 11:160-163. 1943.

64. Nielsen, H. H. The vibration-rotation energies of molecules. Reviews of Modern Physics 23:90-136. 1951.

65. Noether, H. D. The ratio rule. Journal of Chemical Physics 11:97-100. 1943.

66. Ogden, M. IR-7 infrared spectrophotometer instruction manual. Beckman Instruments,Inc. Fullerton, California. 1960. 85p.

67. Ogden, M. Instruction manual, tracking accuracy control and variable scale expansion for IR-4 and IR-7 spectrophotometers. Beckman Instruments, Inc., Fullerton, California. 1961. 21p.

68. Pal, N. N. and P. N. Sen Gupta. Raman effect in some organic and inorganic substances. Indian Journal of Physics 5:13-34. 1930.

69. Papousek, D. and J. Pliva. Computer calculation of quadratic molecular potential constants. Collection of Czechoslovakian Chemical Communications 28:755-775. 1963.

70. Papousek, D. and J. Pliva. Anharmonic potential function of polyatomic molecules, part VI: The role of non-bonded interaction. Collection of Czechoslovakian Chemical Communications 29:1973-1997. 1964.

71. Papousek, D., S. Toman and J. Pliva. Calculation of quadratic molecular potential constants by the method of damped least squares. Journal of Molecular Spectroscopy 15:502-505. 1965.

72. Pariseau, M. A. The empirical calculation of anharmonic force constants of polyatomic molecules. Doctorial Dissertation, University of Minnesota. October 1963. 149p.

73. Pariseau, M. A., I. Suzuki and J. Overend. Least squares adjustment of anharmonic potential constants: Application to $^{12}CO_2$ and $^{13}CO_2$. Journal of Chemical Physics 42:2335-2344. 1965.

74. Pauling, L. The nature of the chemical bond, 2nd Ed. Cornell University Press. Ithaca, New York. 1948. 450p.

75. Pauling, L. and E. B. Wilson. Introduction to quantum mechanics. McGraw Hill, Inc. New York. 1935. 453p.

76. Pliva, J. Anharmonic potential function for polyatomic molecules. Collection of Czechoslovakian Communications 23:777-790. 1958.

77. Pliva, J., V. Spirko and D. Papousek. Anharmonic potential function of polyatomic molecules, part VII: Iterational calculation of anharmonic corrections to fundamental frequencies. Journal of Molecular Spectroscopy 23:331-342. 1967.

78. Porterin, A. Sur la decomposition du cyanate de potassium par la chaleur. Comptes Rendus de Se'ances de l'Acade'mie des Sciences 161:308-310. 1915.

79. Potts, W. J., Jr. Chemical infrared spectroscopy, volume 1: Techniques. John Wiley and Sons, Inc. New York, 1963. 321p.

80. Rao, K. N. and H. H. Nielsen. Fermi diad 10^00 and 02^00 of N_2O. Canadian Journal of Physics 34:1147-1152. 1956.

81. Rao, K. N., R. V. deVore and E. K. Plyler. Wavelength calibrations in the far infrared (30-1000 microns). Journal of Research 67A:351-358. 1963.

82. Redlich, O. Bine allgemeine beziehung zwischen den schwingungsfrequenzen isotoper molekeln. Zeitschrift für Physikalische Chemie B28:371-382. 1935.

83. Reichman, S. and J. Overend. Importance of quadratic force constants in Fermi resonance. Journal of Chemical Physics 47:1525-1530. 1967.

84. Schettino, V. and I. C. Hisatsune. Infrared spectrum of matrix isolated cyanate ion I: Vibrational analysis, band widths, and absolute intensities in potassium halides. Journal of Chemical Physics 52:9-27. 1970.

85. Slyhouse, T. E. and H. O. Drickamer. Effect of pressure on CN^- dissolved in an alkali halide lattice. Journal of Chemical Physics 27:1226-1227. 1957.

86. Smith, D. F., Jr. and J. Overend. A simplification of the general quartic force field of linear triatomic molecules. A prepublication preprint accepted for publication in the Journal of Chemical Physics in 1971.

87. Smith, L. H. and P. Yates. The synthesis of 4-amino-2(3H)-oxo-5-imidazolecarboxamide. Journal of the American Chemical Society 76:6080-6085. 1954.

88. Steele, W. C. and J. C. Decius. Infrared absorption of lanthanum, scandium, and indium borate and the force constants of borate ion. Journal of Chemical Physics 25: 1184-1188. 1956.

89. Suzuki, I. General force sonstants of N_2O. Journal of Molecular Spectroscopy 32:54-73. 1969.

90. Suzuki, I., M. A. Pariseau and J. Overend. General quartic force fields of HCN. Journal of Chemical Physics 44:3561-3567. 1966.

91. Waddington, T. C. Lattice parameters and infrared spectra of some inorganic cyanates. Journal of the Chemical Society 1959:2499-2504.

92. Walnut, T. H. A study of selection rules for vibration spectra of complex crystals. Journal of Chemical Physics 20:58-62. 1952.

93. Wang, J. H. and E. B. Fleischer. Tracer studies on the mechanism of combustion of carbon, sulfur, mercuric(II) sulfide. Journal of the American Chemical Society 80: 3874-3875. 1955.

94. Williams, D. The infrared spectrum of potassium cyanate solutions. Journal of the American Chemical Society 62: 2442-2444. 1940.

95. Wilson, E. B., J. C. Decius and P. C. Cross. Molecular vibrations. New York, McGraw-Hill. 1955. 388p.

96. Witchel, W. Calculations of vibration partition functions of polyatomic molecules including Fermi or Darling-Dennison resonances. Chemical Physics Letters(Netherlands) 2:349-350. 1968.

APPENDICES

APPENDIX I

Normal Coordinate Analysis

The following treatment refers to the situation depicted in Figure 2-1 and described by equations 2-1 through 2-9 for the linear XYZ case. Define a set of general displacement coordinates, x, y, z, using the Ekhart-Savetz conditions:

$$x = 2[(m_1 + m_2 + m_3)/3(m_1 + m_3)][(-m_1x_1/2m_2) + x_2 - (m_3x_3/2m_2)],$$
$$y = 2[(m_1 + m_2 + m_3)/3(m_1 + m_3)][(-m_1y_1/2m_2) + y_2 - (m_3y_3/2m_2)],$$
$$z = 2[(m_1 + m_2 + m_3)/3(m_1 + m_3)][(-m_1z_1/2m_2) + z_2 - (m_3z_3/2m_2)],$$

and $r_{NO} = z_1 - z_3$, $r_{NC} = z_1 - z_2$, and $r_{CO} = z_2 - z_3$. Then using equations 2-1 and 2-2, the following relations can be derived from the above coordinates:

$$x_1 = -[m_2(m_1 + m_3) r_{CO} / m_1(m_1 + m_2 + m_3) r_{NO}]\, x,$$
$$x_2 = [(m_1 + m_3)/(m_1 + m_2 + m_3)]\, x,$$
$$x_3 = -[m_2(m_1 + m_3) r_{NC} / m_1(m_1 + m_2 + m_3) r_{NO}]\, x,$$
$$y_1 = -[m_2(m_1 + m_3) r_{CO} / m_1(m_1 + m_2 + m_3) r_{NO}]\, y,$$
$$y_2 = [(m_1 + m_3)/(m_1 + m_2 + m_3)]\, y,$$
$$y_3 = -[m_2(m_1 + m_3) r_{NC} / m_1(m_1 + m_2 + m_3) r_{NO}]\, y,$$
$$z_1 = -[m_2 z / (m_1 + m_2 + m_3)] + (m_3 r_{NO})/(m_1 + m_3),$$
$$z_2 = [(m_1 + m_3)/(m_1 + m_2 + m_3)]\, z,$$
$$z_3 = -[m_2 z / (m_1 + m_2 + m_3)] + (m_2 r_{NO})/(m_1 + m_3).$$

Substituting these relations into equation 2-7 gives the following kinetic energy equation:

$$2T = [m_1m_3\dot{r}^2_{NC}/(m_1 + m_3)] + [m_2(m_1 + m_3)^2 I(\dot{x}^2 + \dot{y}^2)/ m_1m_3(m_1 + m_2 + m_3) r^e_{NC}] + [m_2(m_1 + m_3)\dot{z}^2/(m_1 + m_2 + m_3)], \quad \text{(I-1)}.$$

In this equation, I is the equilibrium moment of inertia as defined in reference 62 (p. 456). This energy expression contains no cross terms. Expanding equation 2-8 gives the following

expression for the potential energy:

$$2V = k_{11}Q_1^2 + k_{22}Q_2^2 + k_{33}Q_3^2 + 2k_{12}Q_1Q_2 + 2k_{13}Q_1Q_3 + 2k_{23}Q_2Q_3 + k_4(x^2 + y^2). \qquad \text{(I-2)}$$

The last term in equation I-2 takes into account the displacement due to the bend off the z-axis. Now define the following:

$$Q_1 = z_2 - z_1 = r_{NC}; \quad Q_2 = z_3 - z_2 = r_{CO}; \quad Q_3 = z_1 - z_3 = r_{NO}.$$

Making these substitutions into equation I-2 and using the definitions presented earlier, enables to write the potential energy as:

$$2V = \{[k_{11}m_3^2/(m_1 + m_3)^2] + [k_{22}m_1^2/(m_1 + m_3)^2] + k_{33} + [2k_{12}m_1m_3/(m_1 + m_3)^2] + [2k_{13}m_3/(m_1 + m_3)] + [2k_{23}m_1/(m_1 + m_3)]\} r_{NC}^2 + [k_{11} + k_{22} - 2k_{12}] z^2 + 2\{[-k_{11}m_3/(m_1 + m_3)] - [k_{12}(m_1 - m_3)/(m_1 + m_3)] - k_{13} + k_{23}\} z\, r_{NO} + k_4(x^2 + y^2). \qquad \text{(I-3)}$$

Now define the following coordinates:

$$\begin{aligned} Q_1' &= [m_1m_3/(m_1 + m_3)]^{1/2}\, r_{NO}\ ; \\ Q_{2a}' &= [m_2(m_1 + m_3)\, I\ /\ m_1m_2(m_1 + m_2 + m_3)\, r_{NO}^e]^{1/2}\, x\ ; \\ Q_{2b}' &= [m_2(m_1 + m_3)\, I\ /\ m_1m_2(m_1 + m_2 + m_3)\, r_{NO}^e]^{1/2}\, y\ ; \\ Q_3' &= [m_2(m_1 + m_3)/(m_1 + m_2 + m_3)]^{1/2}\, z\ . \end{aligned} \qquad \text{(I-4)}$$

Substituting equations I-4 into I-1 and I-3, gives:

$$\begin{aligned} 2T &= (\dot{Q}_1')^2 + [(\dot{Q}_{2a}')^2 + (\dot{Q}_{2b}')^2] + (\dot{Q}_3')^2; \quad \text{and} \\ 2V &= \{[(k_{11}m_3 + 2k_{13})/m_1] + [(k_{22}m_1 + 2k_{23})/m_3] + [k_{33}(m_1 + m_3) + 2k_{12}]/(m_1 + m_3)\}(Q_1')^2 + [k_4m_1m_3(m_1 + m_2 + m_3)\, r_{NO}^e/m_2(m_1 + m_3)\, I][(Q_{2a}')^2 + (Q_{2b}')^2] + [(k_{11} + k_{22} - 2k_{12})(m_1 + m_2 + m_3)/m_2(m_1 + m_3)]\,(Q_3')^2 + 2\{[-k_{11}m_3/(m_1 + m_3) + k_{22}m_2/(m_1 + m_3) - k_{12}(m_1 - m_3)/(m_1 + m_3) - k_{13} + k_{23}]/[m_1m_2m_3/(m_1 + m_2 + m_3)]\}\,[(Q_1'\,Q_3'] \equiv a(Q_1')^2 + b[(Q_{2a}')^2 + (Q_{2b}')^2] + c(Q_3')^2 + 2dQ_1'Q_3'. \end{aligned} \qquad \text{(I-5)}$$

Equation I-5 still contains the cross-term $Q_1'Q_3'$. This can be eliminated with the following transformation equations:

$$\begin{aligned} Q_1' &= q_1 \sin\gamma + q_3 \cos\gamma\ ; \quad Q_{2a}' = q_{21},\ Q_{2b}' = q_{22}; \text{ and,} \\ Q_3' &= -\,q_1 \cos\gamma + q_3 \sin\gamma\ . \end{aligned} \qquad \text{(I-6)}$$

In equation I-6, $\sin\gamma = (1/\sqrt{2})\{1 + (a - c)/[4d + (a - c)]\}^{1/2}$.

Effecting the transformations indicated by equation I-6 yields the equations 2-9, where the constants are as shown below:

$$k' = a \sin^2\gamma + c \cos^2\gamma - 2d \sin\gamma \cos\gamma \,, \; k' = b, \text{ and}$$

$$k' = a \cos^2\gamma + c \sin^2\gamma + 2d \sin\gamma \cos\gamma \,. \qquad \text{(I-7)}$$

The displacement coordinates, x_i, y_i, and z_i, can be expressed as linear combinations of the normal coordinates as stated in equation 2-3. The transformation ℓ_{ik}'s are shown below:

$$\ell^{(x)}_{121} = \ell^{(y)}_{122} = -[m_2 m_3 (r^e_{CO})^2/(m_1 + m_2 + m_3)\, I^e]^{1/2}$$

$$\ell^{(x)}_{221} = \ell^{(y)}_{222} = [m_1 m_3 (r^e_{NO})^2/(m_1 + m_2 + m_3)\, I^e]^{1/2}$$

$$\ell^{(x)}_{321} = \ell^{(y)}_{322} = -[m_1 m_2 (r^e_{NC})^2/(m_1 + m_2 + m_3)\, I^e]^{1/2}$$

$$\ell^{(z)}_{11} = [m_1 m_2/(m_1 + m_3)(M_1 + m_2 + m_3)]^{1/2}\cos\gamma + [m_3/(m_1 + m_3)]^{1/2}\sin\gamma$$

$$\ell^{(z)}_{21} = -[(m_1 + m_3)/(m_1 + m_2 + m_3)]^{1/2}\cos\gamma$$

$$\ell^{(z)}_{31} = [m_2 m_3/(m_1 + m_3)(m_1 + m_2 + m_3)]^{1/2}\cos\gamma - [m_1/(m_1 + m_3)]^{1/2}\sin\gamma$$

$$\ell^{(z)}_{13} = -[m_1 m_2/(m_1 + m_3)(m_1 + m_2 + m_3)]^{1/2}\sin\gamma - [m_3/(m_1 + m_3)]^{1/2}\cos\gamma$$

$$\ell^{(z)}_{23} = [(m_1 + m_3)/(m_1 + m_2 + m_3)]^{1/2}\sin\gamma$$

$$\ell^{(z)}_{33} = -[m_2 m_3/(m_1 + m_3)(m_1 + m_2 + m_3)]^{1/2}\sin\gamma + [m_1/(m_1 + m_3)]^{1/2}\cos\gamma$$

It should be recalled that for cyanate ion, m_1 is the nitrogen atomic mass, m_2 is the carbon atomic mass, and m_3 is the oxygen atomic mass.

APPENDIX II

Nielsen's Equations

Nielsen (64, p. 119) has utilized a second-order perturbation treatment to derive the following equations relating the spectroscopic anharmonicity constants to the cubic and quartic normal potential energy constants from equation 2-21 for the XYZ case:

$$x_{ii} = (1/4)[6k_{iiii} - 15(k^2_{iii}/\omega_i) - (k^2_{iij}/\omega_j)(8\omega_i^2 - 3\omega_j^2)/(4\omega_i^2 - \omega_j^2)] \qquad (i \neq j \neq 2) \qquad \text{(II-1)}$$

$$x_{22} = (1/4)[6k_{2222} - \sum_{j=1,3}(k^2_{22j}/\omega_j)(8\omega_2^2 - 3\omega_j^2)/(4\omega_2^2 - \omega_j^2)] \qquad (j = 1, 3) \qquad \text{(II-2)}$$

$$x_{2i} = (1/2)[k_{22ii} - (4k^2_{22i}\omega_2/(4\omega_2^2 - \omega_j^2)) - (k_{22j}k_{iij}/\omega_j) + 2(\omega_i/\omega_2)(\xi_{2i})^2 B_e] \qquad (i = 1,3;\ j = 3,1) \qquad \text{(II-3)}$$

$$x_{i2} = (1/2)[k_{ii22} - 6(k_{iii}k_{i22}/\omega_i) - (k_{iij}k_{j22}/\omega_j) + 2(\omega_2/\omega_i)(\xi_{i2})\ B_e] \qquad (i = 1,3;\ j = 3,1) \qquad \text{(II-4)}$$

$$x_{ij} = (1/2)[k_{iijj} - 6(k_{iii}k_{ijj}/\omega_i) - 4k^2_{iij}\omega_i/(4\omega_i^2 - \omega_j^2)] \qquad (i = 1,3;\ j = 3,1) \qquad \text{(II-5)}$$

$$x_{\ell_2\ell_2} = -(1/4)[2k_{2222} + \sum_{i=1,3}k_{22i\ i}/(4\omega_2^2 - \omega_i^2)] \qquad \text{(II-6)}$$

where the k_{ijk} are the normal coordinate potential constants, the ω_i are the harmonic frequencies, ξ_{2i} is the Coriolis interaction constant, and B_e is the equilibrium rotational constant.

When Fermi resonance occurs, the term $(4\omega_i^2 - \omega_j^2)$ becomes small and invalidates the above equations because $\omega_j \approx 2\omega_i$. This effect is attributed to the cubic potential constant k_{jii}.

In this situation, the constants, x_{ii}, x_{ij}, and $x_{\ell_2\ell_2}$ (if ω_2 is the degenerate vibration) will be effected, but only by the terms involving k_{iij}^2. These terms will no longer be present in the forms given above. In their place, the following substitutions are made:

1. in equation II-1 and II-2: $-k_{iij}^2[(\omega_j/2) + (2\omega_i + \omega_j)/8]$
2. in equations II-3, II-4, and II-5:

   $-(k_{iij}^2/2)[(2\omega_i + \omega_j)]$
3. in equation II-6: $(k_{iij}^2/4)/(2\omega_i + \omega_j)$.

APPENDIX III

The $C_{\infty v}$ Symmetry Group

TABLE III-1. SYMMETRY SPECIES AND CHARACTERS FOR $C_{\infty v}$.

$C_{\infty v}$	I	$2C_\infty^{\phi}$	$2C_\infty^{2\phi}$	...	$2C_\infty^{n\phi}$	...	$\infty\sigma_v$	
$A_1(\Sigma^+)$	1	1	1	...	1	...	1	T_z
$A_2(\Sigma^-)$	1	1	1	...	1	...	-1	R_z
$E_1(\Pi)$	2	$2\cos\phi$	$2\cos 2\phi$	...	$2\cos(n\phi)$	...	0	T_x, T_y, R_x, R_y
$E_2(\Delta)$	2	$2\cos 2\phi$	$2\cos 2(2\phi)$	...	$2\cos 2(n\phi)$	...	0	
$E_3(\Phi)$	2	$2\cos 3\phi$	$2\cos 2(3\phi)$	...	$2\cos 3(n\phi)$	...	0	
...	...	...	...	...	...	...	...	

ϕ is an arbitrary angle of rotation about the principal axis.

Symmetry types for higher vibrational levels are determined in the following way. The characters of the resultant species are obtained by multiplying for each symmetry element, the characters of the species of the component normal vibrations taken to the v_k^{th} power. v_k is the vibrational quantum number of the vibration of interest, k. This is done with the symmetry species of combinations by taking direct products of the irreducible representations.

TABLE III - 2. NON-DEGENERATE SPECIES COMBINATION TYPES IN WHICH TWO DIFFERENT VIBRATIONS, AT LEAST ONE OF WHICH IS NON-DEGENERATE, ARE SINGLY EXCITED ($v_k = 1$) IN THE $C_{\infty v}$ SYMMETRY GROUP.

Vibrations Excited	Resultant State
$\Sigma^+ \times \Pi$	Π
$\Sigma^+ \times \Delta$	Δ
$\Sigma^- \times \Pi$	Π
$\Sigma^- \times \Delta$	Δ

TABLE III- 3. SYMMETRY SPECIES OF HIGHER VIBRATION LEVELS OF DEGENERATE VIBRATIONS OF THE $C_{\infty v}$ SYMMETRY GROUP.

Vibrational Level	Resulting Species
$(\Pi)^{n=2}$	$\Sigma + \Delta$
$(\Pi)^{n=3}$	$\Pi + \Phi$
$(\Pi)^{n=4}$	$\Sigma^+ + \Delta + \Gamma$
$(\Pi)^{n=5}$	$\Pi + \Phi + H$

APPENDIX IV

Numerical Data and Potential Calculations

This supplement contains information alluded to in Chapter Seven and numerical values used in calculations throughout this thesis. The following sections are in this appendix:

A. The mass weights used in all calculations in the text;
B. A schematic flow chart of the computer program outlined in Chapter Seven;
C. The numerical values of the final model parameters used in the potential energy calculations;
D. The correlation matrix output with the final potential constants.

A. Mass Weights.

The mass weights and respective reciprocals which were used in isotopic calculations are shown below:

TABLE IV-1. ATOMIC MASS WEIGHTS AND RECIPROCALS.

Atom	Isotope Number	Mass(amu)	Reciprocal (μ, amu^{-1})
Carbon	12	12.00000	0.0833333
	13	13.00335	0.0769032
Nitrogen	14	14.00307	0.0714129
	15	15.00011	0.0666662
Oxygen	16	15.99491	0.062520
	18	17.99916	0.0555581

TABLE IV-2. CYANATE ION MOLECULAR WEIGHTS.

Molecule	Mass(amu)
$^{14}N^{12}C^{16}O^-$	41.9980
$^{15}N^{12}C^{16}O^-$	42.9950
$^{14}N^{13}C^{16}O^-$	43.00133
$^{14}N^{12}C^{18}O^-$	44.00223
$^{15}N^{13}C^{16}O^-$	43.99837
$^{15}N^{12}C^{18}O^-$	44.99927
$^{14}N^{13}C^{18}O^-$	45.00558
$^{15}N^{13}C^{18}O^-$	46.00262

The values listed for the atomic weights were found in the Handbook of Chemistry and Physics, 46th Edition, The Chemical Rubber Company, Cleveland, Ohio(1966), on page B7.

B. Computer schematic flow Diagram.

(1) a. Equilibrium bond lengths (r^e) and initially transferred Morse parameters(a_i) are used to express k_{iiii} and k_{iii} as a function of k_{ii}(in internal coordinates) and a_i.
b. An initial set of k_{ii} are entered.

(2) Model is used to generate a, b, and c coefficients:
a. The inverse power relation is used for the stretch-stretch interactions using initially transferred γ_i, and d_{ij}(Badger's Rule parameters);
b. the Smith-Overend exponential relation is used for the stretch-bend interactions, using model parameters A and B.

Stretch-stretch and stretch-bend interactions are expressed in terms of the a, b, and c coefficients and the principal force constants (k_{ii}, k_{iii}, k_{iiii}) in internal coordinates.

This quartic field in instantaneous internal coordinates undergoes a non-linear transformation to normal coordinates.

Calculate ω_i, x_{ii}, x_{ij} and the energy levels using Nielsen's equations in the proper form to allow for the Fermi resonances.

Compare calculated energy levels to the observed levels. Calculates corrections to the force constants in (1) and (2) by a non-linear least squares routine.

If force constant corrections are greater than 0.005, then go to (1) and (2), if not, then go to (3).

(3) Output results:
- a. least squares $V(R_i)$
- b. least squares $V(Q_i)$
- c. model parameters
- d. anharmonic constants
- e. harmonic frequencies
- f. correlation matrix
- g. energy levels
- h. statistical dispersions

C. Model parameters for cyanate ion in KCl, KBr, and KI.

The model parameters discussed in Chapter Seven are presented in this section. Table IV-3 lists the values which generated the potential constants tabulated in Chapter Seven.

Table IV-3. SMITH-OVEREND MODEL PARAMETERS FOR CYANATE ION IN POTASSIUM HALIDE LATTICES.

A. The a, b, and c coefficients:

for Bond 1 (N-C)

Parameter	in KCl	in KBr	in KI
a_2^1	-0.0810	-0.0794	-0.0760
a_{22}^1	0.1969	0.1907	0.1755
a_{33}^1	0.0326	0.0292	0.0360
a_{222}^1	-0.3725	-0.3570	-0.3175
a_{233}^1	-0.3345	-0.3141	-0.3509
b_2^{11}	0.2552	0.2695	0.2620
b_1^{33}	-1.3697	-1.2040	-1.4604
b_{22}^{11}	-1.0415	-1.0099	-0.9297
b_{33}^{11}	-0.1674	-0.1588	-0.1811
b_{11}^{33}	0.9381	0.7249	1.0665
b_{12}^{33}	2.7112	2.5306	2.8678
c_2^{111}	0.2456	0.2617	0.2540

for Bond 2 (C-O)

a_1^2	-0.1095	-0.1062	-0.0988
a_{11}^2	0.1667	0.1576	0.1398
a_{33}^2	0.0637	0.0681	0.0628
a_{111}^2	-0.2168	-0.2009	-0.1717
a_{133}^2	-0.3205	-0.2968	-0.3399
b_1^{22}	0.2255	0.2227	0.2331

Table IV-3. (continued)

Parameter	for Bond 2 (C-O) in KCl	in KBr	in KI
b_2^{33}	-1.9794	-2.1018	-1.9636
b_{11}^{22}	-0.6716	-0.6361	-0.5688
b_{33}^{22}	-0.3159	-0.3261	-0.3129
b_{22}^{33}	1.9590	2.2087	1.9290
c_1^{222}	0.1942	0.1921	0.2136

B. Other model parameters(dispersions in parenthesis)

A	-1.3697	-1.2116	-1.4604
B	1.4451	1.7547	1.3446
a_{NC}	2.168(0.085)	2.216(0.078)	2.165
a_{CO}	2.312(0.047)	2.297(0.044)	2.315
γ_1	4.9806	4.9090	4.6764
γ_2	2.5627	2.4732	2.3112
δ_1	0.0200	0.0199	0.0200
δ_2	0.0500	0.0502	0.0500

A and B are the Smith-Overend stretch-bend parameters.
a_{NC} and a_{CO} are the adjusted Morse parameters.
γ_1 and γ_2 are the inverse power stretch-stretch parameters.
δ_1 and δ_2 express the change in bond length between triatomic and diatomic bonds for the respective atom-pair.

D. Correlation Matrix.

The correlation matrix for the potential constant calculations in Chapter Seven is shown below. Only nine parameters are shown. For each entry, row one is for the KCl calculation, row two is for KBr, and row three is for KI. In the latter case, the Morse parameters were held constant.

TABLE IV-4. CORRELATION MATRIX FOR POTENTIAL CALCULATIONS IN KCL, KBR, AND KI.

	K_{11}	K_{12}	K_{22}	K_{33}	K_{133}	K_{233}	K_{3333}	a_{NC}	a_{CO}
K_{11}	1.00	0.91	0.90	0.08	0.39	0.41	0.10	0.01	0.02
	1.00	0.90	0.90	0.01	0.36	0.36	0.04	0.01	0.01
	1.00	0.99	0.99	0.17	0.38	0.44	0.14		
K_{12}		1.00	0.89	0.05	0.36	0.38	0.15	0.37	0.18
		1.00	0.89	0.01	0.29	0.33	0.10	0.41	0.23
		1.00	0.98	0.16	0.26	0.33	0.10		
K_{22}			1.00	0.13	0.61	0.64	0.21	0.24	0.23
			1.00	0.10	0.56	0.60	0.20	0.27	0.18
			1.00	0.20	0.35	0.40	0.20		
K_{33}				1.00	0.50	0.53	0.94	0.00	0.21
				1.00	0.56	0.58	0.92	0.03	0.25
				1.00	0.35	0.38	0.93		
K_{133}					1.00	0.98	0.52	0.29	0.42
					1.00	0.98	0.62	0.19	0.46
					1.00	0.98	0.25		
K_{233}						1.00	0.60	0.27	0.47
						1.00	0.67	0.18	0.51
						1.00	0.31		
K_{3333}							1.00	0.16	0.26
							1.00	0.16	0.35
							1.00		
a_{NC}									0.43
									0.46